EGG-CDAP-5379

July 1981

ZIRCALOY CLADDING SHAPE AT FAILURE (BALON2)

D. L. Hagrman

Idaho National Engineering Laboratory

Operated by the U.S. Department of Energy

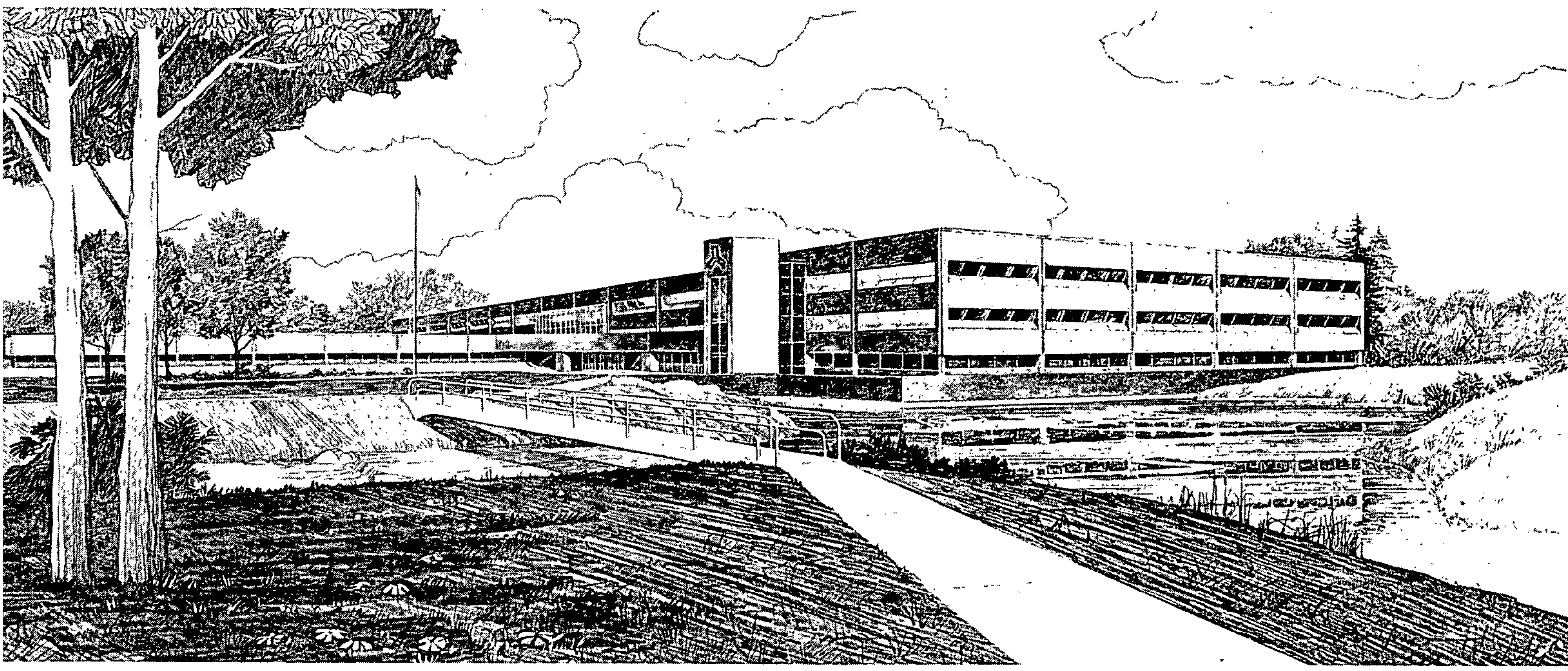

This is an informal report intended for use as a preliminary or working document

Prepared for the
U.S. Nuclear Regulatory Commission
Under DOE Contract No. DE-AC07-76ID01570
FIN No. A6050

EG&G Idaho

EG&G Idaho, Inc.

FORM EG&G-398
(Rev. 11-79)

INTERIM REPORT

Accession No. ______

Report No. EGG-CDAP-5379

Contract Program or Project Title: Fuel Behavior Model Development

Subject of this Document: Zircaloy Cladding Shape at Failure (BALON2)

Type of Document: Status Report

Author(s): D. L. Hagrman

Date of Document: July 1981

Responsible NRC Individual and NRC Office or Division: G. P. Marino, NRC-RES

This document was prepared primarily for preliminary or internal use. It has not received full review and approval. Since there may be substantive changes, this document should not be considered final.

EG&G Idaho, Inc.
Idaho Falls, Idaho 83415

Prepared for the
U.S. Nuclear Regulatory Commission
Washington, D.C.
Under DOE Contract No. DE-AC07-76ID01570
NRC FIN No. A6050

INTERIM REPORT

ABSTRACT

The derivation and some implications of a simple true stress cladding failure criterion are presented in this report. An associated model, BALON2, which uses the true stress failure criterion to calculate cladding shape at failure is described, and the results of a sensitivity study to determine the important parameters affecting cladding shape are included. Recently proposed licensing standards for LOCA analysis are compared with the BALON2 model predictions and are shown to be inconsistent when the pressure differential across the cladding varies.

SUMMARY

The main progress represented by this report is the use of local stress to predict cladding failure. The large scatter inherent in engineering stress or engineering strain expressions has been eliminated as have numerous limitations and special correlations for such effects as heating rate, circumferential temperature gradients, etc., which are necessary when improper failure criteria are employed. The failure stress is only a function of temperature and oxygen content once cold work and irradiation damage are annealed.

Although the failure criterion is simplified by the use of true stress, the calculation of cladding shape at failure is made fairly complex by the interaction of deformation, cladding temperatures and local stress. BALON2, a model for cladding deformation which deals with these interactions is developed and demonstrated. The model shows that circumferential temperature gradients tend to decrease circumferential strain at failure, and that slow heating rates cause both large circumferential strains at failure and small circumferential temperature gradients because they allow time for removal of circumferential temperature gradients. The rate of change of the pressure differential across the cladding is shown to have an effect on the cladding shape. BALON2 model predictions are compared to recently proposed liscensing standards for LOCA analysis. Results of this comparison suggest that the standards may be inadequate because they do not consider several of the parameters that affect cladding shape.

CONTENTS

FIGURES

TABLES

INTRODUCTION

A key consideration in assessing the severity of postulated light water reactor accidents is the post-accident configuration of fuel cladding. Events which could lead to final configurations that restrict coolant flow are more hazardous than scenarios which lead to more easily cooled reactor core geometries. An analysis of data provided by the U.S. Nuclear Regulatory Commission's research program has provided a simple failure criterion and a concise computer subcode which have had success in reducing the uncertainty of predictions of posttest cladding shapes. The criterion and associated subcode, BALON2, are described in this report. In addition, the results of a sensitivity study to determine the important parameters affecting cladding shape and a comparison with detailed measurements of cladding shape at burst are presented.

Predictions for cladding shape at rupture have traditionally been based on correlations of total circumferential elongation (the difference between circumference and initial circumference divided by the initial circumference) versus burst temperature. These correlations display major trends like the minimum elongation found in the alpha plus beta region (1090 to 1255 K burst temperatures) but there is at least a fifty percent uncertainty associated with this approach. Efforts to improve the correlations by adding more variables, like heating rate or circumferential temperature variation at failure, have had very little success.

As experiments improved, it became obvious that a significant part of the problem with correlations for the circumference of cladding at failure is the fact that failure is a local event occurring at one part of the circumference while the circumferential elongation is a global quantity made up of the sum of local elongations at all locations around the circumference. The logical approach, then, was to look for a simple local failure criterion. The success of this effort encouraged development of a computer code to sum all the local elongations as a function of time to obtain a total circumferential elongation at the moment of failure. Early experience with the code has shown it to be successful at explaining much of the previously confusing scatter in total circumferential elongation data.

THE FAILURE CRITERION

Arguments are presented in this section which demonstrate that zircaloy cladding failure can be predicted by comparing the tangential component of true or local stress with a failure stress which is a function of cladding temperature, irradiation and cold work. Heating rate and strain rate do not affect this criterion. The failure stress as a function of temperature is given by the following expressions.

For cladding temperatures between or equal to 300 and 750 K,

$$\sigma_{\theta F} = 1.36\ K_A\ . \tag{1a}$$

For cladding temperatures between 750 and 1050 K,[a]

$$\sigma_{\theta F} = 46.861429\ K_A\ \exp\ -\frac{1.9901087\ 10^6}{T^2}\ . \tag{1b}$$

For cladding temperatures between or equal to 1050 and 2100 K

$$\sigma_{\theta F} = 7.7\ K_A \tag{1c}$$

where

$\sigma_{\theta F}$ = tangential component of true stress at burst (Pa)

K_A = strength coefficient used to describe the plastic deformation of annealed cladding (Pa). Correlations for the strength coefficient are given in Appendix A

T = cladding temperature (K).

---

a. Several significant figures are used in this expression in order to minimize discontinuities at 750 and 1050 K.

For cold worked or irradiated cladding the failure stress is increased by four tenths of the increase of the strength coefficient due to irradiation and cold work.

Equation (1) is estimated to have a standard error of 0.2 times the failure stress. The error and the error estimate are discussed later in this section.

The failure criterion given by Equation (1) is based on data from tests which reported initial cladding dimensions, temperature at failure, pressure at failure, wall thickness at the failed region and some means of estimating the axial and azimuthal radii of curvature at the burst region. In all cases the wall thickness measurements were accurate to no better than ten percent and the azmimuthal radii of curvature were obtained from circumference measurements by assuming a circular cladding cross section. The assumption that the cross section was circular at the moment of burst may be suspected of introducing some systematic error in the failure stress, but cross sections observed close to ruptures (where the shape has not been changed by the rupture tear) are circular.

The most useful data have been produced by the Multirod Burst Test Program sponsored by the U.S. Nuclear Regulatory Commission. All of these tests used internal heaters and an external steam environment. Heating rates varied from 0 to 28 K/s. Estimated burst temperatures, burst pressures and burst strains (average circumferential strain) have been published for a number of single rod tests.[1,2] Also, calibrated photographs of cross sections through the burst regions of some of the tests have been published.[2-5] These cross sections were used to determine wall thickness at burst. The axial radius of curvature at burst was estimated from side view photographs of the burst tubes.[6-8] The Multirod Burst Test Program data from tests for which complete data are available are summarized in Table 1.

TABLE 1. SUMMARY OF MULTIROD BURST TEST DATA

Test No.	Burst Temperature (K)	Differential Pressure at Burst (MPa)	Average Circumferential Strain (m/m)	Wall Thickness as Burst (mm)	Axial Radius of Curvature (cm)
PS-10	1174[a]	6.000[a]	0.20[a]	0.079[c]	2.1[c]
PS-17	1051[a]	12.130[a]	0.25[a]	0.176[c]	1.2[c]
PS-18	1444[a]	0.772[a]	0.24[a]	0.111[d]	0.9[g]
PS-19	1232[a]	2.590[a]	0.28[a]	0.079[c]	0.6[c]
SR-23	1350[a]	0.960[a]	0.35[a]	0.164[e]	1.1[h]
SR-25	1365[a]	0.960[a]	0.78[a]	0.077[e]	0.6[i]
SR-34	1039[b]	5.820[b]	0.316[b]	0.109[b]	1.6[c]
SR-35	1048[b]	4.470[b]	0.290[b]	0.073[f]	3.1[c]
SR-37	1033[b]	13.560[b]	0.231[b]	0.263[f]	3.7[c]
SR-41	1030[b]	9.765[b]	0.274[b]	0.199[b]	2.7[c]
SR-43	1046[b]	7.620[b]	0.290[b]	0.179[b]	3.5[c]

a. Reference 1 pages 18 and 19.

b. Reference 2 pages 7 and 31.

c. From photographs sent by R. H. Chapman, ORNL.

d. Reference 3 page 35.

e. Reference 4 pages 120 and 121.

f. Reference 5 page 26.

g. Reference 6 page 19.

h. Reference 7 page 22.

i. Reference 8 page 17.

Data from tests by Hobson and Rittenhouse[9] were also employed. The Hobson-Rittenhouse tests were conducted with a radiant heating furnace and BWR cladding in an argon environment. Heating rates from 5.6 to 56 K/s were used. Table 2 is a summary of the data that were used from the tests by Hobson and Rittenhouse. Burst temperatures, wall thickness measurements, and the average circumferential strains were obtained from figures in Reference 9. Burst pressures were obtained by private communication from R. H. Chapman, and axial radii of curvature were estimated from cladding samples sent by D. O. Hobson.

Table 3 is a summary of data obtained from tests by H. M. Chung and T. F. Kassner[10] which were used in the development of Equation 1. The burst temperature, differential pressure at burst, average circumferential strain and axial radius of curvature were obtained from Reference 10. The wall thickness at burst was obtained from photographs of cross sections obtained from Chung. An important feature of these tests is that the tests in Table 3 have an internal mandrel which applied an unknown axial stress to the cladding.

None of the data discussed so far were obtained from irradiated cladding or at temperatures below 1000 K. The only available low temperature data with irradiated cladding were obtained from studies by A. A. Bauer, L. M. Lowry, W. J. Gallagher, A. J. Markworth and J. S. Perrin[11,12,13] on spent fuel cladding obtained from the H. B. Robinson reactor. The data from this project which were used to develop Equation (1) are presented in Table 4. Tests M12-16, M12-4 and M12-15 were conducted on as-received cladding while tests D9-7, D9-8, D9-13 and D9-14 were conducted on cladding which had been annealed. Wall thicknesses adjacent to the burst were obtained from unpublished photographs similar to Figure 7 of Reference 11. The axial radii of curvature in these tests is unknown.

Two sources of in-reactor data were employed. One is the irradiation effects test IE-5 conducted in the Power Burst Facility.[14,15] The measured rod internal gas pressure in this test was reported (page 12 of

TABLE 2. SUMMARY OF DATA FROM THE HOBSON-RITTENHOUSE TESTS

Test No.	Burst Temperature (k)	Differential Pressure at Burst (MPa)	Average Circumferential Strain (m/m)	Wall Thickness at Burst (mm)	Axial Radius of Curvature (cm)
35	1061	6.170	0.63	0.25	2.9
34	1081	7.584	0.58	0.23	1.8
40	1111	4.654	0.79	0.18	1.8
18	1145	4.826	1.25	0.18	3.0
18	1158	4.205	0.57	0.20	2.5
19	1160	4.895	0.51	0.23	1.8
21	1171	3.102	0.30	0.18	1.7
8	1179	3.826	0.22	0.20	1.3
16	1195	3.999	0.42	0.25	1.7
5	1196	3.757	0.44	0.20	1.0
26a	1205	3.068	0.27	0.28	1.8
27	1213	2.241	0.55	0.15	1.1
15	1214	2.275	0.41	0.18	1.1
37	1215	2.344	0.40	0.18	1.4
26	1220	3.033	0.53	0.13	1.5
9	1235	1.448	0.43	0.20	2.7
28	1253	1.413	0.85	0.18	2.8
11	1299	1.434	0.68	0.25	1.5
32	1302	0.745	0.93	0.25	2.1
29	1432	0.676	0.92	0.23	2.5
36	1440	0.827	0.50	0.23	1.5
4	1472	0.689	1.11	0.20	2.5
36a	1487	0.662	0.74	0.25	1.5

TABLE 3. SUMMARY OF DATA FROM THE CHUNG-KASSNER TESTS

Test No.	Burst Temperature (K)	Differential Pressure at Burst (MPa)	Average Circumferential Strain (m/m)	Wall Thickness at Burst (mm)	Axial Radius of Curvature (cm)
AS-40	1089	5.302	1.01	0.39	2.9
AS-36	1310	0.558	1.11	0.26	2.9
AS-9	1329	1.282	1.24	0.12	3.2
AS-5	1348	1.334	1.02	0.42	1.6

TABLE 4. SUMMARY OF DATA FROM THE BAUER ET AL. TESTS

Test No.	Burst Temperature[a] (K)	Burst Strength[a] (MPa)	Average Circumferential Strain[a] (m/m)	Wall Thickness at Burst[b] (mm)
M12-16	477	749.4	0.026	0.57
M12-4	644	659.1	0.052	0.60
M12-15	644	684.6	0.028	0.61
D9-7	644	356.4	0.212	0.45
D9-8	644	350.9	0.204	0.46
D9-13	644	372.3	0.225	0.51
D9-14	644	367.5	0.292	0.48

a. From Reference 12, pages 3 and 7.

b. From photographs sent by A. A. Bauer and L. W. Lowry of Battelle Columbus Laboratories.

Reference 15) to be 5.2 MPa in excess of the coolant pressure and the cladding temperature was estimated from microstructure studies to be near 1100 K. The average circumferential elongation (engineering strain) was reported to be 0.25 (page 16 of Reference 15). The wall thickness at burst was estimated to be 0.09 mm using Figure 5 of the post-irradiation examination results report[15] and the axial radius of curvature was estimated to be approximately four times the rod diameter from the photograph on page 91 of Reference 15.

The second source of in-reactor data is a series of tests in the FR2 reactor in Germany.[16] Complete data from three tests were presented (A2.3, B1.2 and B1.3) but two of the cladding cross sections had burst edges rolled in--evidence of contact with the shroud. For that reason, only data from test B1.2 were used. The average circumferentail elongation, axial radius of curvature, burst pressure, burst temperature and wall thickness at burst (0.249, 1.5 cm, 4.52 MPa, 1188 K and 0.16 mm, respectively) were taken from Reference 16. The coolant pressure was assumed to be the typical value of 0.3 MPa given on page 2 of the reference.

One out-of-pile test result from Germany[17] was used in developing the failure criterion. The test was performed in air (0.1 MPa pressure) with an internal heater. The burst temperature, internal gas pressure at burst, average circumferential elongation and wall thickness at burst (1114 K, 7.1 MPa, 0.37 mm, and 0.215 mm, respectively) were taken from Figure 13 of Reference 17. The axial radius of curvature was estimated to be approximately three times the cladding radius at burst by inspection of X-ray photographs of similar tests just prior to burst.

The development of Equation (1) was preceded by attempts to use average circumferential elongation, engineering hoop stress and wall thinning versus burst temperature as failure criteria, but these criteria all exhibited unacceptable scatter when the data base just discussed was used to test them. Local stress versus burst temperature not only showed less scatter, but those data that exhibited scatter could be explained by a careful examination of experiment details.

Local stresses at failure were estimated from the data just presented and the equilibrium equation for a membrane element at the time of failure[18]

$$\frac{\sigma_{ZF}}{r_Z} + \frac{\sigma_{\theta F}}{r_\theta} = \frac{P_F}{t_F} \tag{2}$$

where

P_F = difference between gas pressure and coolant pressure at failure (Pa)

σ_{ZF} = axial stress at failure (Pa)

$\sigma_{\theta F}$ = tangential stress at failure (Pa)

r_z = axial radius of curvature at failure (m)

r_θ = circumferential radius of curvature at failure (m)

t_F = cladding thickness at burst (m).

Two approximations are needed to deduce an estimate of $\sigma_{\theta B}$ from Equation (2) and the data. The first approximation is that the cross section perpendicular to the cladding axis is approximately circular, or

$$r_\theta \approx \text{undeformed radius} \cdot \frac{\text{circumference at burst}}{\text{undeformed circumference}} \cdot \tag{3}$$

This approximation is necessary because the shape at the moment the burst tear begins is unknown.

The second approximation is needed to estimate the axial stress, σ_{ZF}. The maximum axial stress is limited by a physical consideration. It must have been less than $\sigma_{\theta F}$ for failure to occur along an axial line. Since r_Z is typically several times r_θ, the first term of Equation (2) is small as long as σ_{ZF} is less than $\sigma_{\theta F}$ so a crude approximation is acceptable. The maximum value of σ_{ZF} ($\sigma_{\theta F}$) is therefore used to estimate the contribution of the first term. This approximation tends to underpredict $\sigma_{\theta F}$ while the assumption of Equation (3) tends to overpredict $\sigma_{\theta F}$ because Equation (3) ignores the reduction of r_θ due to local bulges in the plane perpendicular to the cladding axis.

The expression for tangential stress at failure obtained from Equation (2) with the two approximations just discussed is

$$\sigma_{\theta F} = \frac{P_F}{t_F}\left[\frac{1}{\frac{1}{r_z}+\frac{1}{r_\theta}}\right]. \tag{4}$$

Figure 1 is a plot of the local tangential failure stress obtained from Equation (4) and the data. Approximate heating rates during burst are indicated to show that there is no systematic variation with heating rate. Comparison of the burst stresses obtained from Hobson's tests with both Chapman's tests and the two in-reactor data show there is no significant effect of oxide films or alpha layers on the burst stress, at least at the heating rates used in these tests. The most probable interpretation of this observation is the suggestion that the relatively thin oxide and alpha layers are cracked before the burst stress of the underlying beta layers is achieved.

Most of the burst stresses shown in Figure 1 form a locus which looks very similar to a plot of the strength coefficient for plastic deformation of zircaloy.[a] The exceptions are not scattered randomly. They all lie

---

a. The strength coefficient is discussed in Appendix A.

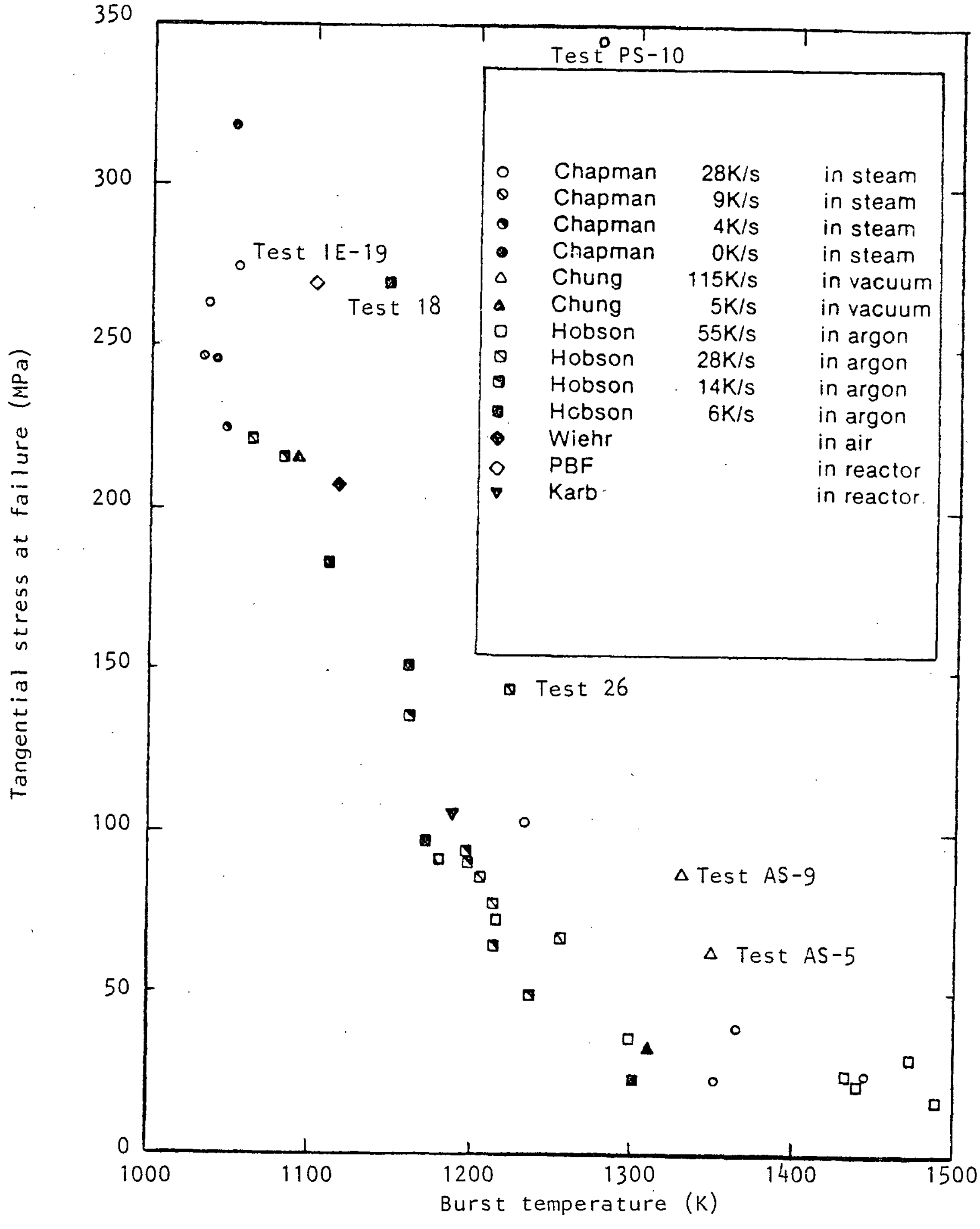

Figure 1. Local tangential stress at failure versus temperature assuming a circular cross section at failure.

above the main collection of points. Closer inspection indicates that the tests which yielded unusually high tangential burst stresses had features which caused the assumptions used in calculating tangential burst stress to be questionable. These features are discussed, on a test by test basis, in the next several paragraphs. The exceptional data are individually labeled in Figure 1.

For rod IE-19 of the PBF Test IE-5 the maximum temperature of the cladding burst region was determined by metallography to be approximately 1100 K. Postirradiation examination results[15] show the maximum temperature of the fracture area was less than the maximum cladding temperature at other azimuthal locations in the axial plane of the fracture. The interpretation given to this information in the postirradiation examination results report is that 1100 K was also the burst temperature because no increase could have occurred on the protruding fracture tips after the rod burst. This conclusion may be slightly overstated. The test results report (see Figure 13 of Reference 19) shows that the adjacent 45 degree thermocouple which also protruded experienced a 50 K temperature rise after the initial temperature increase. Therefore a more realistic estimate of the burst temperature of the cladding in rod IE-19 is 1000 to 1050 K.

Test PS-10 from Chapman's studies was performed with a heater which has an unusually large circumferential variation in temperature.[20] In this case very local ballooning is likely, and Equation (4) is probably a poor approximation for the circumferential radius of curvature near the time of burst. Because of the questionable validity of Equation (4) for this test and because of the large difference between the calculated burst stress of this test and several other data obtained at similar burst temperatures, this test was omitted from the failure analysis.

Test 18 from the Hobson-Rittenhouse series burst at a thermocouple temperature of 1145 K, yet had an average circumferential strain characteristic of temperatures in the alpha phase. Moreover, the axial profile of this test is almost triangular (see Figure 4 of Reference 9). In all probability the axial radius of curvature given in Table 2 (estimated from the bottom half of the sample) is much too large. The test was therefore eliminated from the data base.

Test 26 from the Hobson-Rittenhouse series is the only sample in the entire test series which did not exhibit approximate mirror symmetry of wall thickness about a plane through the burst area and the cladding centerline. In this test, one half of the cross section is essentially undeformed and one half is uniformly thin. Thus, both the axial and circumferential radii of curvature estimated for this test are questionable. Therefore the test was removed from the data base.

Tests AS-9 and AS-5 by Chung are the most difficult of all the data shown in Figure 1 to understand. It is probable that the constraining mandrel used in these tests caused a large axial stress which perturbed the test. Moreover, test AS-36 which differed only in heating rate from AS-5 and AS-9 does not differ from the Hobson or Chapman tests which burst at similar temperatures. Tests AS-5 and AS-9 were removed from the data base solely because they differ markedly from the two tests by Chapman which were conducted in steam with an internal heater--two features which are believed to make Chapman's test more representative of in-reactor cladding failure.

The remaining data shown in Figure 1 were used to find the tangential burst stress at failure above 1000 K. The failure stress derived from the data was divided by the strength coefficient obtained from the correlation given in Appendix A and the quotients were averaged. For the alpha phase data with burst temperatures above 1000 K, the average quotient is 7.48 ± 0.91; for the alpha plus beta region, it is 7.54 ± 1.03; and for the beta phase, it is 8.14 ± 1.84. Since there is no significant variation of the quotient, the average obtained for the entire temperature range above 1000 K, 7.70 ± 1.29, was used in Equation (1).

The estimated uncertainty of ±0.2 times the predicted failure stress is slightly larger than the fractional standard error[a] of the preliminary fit (±0.17) because of the additional error associated with possible variations in shape. The additional factor of 0.03 is the author's intuitive judgement.

Equations (3) and (4)[b] were also used with the low temperature data of Table 4 to estimate low temperature failure stresses. In this case the ratios of failure stress to strength coefficient obtained were much smaller than those of the high temperature data. A ratio of 0.84 ± 0.03 was found for the annealed cladding and 0.80 ± 0.06 was found for the irradiated cladding. These ratios were not used for the failure stress correlation because the axial radii of curvature needed to accurately calculate the failure stresses were not known (infinity was assumed). Instead, the measured failure strains were used with the equation of state for zircaloy plastic deformation (Appendix A), an assumed strain rate sensitivity exponent of zero, and typical anisotropy coefficients[c] to calculate failure stresses consistent with the equation of state and the measured strain. This approximation is more reasonable than estimating axial radii of curvature at low temperature because (a) the unknown strain rate at failure is unimportant at low temperature and (b) the stress-strain curve at low temperature is very flat so that small uncertainties in stress are equivalent to large uncertainties in strain. The factor of 1.36 for

---

a. The standard error of the preliminary fit was estimated with the expression $\left[\sum\left(\frac{\sigma_{\theta F}}{7.7 \text{ strength coefficient}} - 1\right)^2 / (\text{number of measurements} - 1)\right]^{0.5}$.

b. The axial radius of curvature was assumed to be three times the circumferential radii of annealed cladding and infinite for the irradiated cladding.

c. The irradiated cladding was assumed to be isotropic when effective stress and strains were calculated but the annealed cladding was assumed to have typical anisotropy coefficients.

annealed cladding and an increase of burst strength equal to four tenths of the increase in the strength coefficient due to cold work or irradiation in Equation (1a) reproduce the failure strains listed in Table 4.

Equation (1b) is simply an assumption contrived to extrapolate between the two regions where data are available without producing unreasonable predictions for failure strain in the temperature range where it is used.

A MODEL FOR CALCULATING CLADDING SHAPE

Equation (1) is sufficient to provide a complete description of both the time of cladding failure and the shape of failed cladding if they are used with an equation of state for zircaloy plastic deformation and a model which determines cladding shape as a function of temperature and pressure histories. A suitable equation of state is available as part of the MATPRO materials properties package and is discussed briefly in Appendix A. More detailed descriptions are available in Reference 21. This section describes a large deformation model, BALON2, which determines cladding shape at failure using the MATPRO equation of state and the failure criterion given by Equation (1). The model has been programmed as a FORTRAN IV computer code. Input/output information and a listing of the BALON2 code are provided in Appendix B.

Time step increments are used to model the deformation of cladding. Figure 2 illustrates the sequence of the calculations. First, local stresses are calculated using given pressures, temperatures, midwall radii and wall thicknesses. Then, the given time step size is checked to see if it is short enough to prevent significant change in the local stresses during the time step. If the given step is too long, it is divided into several shorter steps. For some options, cladding temperatures are recalculated to account for effects of the deformation during the previous time step on cladding temperature. The effects of annealing are also considered for these options.

Next, requested start-of-step information is printed and all nodes are checked for failure. If failure has occurred, final shape information is printed and the calculation is complete.

If cladding failure has not occurred, the description of the cladding texture (anisotropy constants) is updated and the effective strain prior to deformation is calculated. This initial effective strain is used to calculate strain component increments, and the increments are used to

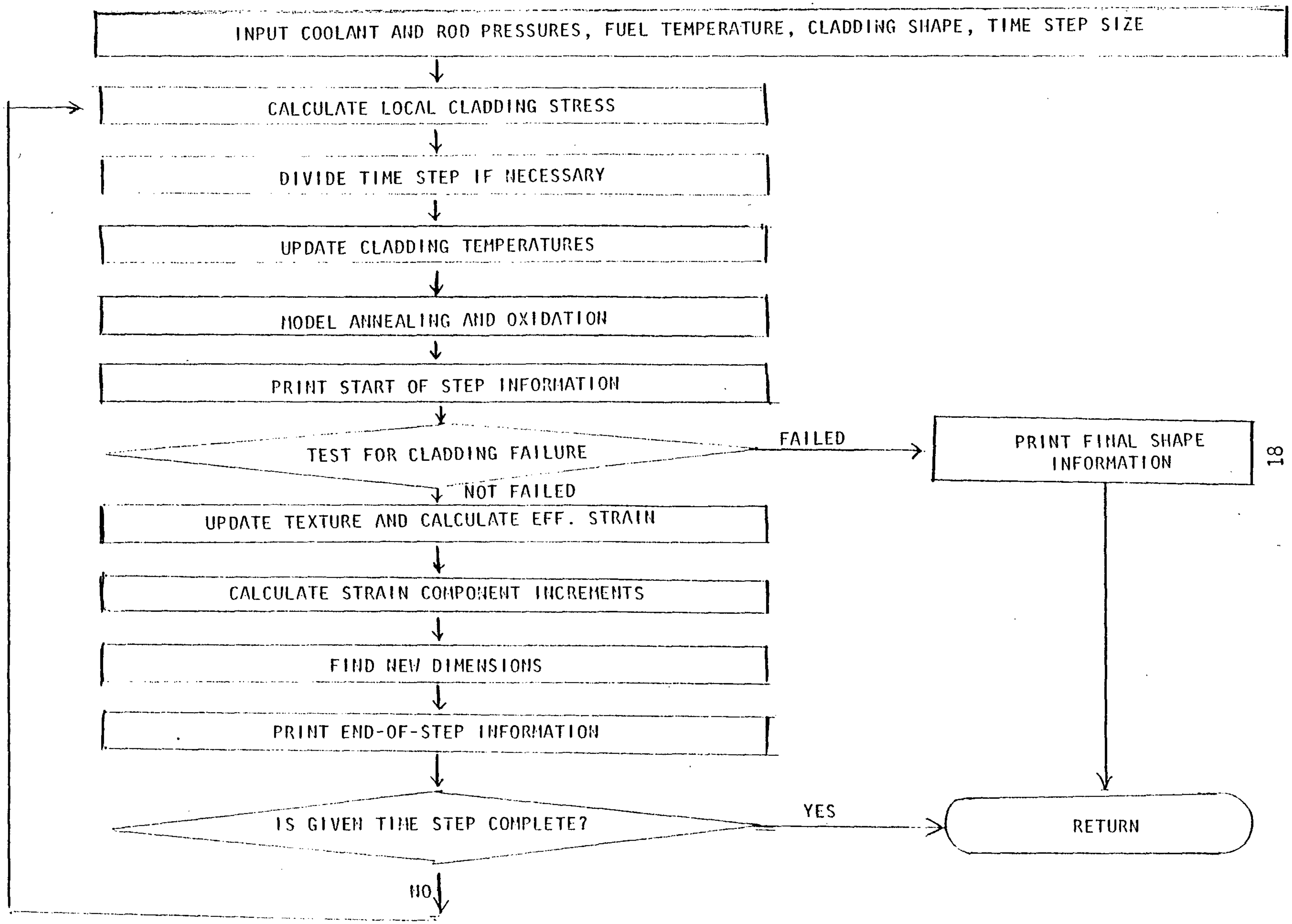

Figure 2. Sequence of model calculations.

calculate new dimensions at the end of the time step under the assumption that local stress and temperatures are constant during the time step. Requested end-of-step information is printed and a check is made to see if deformation for all of the given time step has been calculated. If it has, control is returned to the driving program and the next time step is considered. If it has not, the remaining part of the given time step is input and the process beginning with the calculation of local stress is repeated. The following sections describe details of the calculations mentioned in Figure 2.

Calculation of Local Stress in the Cladding

The internal rod gas pressure, the external coolant pressure, cladding shape, forces from the fuel pellets and forces from the spacer grids all contribute to local cladding stresses. It is assumed in this model that the cladding experiences only an axial constraint force from the grids or fuel stack. The constraint force is an input parameter.

The effect of pressure and shape changes is discussed in more detail below. First, a thin-wall approximation is used to find the principal stress components in a right circular cylinder. The thin wall approximation is based on the expressions for tangential and radial stress in a thick walled cylinder.[22] The expressions used for the thick walled cylinder are

$$\sigma_{\theta\theta} = \frac{P_i\left(c^2 + \frac{c^2b^2}{r^2}\right) - P_o\left(\frac{c^2b^2}{r^2} + b^2\right)}{b^2 - c^2} \tag{5}$$

$$\sigma_{rr} = \frac{P_i\left(c^2 - \frac{c^2b^2}{r^2}\right) + P_o\left(\frac{c^2b^2}{r^2} - b^2\right)}{b^2 - c^2} \tag{6}$$

where

$\sigma_{\theta\theta}$ = tangential component of stress

σ_{rr} = radial component of stress

P_o = pressure of fluid outside the cylinder

P_i = pressure of fluid inside the cylinder

c = inner radius of the cylinder

b = outer radius of the cylinder.

The thin-wall expression used for the radial stress is obtained by replacing $\frac{1}{r^2}$ by its average value across the wall of the cylinder,

$$\frac{1}{b - c} \int_c^b \frac{1}{r^2}\, dr = \frac{1}{cb} \quad . \tag{7}$$

Thus,

$$\sigma_{rr} \approx - \frac{P_o b + P_i c}{b + c} \quad . \tag{8}$$

In order to derive a thin wall expression for $\sigma_{\theta\theta}$ that is compatable with the perturbation theory to be introduced shortly for a noncylindrical shape, the variables

$$h_{cyl} = b\text{-}c \tag{9}$$

and

$$a = \frac{b + c}{2} \tag{10}$$

are substituted into Equation (5) and the resultant equation is expressed in powers of wall thickness, h_{cyl}.

$$\sigma_{\theta\theta} = \frac{P_i \left\{ a^2 \left[1 + \frac{a^2}{r^2} \right] - h_{cyl} \left[a\left(1 + \frac{a^2}{r^2}\right) - \frac{a^3}{r^2} \right] + \text{higher powers of } h_{cyl} \right\}}{2\, a\, h_{cyl}}$$

$$\frac{-P_o \left\{ a^2 \left[1 + \frac{a^2}{r^2} \right] + h_{cyl} \left[a\left(1 + \frac{a^2}{r^2}\right) - \frac{a^3}{r^2} \right] + \text{higher powers of } h_{cyl} \right\}}{2\, a\, h_{cyl}} \tag{11}$$

The quantity $\frac{1}{r^2}$ in Equation (11) is again replaced by its average value over the wall of the cylinder [see Equation (7)] to obtain

$$\sigma_{\theta\theta} \approx (P_i - P_o) \frac{a}{h_{cyl}} - \frac{P_i + P_o}{2} \tag{12}$$

to order $\left(\frac{h_{cyl}}{a}\right)^0$. The second term is frequently dropped but is kept in this case in order to have zero effective stress[a] for isotropic cladding with $P_i = P_o$.

The expression used for the axial stress, σ_{zz}, is the net axial force for a closed cylindrical tube divided by the cross sectional area of cladding:

---

a. The effective stress is given by Equation (25).

$$\sigma_{zz} = \frac{\pi P_i c^2 - \pi P_o b^2 + F_z}{\pi (c^2 - b^2)} \tag{13}$$

where

σ_{zz} = axial component of stress

F_z = additional axial force applied by any constraints.

When the snape of the cladding departs from a right circular cylinder, the stresses change significantly. A perturbation theory developed by *Kramer and Deitrich*[23] *is used to approximate the effect of shape on* stress. The derivation of the expression for the effect of shape change on stress is summarized in Appendix C. It is shown that to first order in $\frac{\delta}{a}$ the σ_{zz} and σ_{rr} components do not change while the $\sigma_{\theta\theta}$ component changes by

$$\sigma_{\delta}{}^{1}{}_{1} \approx \frac{\Delta P \delta}{h_{cyl}} - \frac{a\ \Delta P h_{\delta}}{h_{cyl}^2} + \frac{\Delta P}{h_{cyl}} \frac{\partial^2 \delta}{\partial \theta_o^2} + \frac{\sigma_{zz}}{\lambda^2} a \frac{\partial^2 \delta}{\partial z_o^2} \tag{14}$$

where

$\sigma_{\delta}{}^{1}{}_{1}$ = change in $\sigma_{\theta\theta}$ due to departure of the cladding shape from a right circular cylinder

ΔP = $P_i - P_o$

δ = local perturbation of the cladding midwall radius (radius - average radius)

h_{δ} = local perturbation of the cladding wall thickness (wall thickness - average wall thickness)

a = average radius

θ_o, z_o

= coordinates that material particle occupied before deformation

λ = exponent of the average true axial strain component of the cylinder, $\exp(\varepsilon_z)$.

The four terms of the right hand side of Equation (14) can be given sound physical interpretations. The first two terms represent the effect of local changes in radius and wall thickness, while the second two terms are the contributions due to local changes in the radii of curvature.

Figure 3 is a schematic illustration of the effect of the fourth term of Equation (14) on a ballooned section of cladding. In the center region the hoop stress is reduced because

$$\frac{\partial^2 \delta}{\partial z_o^2} \left(\text{which is equal to } \frac{\partial^2 r}{\partial z_o^2} \right)$$

is negative. The curvature of the cladding allows σ_{zz} to exert a force on the bulged section which pulls with the force exerted by $\sigma_{\theta\theta}$ against the internal pressure, P_i. At the ends of the bulged region

$$\frac{\partial^2 \delta}{\partial z_o^2}$$

is positive. In this region σ_{zz} exerts a force which pulls with the internal pressure against the restraining force exerted by $\sigma_{\theta\theta}$. A larger $\sigma_{\theta\theta}$ is thus required to hold the internal pressure at the ends of the ballooned regions. The fourth term of Equation (14) is thus the term which describes the axial propagation of ballooned regions.

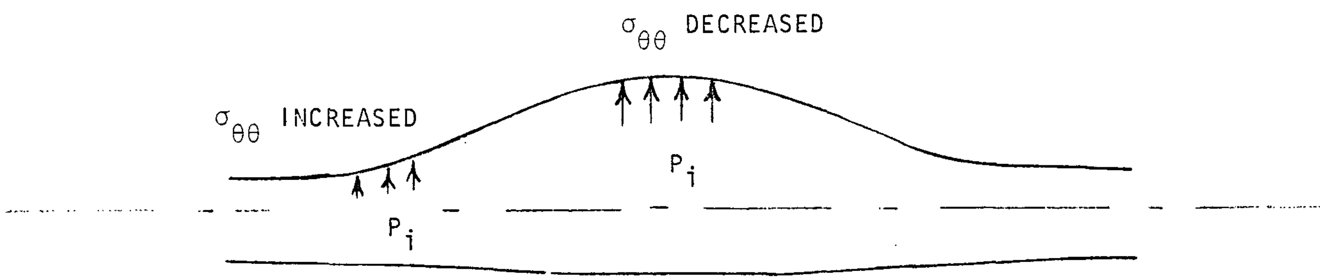

Figure 3. Effect of $\sigma_{zz} \frac{d^2\delta}{dz_o^2}$ term.

Figure 4 is a schematic illustration of the effect of the third term of Equation (15) on a ballooned section of cladding. In the bulged section,

$$\frac{\partial^2 \delta}{\partial \theta_o^2} \left(\text{which is equal to } \frac{\partial^2 r}{\partial \theta_o^2} \right)$$

is negative. The small local radius of curvature allows the force exerted by $\sigma_{\theta\theta}$ to act at a relatively acute angle to P_i and thus counter the force exerted by P_i with a smaller $\sigma_{\theta\theta}$. At the ends of the local bulge,

$$\frac{\partial^2 \delta}{\partial \theta_o^2} \text{ is positive } \left(\frac{\partial^2 \delta}{\partial \theta_o^2} = 0 \text{ for a circle} \right).$$

In this region, $\sigma_{\theta\theta}$ acts more nearly at right angles to P_i, and a large $\sigma_{\theta\theta}$ is required to have a sufficiently large force to oppose the normal force exerted by P_i. The third term of Equation (14) is thus the term which tends to propagate local bulges around the circumference to form a circular cross section.

Since all four terms of Equation (14) act simultaneously, determining which term will dominate for a given deformation is difficult. The problem is complicated further by the interactions between heat sources, heat sinks, cladding shape, cladding temperatures and cladding strength.

Check for Sufficiently Small Time Step Size

Once the local stress is known, it is possible to test the given time step to see if it is sufficiently small to prevent significant change in the local stress during the time step. The test begins with a comparison of the tangential stress at each node with the cladding strength coefficient times the strain raised to the strain hardening exponent. If

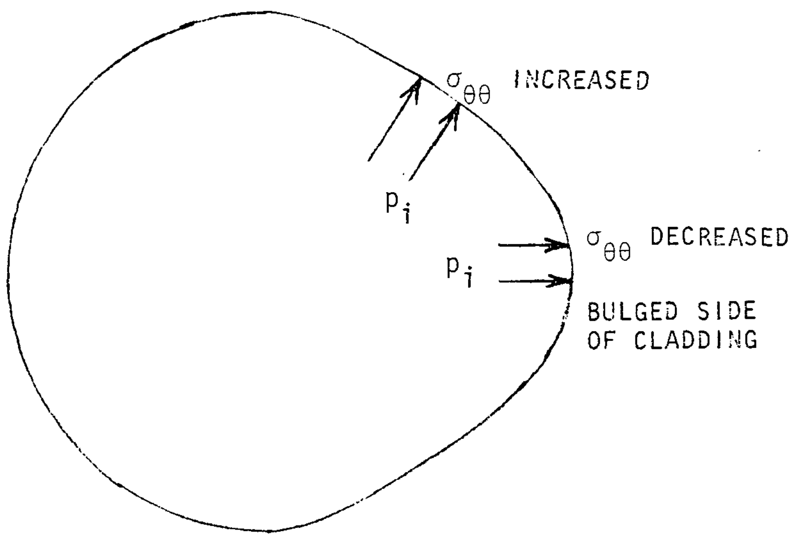

Figure 4. Effect of $\dfrac{\Delta P}{h_{cyl}} \dfrac{\partial^2 r}{\partial \theta_0^2}$ term.

the tangential stress is less than this product, the given time step size is adopted. For tangential stresses greater than the product, the maximum allowed time step interval is determined with the relation

$$\Delta t = \left(\frac{\varepsilon_{\theta\theta}^{h} K}{\sigma_{\theta\theta}} \right)^{\frac{1}{m}} 10 \qquad (15)$$

where

Δt = maximum allowed time step interval

K = cladding strength coefficient

m = cladding strain rate sensitivity exponent

n = cladding strain hardening exponent

$\varepsilon_{\theta\theta}$ = tangential component of strain at start of step.

Equation (15) results from a Taylor series approximation used with the MATPRO equation of state for zircaloy plastic deformation and the requirement that the strain increment be limited to no more than 0.01. The form of the equation of state used is

$$\varepsilon_f = \left[\left(\frac{n}{m} + 1 \right) 10^{-3} \left(\frac{\sigma}{K} \right)^{\frac{1}{m}} \Delta t + \varepsilon_i^{\left(\frac{n}{m} + 1 \right)} \right]^{\frac{m}{n + m}} \qquad (16)$$

where

ε_f = effective strain at the end of the time interval

ε_i = effective strain at the start of the time interval

σ = effective stress during the time interval

and the other variables have been defined previously. Using the Taylor series approximation for a small time interval, Equation (16) can be rewritten as

$$\varepsilon_f \approx \varepsilon_i \left[1 + \frac{10^{-3} \left(\frac{\sigma}{K}\right)^{\frac{1}{m}} \Delta t}{\varepsilon_i^{\frac{(n+m)}{m}}} + \cdots\cdots \right] . \tag{17}$$

Solution of Equation (17) for Δt yields

$$\Delta t \approx 10^3 \left(\varepsilon_i^h \frac{K}{\sigma}\right)^{\frac{1}{m}} (\varepsilon_f - \varepsilon_i) . \tag{18}$$

Substitution of $\varepsilon_f - \varepsilon_i = 0.01$ and approximation of the effective stress and strain with the tangential components converts Equation (18) to Equation (15), the expression used for calculating the maximum allowed time interval, Δt.[a] If the given time step is greater than Δt, it is replaced by Δt and the given time step less Δt is resubmitted as a subsequent given time step when the calculation with Δt is complete.

---

a. For temperatures in the alpha and beta phase region, the Δt given by Equation (15) is increased by a factor of five because experience showed too many time steps were being used without this adjustment.

Update of Cladding Temperatures

After the time step size is determined, the cladding temperature can be calculated. There are several options that can be used to calculate the cladding temperature:

1. Assume constant fuel surface heat flux

2. Assume constant fuel surface temperature

3. Interpolate cladding temperatures from tables of measured values

4. Assume cladding temperatures are constant for the length of the given time step [which can be much longer than the time step determined with Equation (18)].

In the FORTRAN listing of BALON2 in Appendix B, the input MODE variable is used to select one of these options. A value of 0 for MODE causes a constant fuel surface heat flux assumption to be used while MODE = 1 causes use of a constant fuel surface temperature assumption. If MODE = 2, temperatures and pressures are interpolated from tables of data that are read in at the start of a problem. If MODE = 3, the input temperatures are used for the duration of the input time step. The MODE = 0 and MODE = 1 options will be discussed in more detail in the remainder of this section.

The equation used to calculate cladding surface temperatures for the constant fuel surface heat flux assumption (MODE = 0) is

$$T_c = T_{c_o} \exp\left(\frac{h_s \Delta t}{\rho C_p h}\right) + \frac{q\, r_f + h_s r_{cl}\, T_s}{h_s r_{cl}} \left[1 - \exp\left(\frac{h_s \Delta t}{\rho C_p h}\right)\right] \tag{19}$$

where

T_c = cladding temperature after time interval Δt

T_{c_o} = cladding temperature at the start of the time interval

h_s = cladding surface heat transfer coefficient

ρ = cladding density

C_p = cladding specific heat capacity

h = cladding wall thickness

$\dot{q}$ = fuel surface heat flux

r_f = fuel surface radius

r_{cl} = cladding midwall thickness

T_s = steam temperature.

Equation (19) is derived by equating the rate of heat loss from the fuel surface to the rate energy is retained in the cladding plus the rate of heat loss from the cladding surface to steam:

$$\dot{q}\, r_f = \left[c_p\, \rho h \frac{dT_c}{dt} + h_s\, (T_c - T_s)\right] r_{cl}\ . \qquad (20)$$

Solution of this equation for the time-dependent cladding temperature with all other quantities assumed constant yields Equation (19). Radiative heat transfer from fuel to cladding or cladding to shroud is not considered in this formulation.

The equation used to calculate cladding surface temperatures for the constant fuel surface temperature assumption (MODE = 1) is

$$T_c = \left[h_g\, T_f + h_s T_s + \frac{C_p\, \rho h}{\Delta t}\, T_{c_o} + e_f \sigma \left(T_f + T_{c_o}\right)\left(T_f^2 + T_{c_o}^2\right) T_f + e_s \sigma \left(T_{c_o} + T_{sh}\right)\left(T_{c_o}^2 + T_{sh}^2\right) T_{sh} \right] \Big/ \left[h_g + h_s + \frac{C_p \rho h}{\Delta t} + e_f \sigma \left(T_f + T_{c_o}\right)\left(T_f^2 + T_{c_o}^2\right) + e_s \sigma \left(T_{c_o} + T_{sh}\right)\left(T_{c_o}^2 + T_{sh}^2\right) \right] \tag{21}$$

where

h_g = gas gap heat transfer coefficient

T_f = fuel or heater element surface temperature

e_f = effective emissivity of the combined fuel and cladding inner surfaces

σ = Stefan's constant

= 5.67×10^{-8} w/m$^2 \cdot$ K^4

e_s = effective emissivity of the combined cladding outer and shroud inner surfaces

T_{sh} = shroud surface temperature.

This equation is derived with an energy balance like Equation (20) but with the different assumption that fuel surface temperature rather than fuel heat flux is approximately constant during the given time step [note that the given time step size may have been reduced considerably due to the limit set by Equation (15) to arrive at Δt, the time step size used in Equations (19) and (21)].

Equation (21) is derived by equating the rate at which heat is supplied to the cladding by convection and radiation to the rate that energy is retained in the cladding plus the rates of heat loss to surrounding steam by convection and a shroud by radiative heat exchange:

$$h_g(T_f - T_c) + e_f\sigma \left(T_f^4 - T_c^4\right) = C_p\rho h \frac{\left(T_c - T_{c_o}\right)}{\Delta t}$$

$$+ h_s \left(T_c - T_s\right) + e_s\sigma \left(T_c^4 - T_{sh}^4\right) \quad . \tag{22}$$

Next, the approximations

$$T_f^4 - T_c^4 \approx (T_f - T_c) \left(T_f + T_{c_o}\right) \left(T_f^2 + T_{c_o}^2\right) \tag{23}$$

and

$$T_c^4 - T_{sh}^4 \approx \left(T_c - T_{sh}\right) \left(T_{c_o} + T_{sh}\right) \left(T_{c_o}^2 + T_{sh}^2\right) \tag{24}$$

are employed to convert Equation (24) to a linear equation. The resultant expression is solved for T_c.

Equations (19) and (21) have both been included because they bracket the usual behavior of a ballooned fuel rod where the heat flux decreases and fuel surface temperature increases as the gas gap resistance increases.

Calculation of Strain Component Increments

With stress, an acceptable time step size, and cladding temperature known, calculation of strain component increments is possible. The effective stress which is needed for the equation of state for zircaloy plastic deformation is calculated with the equation

$$\sigma_e = \left[A1S\ (\sigma_{\theta\theta} - \sigma_{zz})^2 + A2S\ (\sigma_{zz} - \sigma_{rr})^2 + A3S\ (\sigma_{rr} - \sigma_{\theta\theta})^2 \right]^{\frac{1}{2}} \tag{25}$$

where

σ_e = effective stress

A1S, A2S, A3S = coefficients of anisotropy (provided by the MATPRO model CANISO).

The effective strain at the end of a time step interval is obtained with the integral form of the equation of state for plastic deformation used in the MATPRO package,[a] Equation (16). Finally strain component increments during the time step are obtained from the Prandtl-Reuss flow rule[18]:

$$d\varepsilon_{\theta\theta} = \frac{d\varepsilon}{\sigma_e} \left[\sigma_{\theta\theta}\ (A1E + A3E) - \sigma_{zz} A1E - \sigma_{rr} A3E\right] \tag{26}$$

$$d\varepsilon_{zz} = \frac{d\varepsilon}{\sigma_e} \left[-\sigma_{\theta\theta} A1E + \sigma_{zz}\ (A2E + A1E) - \sigma_{rr} A2E\right] \tag{27}$$

$$d\varepsilon_{rr} = \frac{d\varepsilon}{\sigma_e} \left[-\sigma_{\theta\theta}\ A3E - \sigma_{zz}\ A2E + \sigma_{rr} (A3E + A2E)\right] \tag{28}$$

where

$d\varepsilon_{\theta\theta}$, $d\varepsilon_{zz}$, $d\varepsilon_{rr}$ = true strain increments in the θ, z and r directions, respectively.

---

a. This form of the equation of state is used by the CSTRNI model.

$d\varepsilon$ = $\varepsilon_f - \varepsilon_i$

A1E, A2E, A3E = coefficients of anisotropy (provided by the MATPRO model CANISO in the FORTRAN program of Appendix B).

Estimation of Cladding Dimensions at the End of the Time Step

Equations (26) to (28) are sufficient to calculate cladding circumference, wall thickness and length change but not the cladding midwall radii. Figure 5 illustrates one of the two additional global considerations required to find the radii--the effect of the relative deformations of all parts of the cladding circumference. The top cross section in Figure 5 represents the deformation of the most rapidly deforming segment of the cladding circumference as it probably happens. There is some tangential component to the displacement and the stiffer, less rapidly deforming segments merely move outword with minimal increase in circumference. The middle cross section of the figure illustrates a pure radial displacement which would be expected by symmetry if all segments were equally stiff. The radial displacement is frequently assumed for simplicity[18,23] and was tried during the development of this model. The assumption was found to be invalid and abandoned in favor of the approximation shown at the bottom of the figure, namely that the tangential component of the cladding displacement is sufficient to maintain a nearly circular cross section. The key observations in favor of the circular cross section assumption are (a) the third term of the local stress expression, Equation (14), causes cross sections to tend to be circular (see Figure 4) and (b) the circular cross section assumption is more consistent with the circular cross section assumption made during the derivation of the failure stress. Calculations using the radial displacement assumption did not match data unless the failure stress was reduced by a factor of 0.6. This was not believed to be realistic.

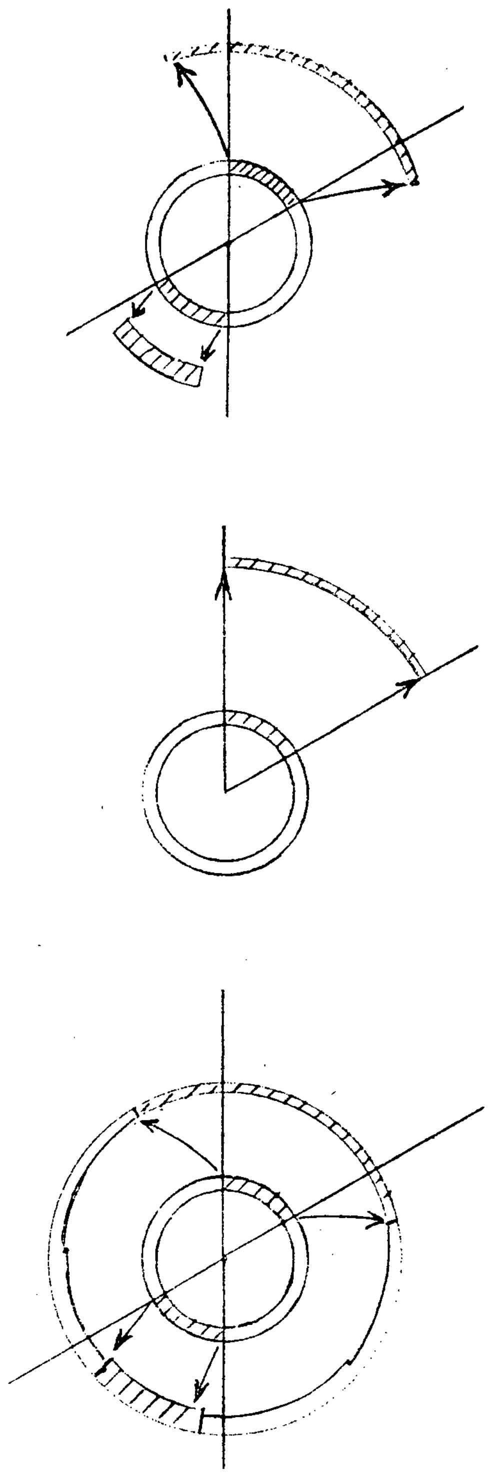

Figure 5. Effect of relative deformation of all segments of the cladding circumference.

The second global consideration required before one can predict the midwall radii of the deforming cladding is the effect of bending due to different changes in cladding length as the ballooning proceeds. The expression used for bending at the K-th axial node through the J and $\frac{NJ}{2}$ - th circumferential nodes is

$$dX = \left[\frac{ZBEND^2}{8\ r_o \left\{\exp\left[\varepsilon_{\theta\theta}(K,J)\right] + \exp\left[\varepsilon_{\theta\theta}\left(K,J+\frac{NJ}{2}\right)\right]\right\}}\right] \left[\frac{d\varepsilon_{zz}\left(K,J+\frac{NJ}{2}\right) - d\varepsilon_{zz}(K,J) - \left[\varepsilon_{zz}\left(K,J+\frac{NJ}{2}\right) - \varepsilon_{zz}(K,J)\right]}{\left[\frac{d\varepsilon_{\theta\theta}(K,J) + d\varepsilon_{\theta\theta}\left(K,J+\frac{NJ}{2}\right)}{2}\right]}\right] \quad (29)$$

where

dX	=	decrease in the midwall radius of the surface element at the K-th axial and J-th circumferential node caused by the incremental strains $d\varepsilon_{zz}$ and $d\varepsilon_{\theta\theta}$
ZBEND	=	average length contributing to the bending
r_o	=	radius of the undeformed cladding.

The derivation of this equation is given in Appendix D.

An important limitation of the bending model is the assumption that length changes at each node around the circumference are independent of local stresses caused by length changes at neighboring nodes. The assumption causes the calculation of unrealistically large variations of bending displacements from node to node around the cladding circumference. Experience with the model has shown that this undesireable feature is avoided by averaging the midwall radius of each circumferential node with its two neighbors when the bending model is used.

Because of the highly simplified nature of the bending model that results in Equation (29), the model is used only up to the time the deforming cladding contacts the fuel (typically ∿1% circumferential elongation). The model thus serves to estimate the most important effect of bending, the local heating due to fuel-cladding contact, but is not used for large strains where the approximations made in the derivation of Equation (29) do not justify use of the model.

Figure 6 illustrates the way that the circular cross section and bending models are combined to determine cladding midwall radii prior to cladding heater contact. The smaller circle represents the fuel and the larger circle represents the deformed cladding. After the radius of each node is increased by a factor equal to the exponent of the tangential strain increment for the node, the bending is calculated with Equation (29). The minimum radius, $\overline{CM}$, at each axial position is then identified. The displacement distance, $\overline{DC}$, is the average radius of the cladding (circumference calculated from $\varepsilon_{\theta\theta}$ values divided by 2π) minus $\overline{CM}$. Once $\overline{DR}$, the average radius, and $\overline{DC}$ are known the midwall radius at an angle θ to the minimum radius is given by

$$\overline{CR} = \left(\overline{DR}^2 - \sin^2\theta\ \overline{DC}^2\right)^{1/2} - \cos\theta\ \overline{DC} \quad . \tag{30}$$

The expression is derived by using the Pythagorean theorem on a right triangle whose hypotenuse is the line $\overline{DR}$ and one leg of which is the constructed line $\overline{CR}$ sin θ.

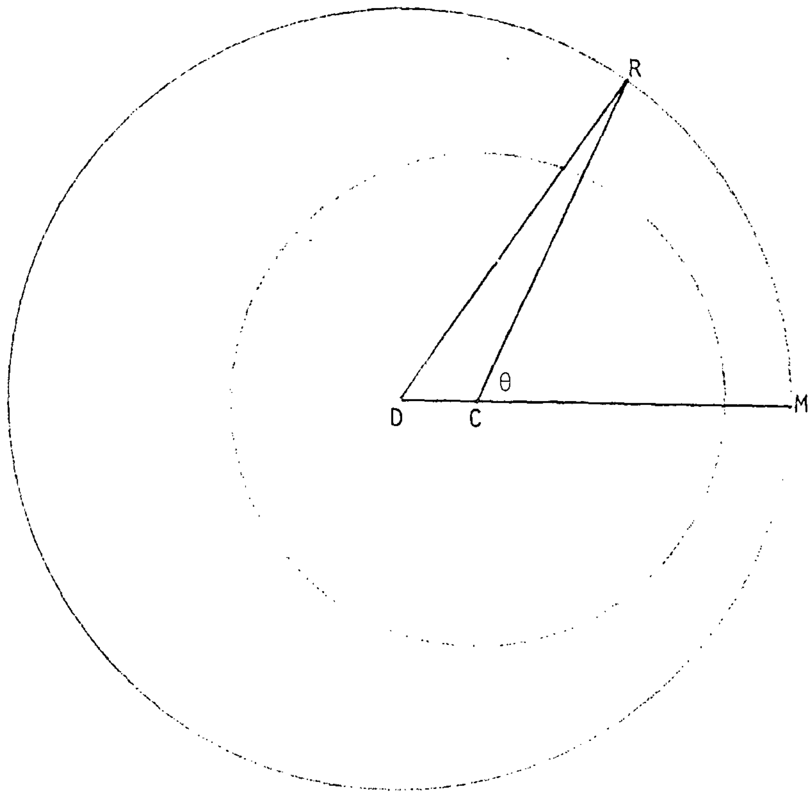

Figure 6. Use of circular cross section and bending models to determine cladding midwall radii.

Once contact between the fuel and cladding has occurred at some orientation, the bending model is inactive. The cladding and fuel are assumed to remain tangent at their initial point of contact.

With midwall radii calculated for each node, the remainder of the cladding shape information can be calculated using the definition and values of axial and radial strain.

$$h = h_o \exp(\varepsilon_{rr}) \tag{31}$$

$$\Delta Z = \Delta Z_o \exp(\varepsilon_{zz}) \tag{32}$$

where

h_o = initial cladding thickness

ΔZ = length of a given axial node

ΔZ_o = initial length of the given axial node.

PARAMETRIC STUDIES AND COMPARISON WITH DATA

This section presents several illustrations of the use of the BALON2 model to understand how various parameters contribute to cladding shape at failure. The main conclusion is that the parameters traditionally used to describe cladding shape interact. That is, burst temperature, heating rates, pressure history, circumferential temperature variations and axial temperature variations affect cladding shape at failure and each of these parameters can affect the others. A second conclusion is that the relatively simple concept of failure caused by true stress exceeding a failure stress (which is primarily a function of temperature) is the most useful guide to understanding cladding shape at failure.

Figure 7 shows the model-predicted effect of variations in the linear heating rate of an internal heater. For the nine analyses shown, a constant pressure difference of 14.5 MPa was assumed. (The figure could look quite different with a different pressure difference.) The heater was assumed to have a 1% axial and a 1% circumferential hot spot. The large number shown next to each analysis is the cladding burst temperature and the small number is the circumferential temperature variation at failure.

As shown in Figure 7, the total circumferential elongation decreases significantly with increasing heating rate. However, the decrease may not be directly due to the heating rate because the increasing heating rate causes increased burst temperature and circumferential temperature variation which also contribute to reduced elongation. The increased burst temperature lowers the failure stress so that less deformation is required to reach the failure stress. The circumferential temperature variation tends to localize the strain at one part of the circumference.

The effect of heating rate is more clearly understood when attempts at correlating elongation with heating rate are abandoned in favor of plots of the true and failure stresses at the hot node versus time. Figures 8 and 9

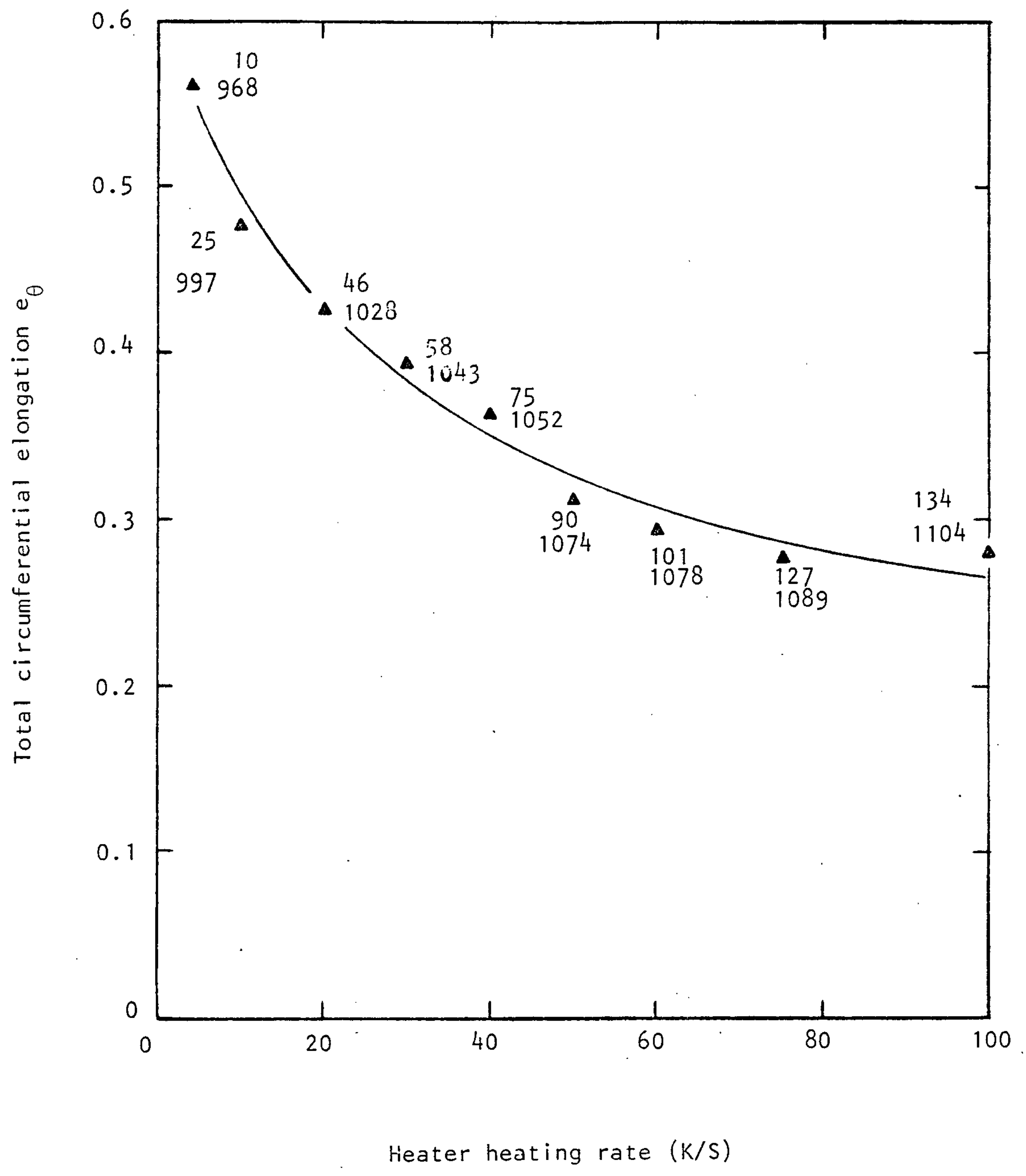

Figure 7. Effect of heating rate on total circumferential elongation.

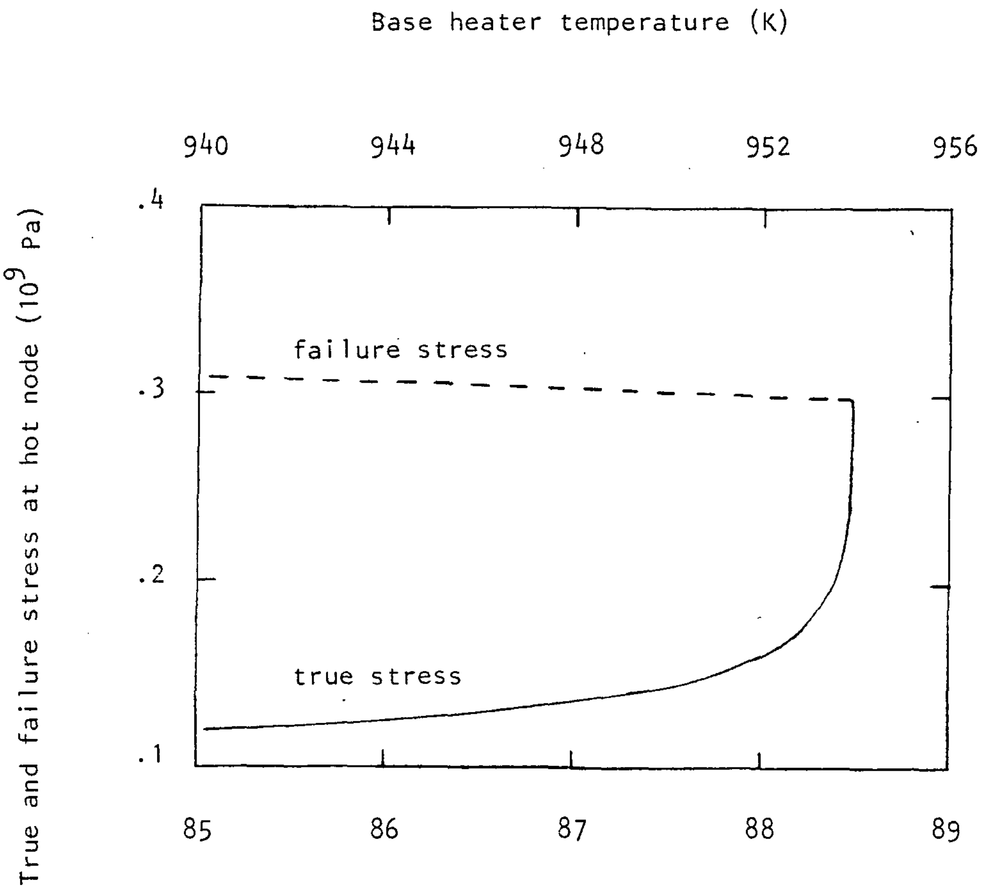

Figure 8. Hot node true and failure stresses for a heater heating rate of 4 K/s.

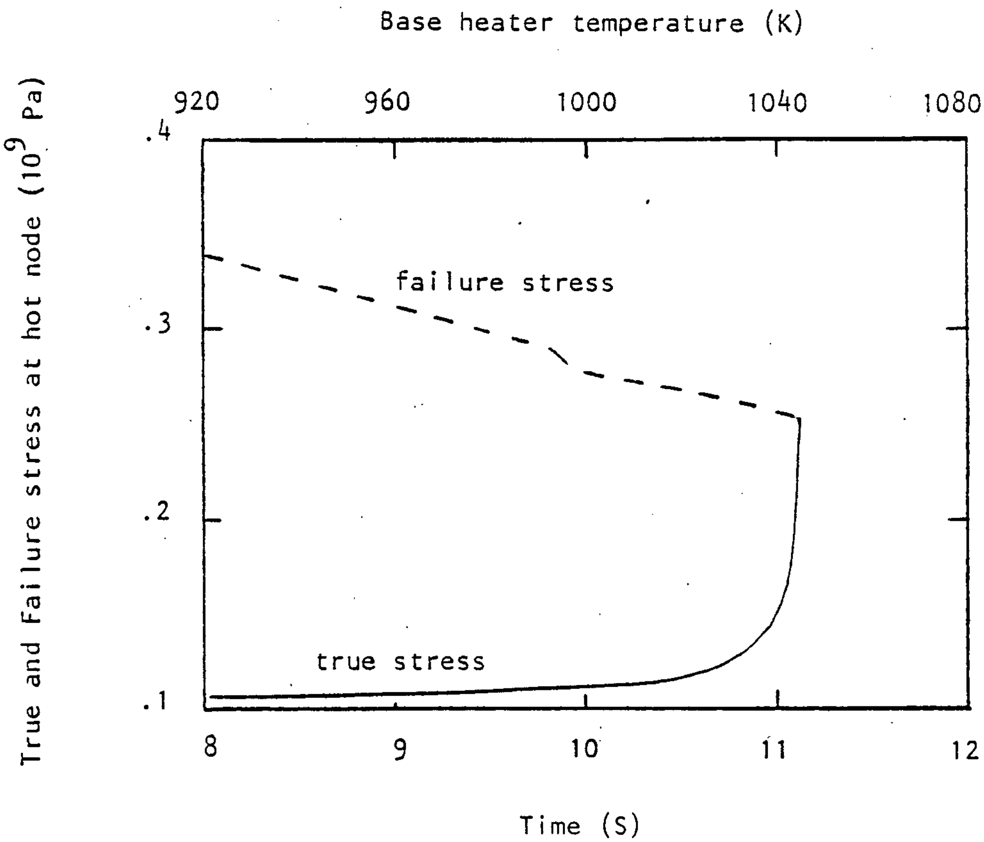

Figure 9. Hot node true and failure stresses for a heater heating rate of 40 K/s.

show these stresses for analyses using 4 K/s and 40 K/s heating rates, respectively. The two figures use equal stress and time scales but begin at much different times.

For the 4 K/s heating rate shown in Figure 8, the failure stress is nearly constant and the true stress increases over a period of several seconds to intersect the failure stress. Burst occurs in the mid 900 K temperature range where the failure stress is high because the cladding temperature remains in that range for the several seconds required for deformation to increase the local stress to the failure stress.

With the 40 K/s heating rate shown in Figure 9, the failure stress has a significant negative slope because of the rapid heating rate.[a] Deformation begins in the 900 K temperature range but is not sufficiently rapid to raise the local stress to the failure stress until a temperature near 1040 K is attained. At that temperature, the failure stress is significantly reduced so less deformation is required to raise the local stress to failure.

Close inspection of Figures 8 and 9 reveals a secondary effect of the heating rate. For equal temperatures the failure stress in Figure 9 is higher than that of Figure 8 and the deformation (rate of true stress increase) is lower in Figure 9 than that of Figure 8. Both differences are caused by the presence of some residual cold work strength in the cladding with the rapid heating rate.

---

a. The nonlinear portion of the failure stress curve near 10 seconds is caused by the nonlinear increase in cladding temperature as deformation begins and the cladding bends into the heater at the hot node. This decrease was not visable in Figure 8 because it occurred prior to 85 seconds.

If a rapid heatup rate can reduce the failure stress and thus require less deformation for failure, it is logical to expect a rapid internal gas pressurization rate (or a rapid decrease in external pressure) to increase local stress to failure with relatively little deformation. This effect is interesting because it has been ignored in most analyses of cladding burst shape and because the small gas volume near the expanding region of a full length fuel rod could lead to large deformations by causing lowered internal gas pressure as the rod deforms. The decreasing internal pressure would require more extensive deformation than a constant pressure test to increase the local stress to the failure stress.

Calculations for the effect of varying pressurization rates are shown in Figure 10. In the six analyses shown, temperature was increased at 100 K/s from 600 K to 1073 K and stopped while internal pressure was ramped at the rate shown in the figure. The decrease in circumferential elongation from 0.9 to 0.4 as the pressurization rate is increased from 0.1 MPa/s to 2 MPa/s shows that cladding shape is sensitive to pressure history.

Figure 11 shows the same trend using data reported by Busby and Marsh.[24] In four tests[a] with temperature held constant at 922 K and pressure increased at 0.09, 0.17 and 0.81 MPa/s, the calculated trend is confirmed.

Another important parameter for determining the cladding shape is the circumferential temperature variation, If the cladding has a hot spot, the deformation will be localized at the hot spot and the total circumferential elongation will be small. Figure 12 shows data from Chapman[2] and Wiehr[25] as well as lines representing a number of model calculations for heater heating rates of 4 K/s and 30 K/s. All of the bursts occurred in

---

a. Samples 8, 9, 24, and 23.

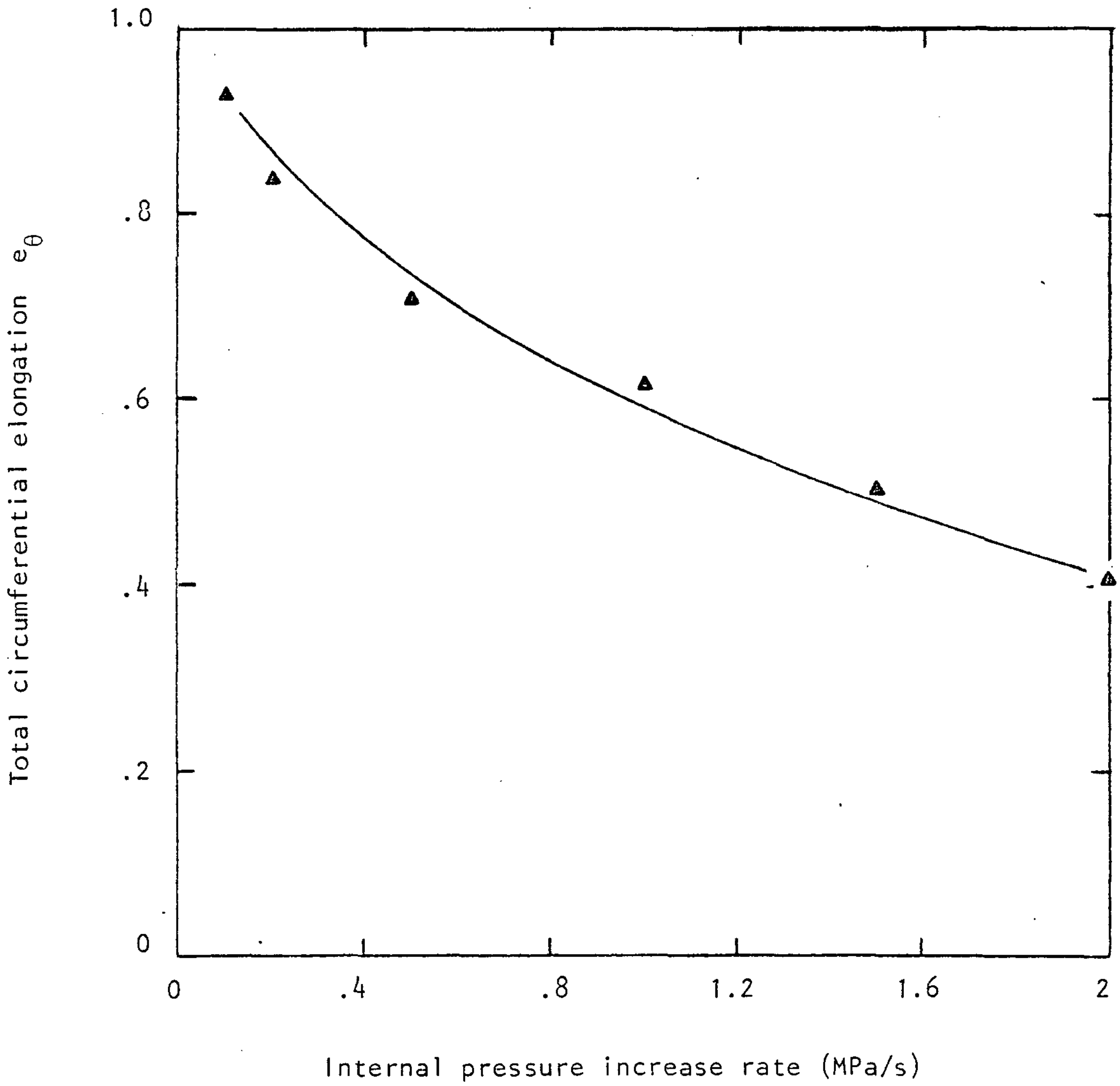

Figure 10. Model calculations for the effect of varying pressurization rates.

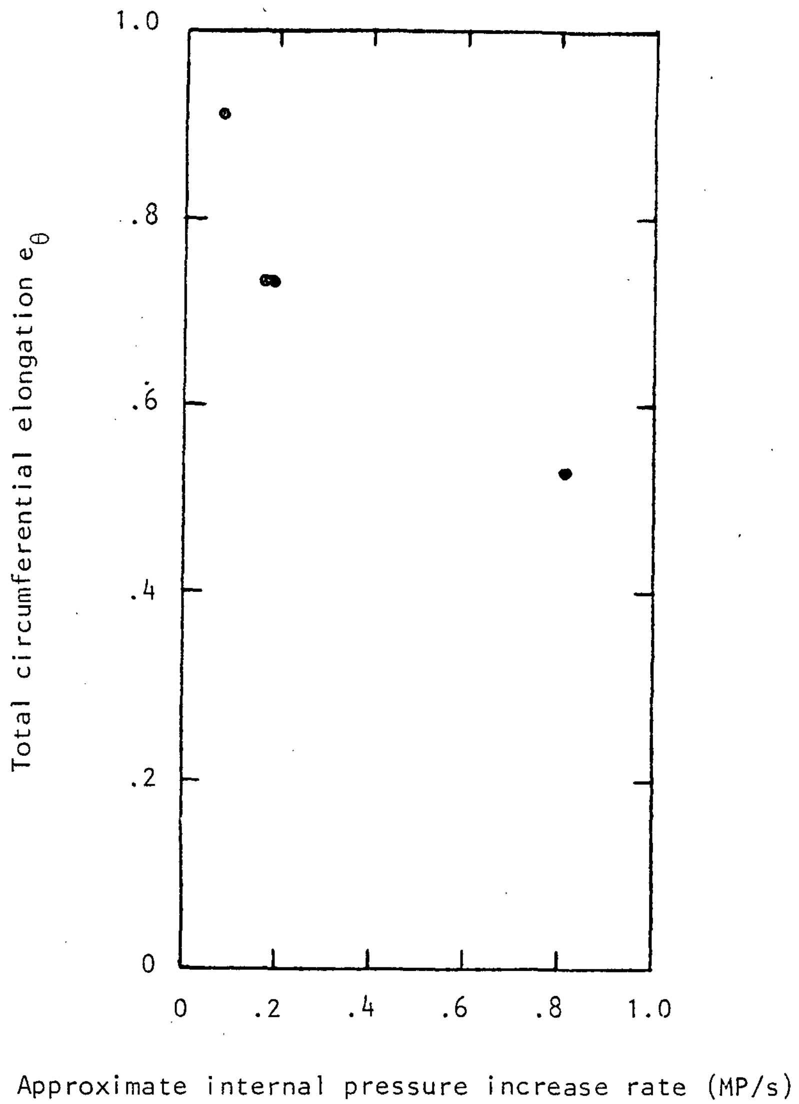

Figure 11. Tests by Busby and March showing the effect of increasing pressurization rates on total circumferential elongation.

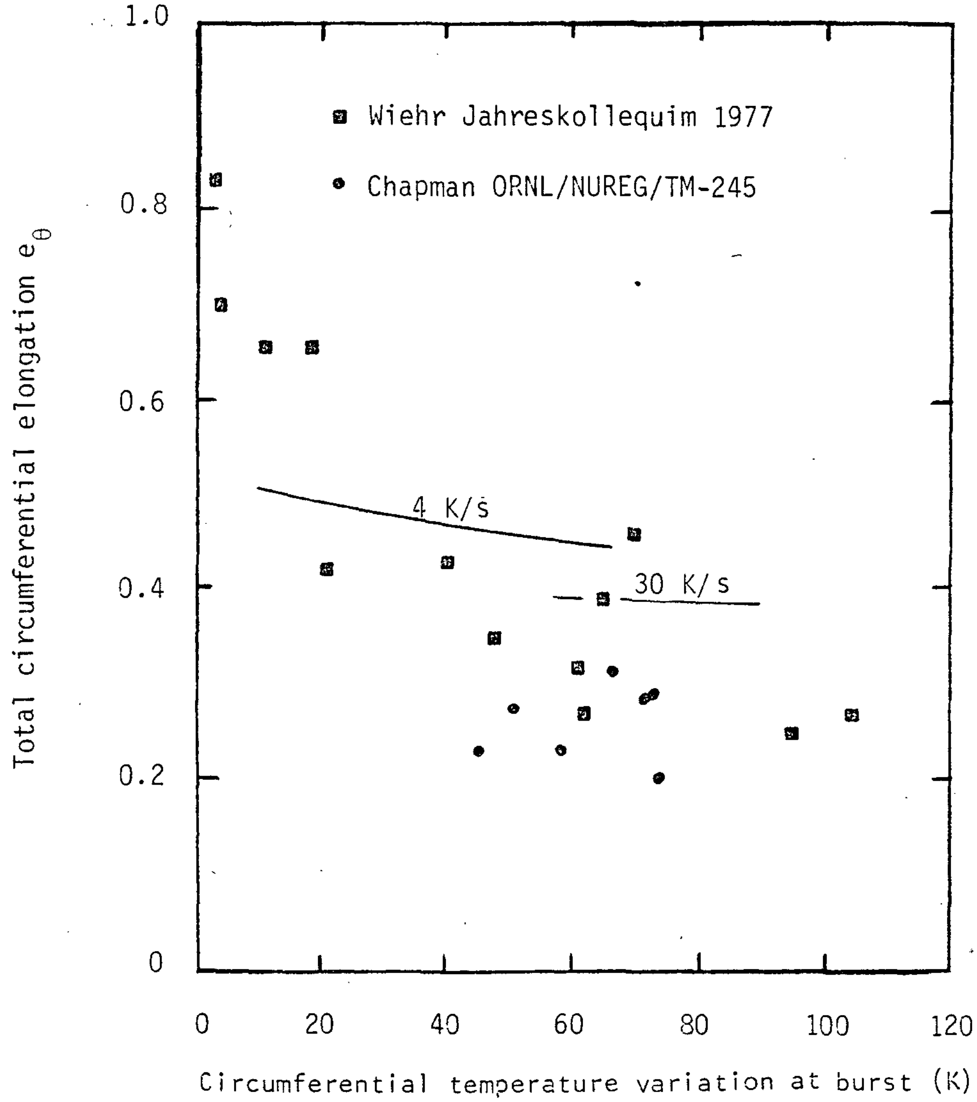

Figure 12. Total circumferential elongation versus circumferential temperature variation at burst and heating rate.

the high temperature alpha phase.[a] The data show considerable scatter because varying internal pressures and heating rates were used, but the trend of decreasing circumferential elongation with increasing circumferential temperature variation at burst is observable.

The calculations are from analyses with a constant pressure difference of 14.5 MPa and 1% axial and circumferential temperature variation (10 K) of the heater temperature. The calculated results not only agree with the trend of the data but also illustrate how heating rate and cladding circumferential temperature variation at burst can be coupled in the alpha phase of Zircaloy (temperature less than 1090 K). The left end of each line represents analyses with high temperature steam and hot shroud (825 K) while the right end represents low temperature steam and cool shroud (600 K). For the 30 K/s heating rate, cladding bending[b] and the cladding mass result in a temperature variation of at least 50 K. The cladding hot spot bends into the internal heat source and fails before the heat flux from the colder side of the heater (which must cross a wide gas gap) can raise the cladding temperature close to the hot-side temperature. For the 4 K/s heating rate, the hot spot does not fail before the cold side of the cladding can be heated across the gas gap. The circumferential variation of the cladding in the 4 K/s test is thus closer to the 10 K difference of the heater. Since the calculation shows both large elongations and small temperature variations are associated with slow heating rates, it is not possible to decide whether the slow heating rate or the small temperature variation is the main cause of the large elongations.

---

a. 950 to 1090 K.

b. The bending is caused by Zircaloy anisotrophy in the alpha phase which in turn causes a reduction in length which is proportional to the amount of deformation.

The final parameter mentioned at the beginning of this section is axial temperature variation. The mechanism for the effect of axial temperature variation was discussed during the interpretation of Equation (14) where it was noted that a positive

$$\frac{d^2r}{dZ^2}$$

term reduces the hoop stress. The reduced stress allows greater deformation to occur before the failure stress is attained. Since increasing axial temperature variations cause increasing values of

$$\frac{d^2r}{dZ^2},$$

increasing elongation with increasing axial temperature variation is expected.

Calculations of this effect are not shown because the simplified treatment of cladding bending used in the model assumes that the hot azimuthal node remains in contact with fuel at each axial node. This in turn causes

$$\frac{d^2r}{dZ^2}$$

to be zero for the hot azimuthal node and no effect is calculated. The expected relation between total circumferential elongation and axial temperature variation at failure was observed with an earlier version of the model which assumed radial displacement of the cladding. Since post-rupture shapes exhibit some displacement from the fuel surface, a moderate increase in elongation with increasing axial temperature gradients should be expected even though calculations with the model described here do not predict the trend.

It is useful to compare the results of the parametric study just discussed with recently proposed liscensing standards for determining cladding deformation for loss of coolant accident analysis.[26] The standards propose using a temperature versus engineering hoop stress and heating rate correlation devised by R. H. Chapman for a best estimate of burst time

$$T_R = 3960 - \frac{20.4\ S}{1 + H} - \frac{8,510,000\ S}{100\ (1 + H) + 2790\ S} \tag{33}$$

where

T_R = rupture temperature (°C)

S = engineering hoop stress (Kpsi)

H = 0 if the heating rate is less than 0

= 1 if the heating rate is greater than 28°C/s

= ratio of the heating rate to 28°C/s if the heating rate is in the range 0 to 28°C/s.

Once the burst temperature is determined from Equation (33), it is used with correlations for total circumferential elongation versus burst temperature. One correlation is supposed to bound the data for heating rates less than or equal to 10°C/s, and another is for heating rates greater than or equal to 25°C/s.

The parametric study discussed at the beginning of this section has already shown that burst temperature is only one of five parameters affecting burst shape. For large circumferential temperature variations, fast heating rates, small local axial temperature variations and increasing differential pressure across the cladding, the elongation correlations of Reference 26 significantly overestimate the circumferential elongation at failure calculated with the model. On the other hand, if circumferential temperature variations are small, heating rates are low or negative, local axial (pellet-to-pellet) temperature variations are large and the gas volume near the ballooning region is small, the correlations of Reference 26 will underestimate the elongation at failure calculated with the model. The arbitrary selection of burst temperature and fast or slow heating rates as shape parameters is restrictive and may not produce meaningful results. The model indicates that more reliable results could be expected by specifying approximate pressure-time and temperature-time tables with assumed typical temperature variations in the heat source. In case of concern about particular problems, more detailed analysis with the model could always be used to confirm the approximate results from the tables because the tables would be based on true stress-true strain considerations.

The procedure just recommended would eliminate the need for Equation (33) and the attendent problems of determining which of a continuously varying series of heating rates to use. However, the fact that Equation (33) is based on excellent data from the Multirod Burst Test (MRBT) program makes comparison useful. Figure 13 is a comparison of the MRBT correlation for heating rates faster than 28°C/s, the MRBT data for heating rates of 28°C/s[26] and several model analyses assuming constant pressure (therefore constant engineering stress) and a heater heating rate of 30°C/s. The model essentially reproduces the correlation as well as the data. The main discrepancy is a trend by the model to predict higher failure temperatures than the data. The probable reason for this discrepancy is the fact that the data report the hottest thermocouple reading, not necessarily the hottest region of the cladding. In the alpha phase region where the cladding bends into the heater at the hot spot, the model calculations show a highly localized hot spot at the point of contact. In the high temperature beta phase region where bending does not occur, the trend does not occur.

All of the MRBT data were taken with nearly constant pressure differentials across the cladding. Since in-reactor tests can involve changing cladding differential pressures due to changing coolant pressure

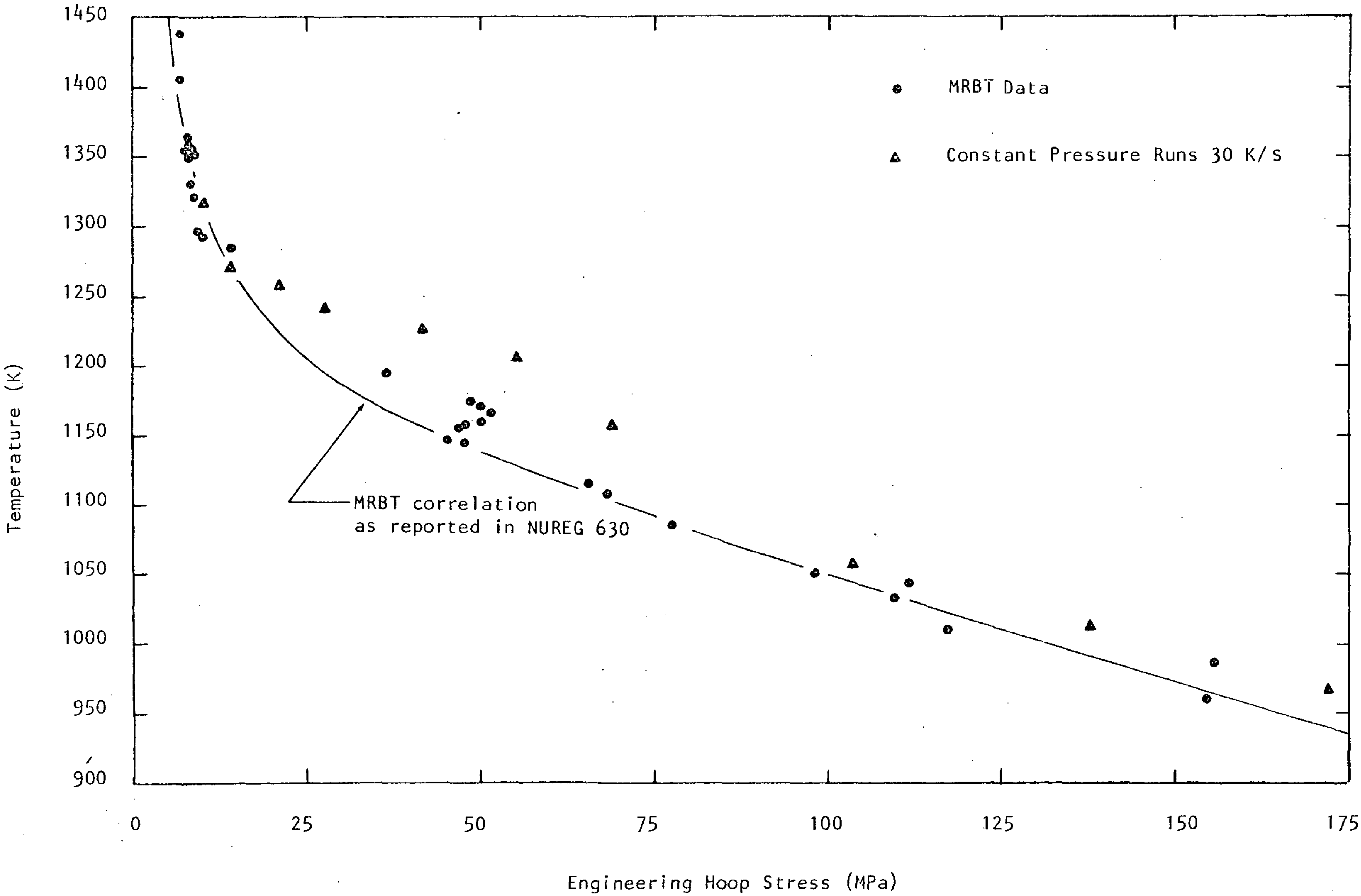

Figure 13. Comparison of MRBT data with constant pressure model calculations.

or increasing rod volume, several ramped pressure runs were compared with the MRBT correlations. Figure 14 illustrates the results. The three curves are the calculations using Equation (33) for heating rates of 28 K/s, 14 K/s and 0 K/s. The triangles represent the results of the constant pressure runs at the various heatup rates that were used to generate Figure 7. These results are in agreement with the MRBT correlation.[a] The squares represent the results of analyses with pressure ramped at 1 MPa/s and temperature ramped to a fixed value, then held constant. These burst points are significantly above and to the right of the 0 K/s line calculated for burst by the MRBT correlation.

Figure 15 compares the 0 K/s MRBT correlation to the 0 K/s data from Busby and Marsh.[24] The data fall above and to the right of the correlation line and the distance from the line increases as the pressurization rate (shown in MPa/s next to each result) increases. Interpretation of this trend is a direct application of the true stress failure criterion. Since failure occurs when the true stress equals the failure stress, the tests with higher pressurization rates achieve the failure stress with higher pressure and less deformation than tests with lower pressurization rates.

Figure 16 is an example of the most complete analysis attempted to date with the model for cladding shape at failure. MRBT test SR-37[2] was selected from a number of well documented tests. The information reported includes temperature versus time data from three groups of four thermocouples placed 90 degrees apart at distances of 18.7, 23.7, and 69.7 cm above the bottom of an internal heater. These data were used to input cladding temperatures for an analysis with the model. In addition,

---

a. The main disagreement is that the models predict no limit to the effect of heating rate at 28°C/s. Since few data are available with internal heat sources and heating rates greater than 28°C/s, it is suggested that removal of the 28°C/s limit based on the model results would improve the correlation of Equation (33).

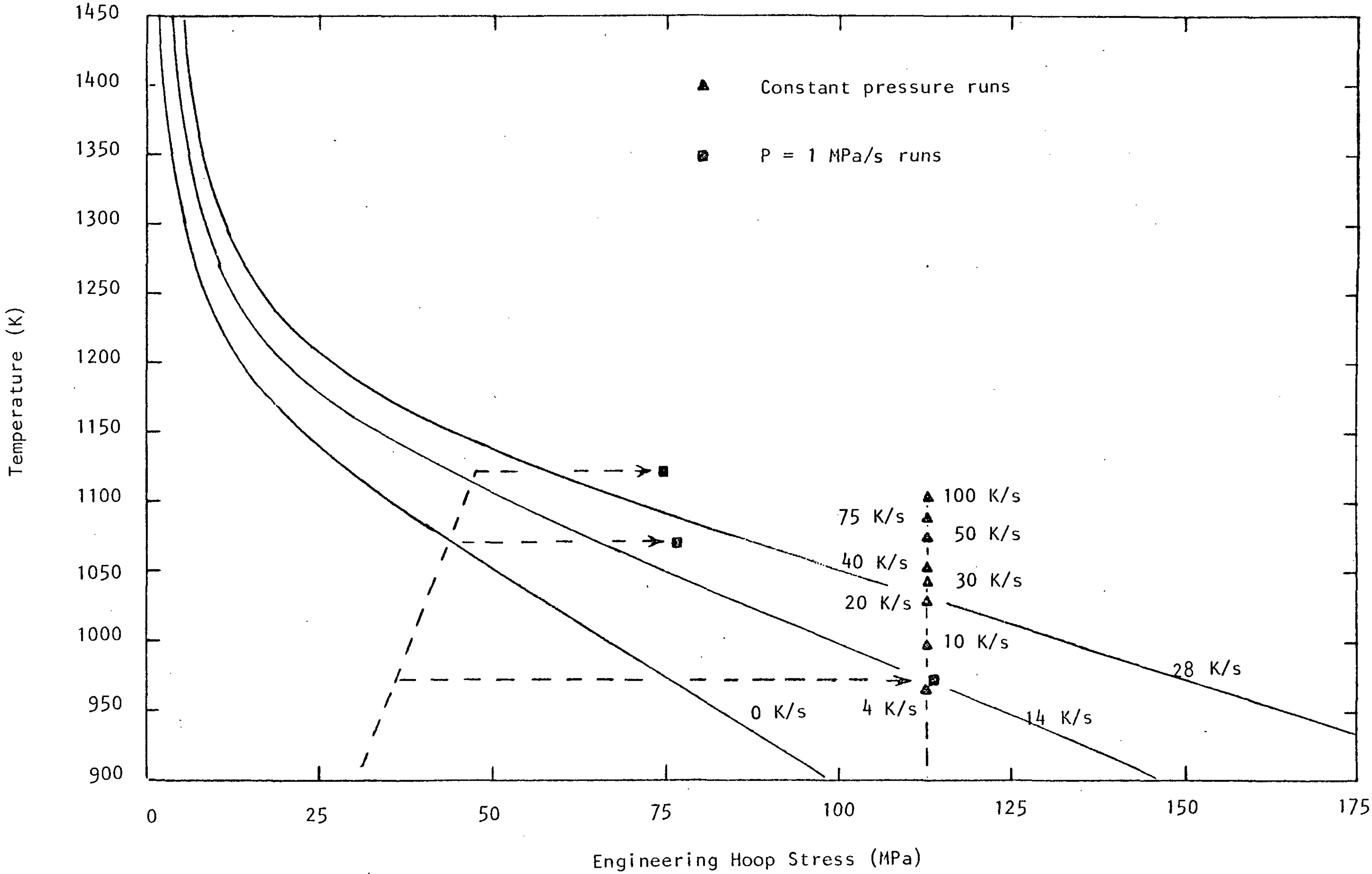

Figure 14. MRBT correlations compared with constant pressure and increasing pressure model calculations.

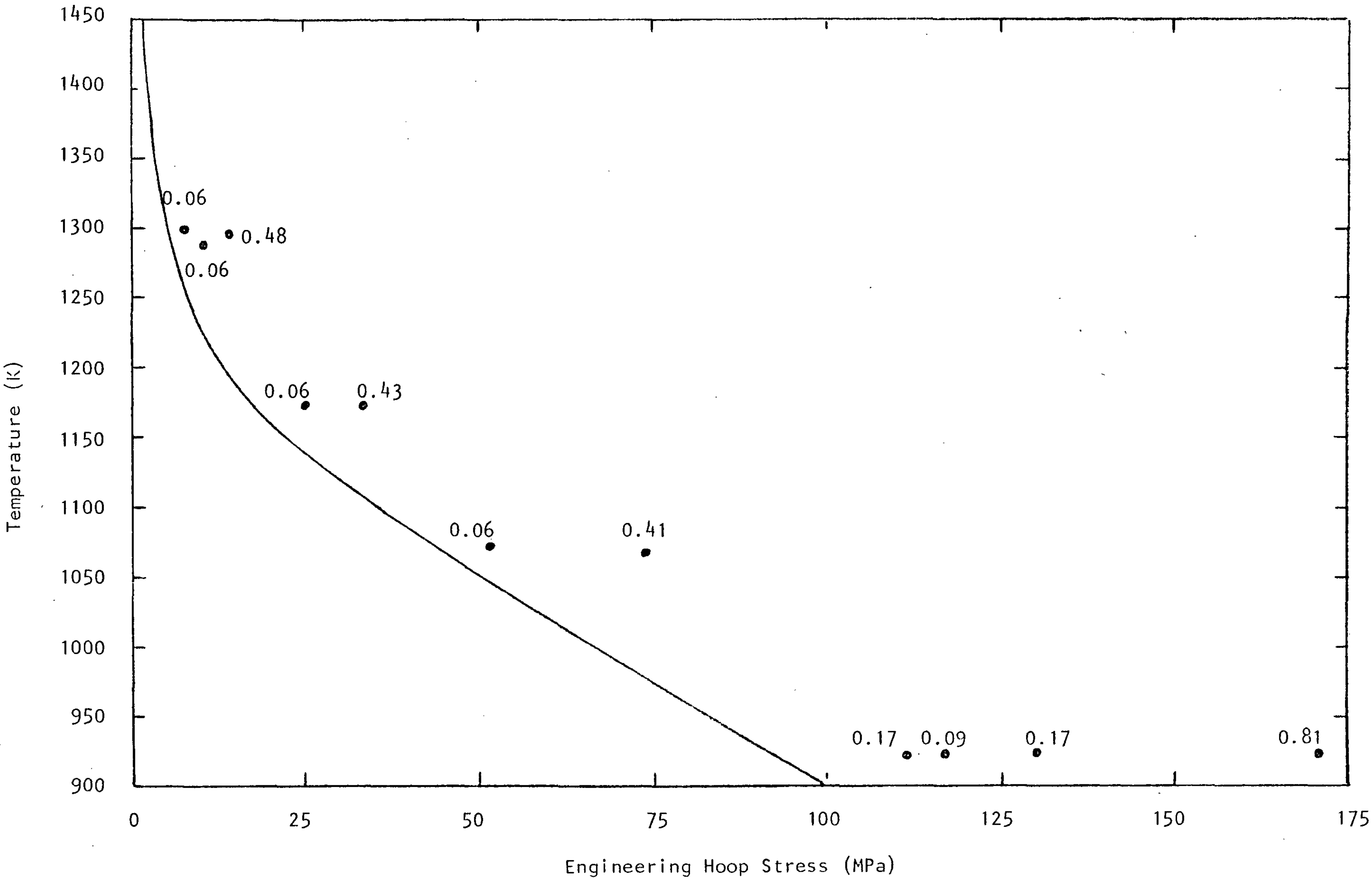

Figure 15. MRBT correlation for 0 K/s compared with 0 K/s data with increasing internal pressure from Busby and Marsh.

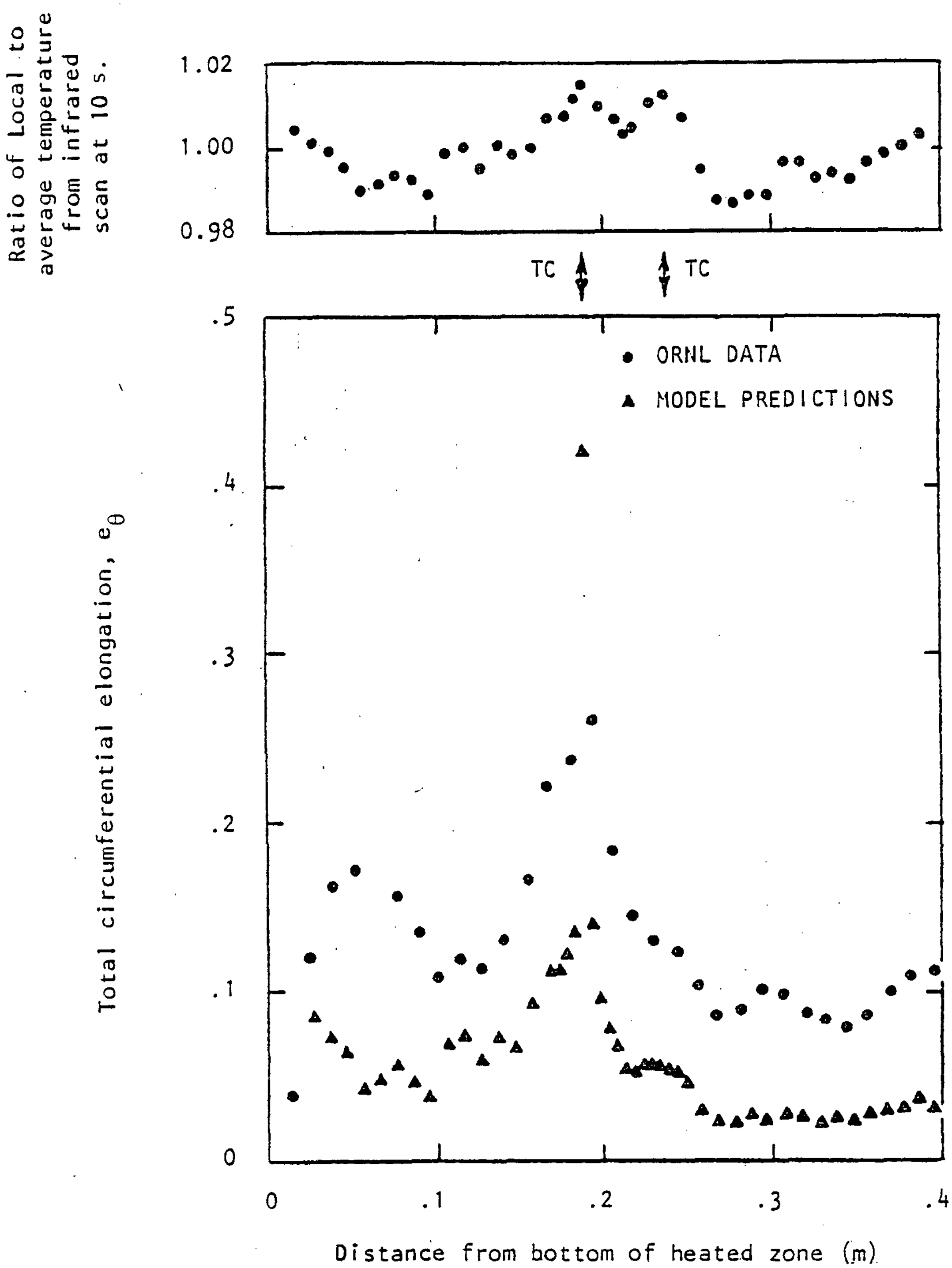

Figure 16. Model calculations versus measured elongation for MRBT Test SR-37.

heater temperature variations obtained during a preliminary infrared scan of one quadrant of the heater surface were reported. The top graph in Figure 16 is a reproduction of the ratio of local-to-average temperature obtained from this scan. The lower graph of the figure shows measured total circumferential elongation and the calculated elongation for the lower 40 cm of the 100 cm specimen.

The reasonable agreement shown between the model calculation and experiment results for the full 40 cm was obtained only after Equation (A-18) was added to the MATPRO equation of state for Zircaloy cladding plastic deformation. Comparison of the shape of the upper and lower curves shows that local maximums and minimums of the heater temperature profile are reproduced by both the measured and calculated elongations. Where differences exist, they can be explained by the difference between the cladding temperatures measured by the thermocouples and the heater temperature profile measured in the infrared scan. An outline of the method used to interpolate the thermocouple measurements is required in order to assess these differences.

Since the model uses sixteen circumferential and sixteen axial nodes, some means of interpolating the data of the twelve thermocouples was required. Temperatures of circumferential nodes not at the azimuthal angle of the thermocouples were obtained by averaging the temperatures at the azimuthal angle of the thermocouples for each axial location. Thus, even at the elevations of the thermocouples, a hot spot falling between the thermocouples would not be entered into the table of temperatures required for this analysis. A missing hot spot is the most likely explanation for the over-prediction of elongation at the location of the 18.7 cm elevation.

Temperatures at axial nodes without thermocouples were obtained with a combination of interpolation of thermocouple data and heat balance estimates. The effect of steam heating is estimated for this unheated shroud test by estimating the heat transfered from the cladding to the steam with the equation

$$h_s[T_c\ (Z) - T_s\ (Z)]\ 2\pi r = \dot{m}_{steam}\ C_{p_{steam}}\ \frac{dT_s\ (Z)}{dZ} \tag{34}$$

where

h_s	=	cladding surface heat transfer coefficient
$T_c(Z)$	=	cladding temperature at elevation Z
$T_s(Z)$	=	steam temperature at elevation Z
r	=	cladding outside diameter
$\dot{m}_{steam}$	=	mass flow rate of steam
$C_{p_{steam}}$	=	specific heat per unit mass of steam.

Since the cladding is far more massive than the steam, it is assumed that the steam temperature varies much more than the cladding temperature. Equation (34) with $T_c(Z)$ assumed constant leads to the following expression for T_{steam} (Z) in terms of the inlet steam temperature, T_{steam} (0), and the average cladding temperature, T_c.

$$\frac{T_c - T_s\ (Z)}{T_c - T_s\ (0)} = \exp\left(\frac{-2\pi r\ h_s\ Z}{\dot{m}_{steam}\ C_{p_{steam}}}\right) \tag{35}$$

Equating the heat flux from the heater at one elevation to the heat lost to steam plus the energy used to raise the cladding temperature at that elevation shows

$$h_g\ [T_f(Z) - T_c(Z)] = h_s\ [T_c(Z) - T_s(Z)] + C_p\ h\ \rho\ \frac{dT_c(Z)}{dt} \tag{36}$$

where

h_g = gas gap heat transfer coefficient

$T_f(Z)$ = fuel or heater surface temperature at elevation Z

C_p = specific heat per unit mass of cladding

h = cladding wall thickness

ρ = cladding density

t = time.

Substitution of Equation (35) into Equation (36) leads to the approximate expression

$$T_c(Z) = T_f(Z) - \frac{h_s}{h_g} [T_c - T_s(0)] \exp \left(\frac{-2\pi r h_s Z}{\dot{m}_{steam} C_{p_{steam}}} \right) + \frac{C_p h_s}{h_g} \frac{dT_c}{dt} . \qquad (37)$$

The first term of Equation (37) shows that the change in cladding temperature with axial position is proportional to the change in heater temperature while the second term represents the effect of steam heating and the third is not a function of Z. The infrared heater scan provides the data necessary for an approximate evaluation of the effect of heater temperature variations. The data necessary to use the second term to evalutate the effect of steam heating are given by Champman. The expression used to estimate cladding temperatures at position Z from a thermocouple measurement at z_o is

$$T_c(Z) = T_c(Z_o)\left[1 + \frac{T_h(Z)}{\bar{T}_h} - \frac{T_h(Z_o)}{\bar{T}_h}\right]$$

$$- \frac{h_s}{h_g}\left[T_c(Z_o) - T_s(Z_o)\right]\left[\exp\left(\frac{-2\pi r h_s Z}{\dot{m}_{steam} C_{p\ steam}}\right) - \exp\left(\frac{-2\pi r h_s Z_o}{\dot{m}_{steam} C_{p\ steam}}\right)\right] \quad (38)$$

where

$\bar{T}_h$ = average heater temperature.

If there are thermocouples both upstream and downstream from a particular Z, a weighted average of the temperatures calculated from the two thermocouples is used. The weighting factor for each thermocouple is proportional to the distance to the other thermocouple

$$f_d = \frac{Z - Z_u}{Z_d - Z_u}$$

$$f_u = \frac{Z_d - Z}{Z_d - Z_u}$$

where

f_d = weighting factor for temperature from downstream thermocouple

f_u = weighting factor for temperature from upstream thermocouple

Z_u = position of upstream thermocouple

Z_d = position of downstream thermocouple.

The principal reason for differences between the shape of the heater temperature profile and the circumferential elongation calculated using the model is the fact that thermocouple measurements did not exactly reproduce the heater temperature profile. The thermocouple at 23.7 cm measured significantly lower temperatures than those at 18.7 cm during test SR-37, in spite of the fact that the infrared scan shows nearly equal peaks at these two points. An obvious explanation for this difference is the fact that the infrared scan sampled only one quadrant of the heater's circumference. The temperature variation on the other quadrants could have been quite different. In spite of this possible difference, the fact that the general features of the shape of the infrared trace and the measured elongation are the same leaves little doubt that the heater temperature profile is an important parameter for this cold-shroud test.

CONCLUSIONS

The principal conclusion from this study is that local or true stress can be used to provide a mechanistic approach to calculating Zircaloy cladding shape at failure. The large scatter inherent in engineering stress or engineering strain expressions has been explained and the need for numerous limitations and special correlations for such effects as heating rate, circumferential termperature gradients, etc., has been eliminated. The correlation for true stress at failure coupled with a mechanical model, BALON2, which calculates local stress reproduces special correlations which have been derived for burst temperature versus burst pressure (engineering stress), total circumferential elongation versus circumferential temperature variation at failure and total circumferential elongation versus heating rate. In addition, other correlations such as total circumferential elongation versus rate of change of pressure differential across the cladding have been demonstrated with model calculations.

There is consistent agreement with experimental data where such data are available. The model has also provided a reasonable means of extrapolating limited data. For example, the model suggests that the arbitrary use of 28°C/s heating rate data to describe faster heating rates is incorrect. The trends observed from 0°C/s to 28°C/s should be continued to at least 100°C/s.

REFERENCES

1. R. H. Chapman, Multirod Burst Test Program Quarterly Progress Report for April--June 1977, ORNL/NUREG/TM-135, December 1977.

2. R. H. Chapman, J. L. Crowley, A. W. Longest and E. G. Sewell, Effect of Creep Time and Heating Rate on Deformation of Zircaloy-4 Tubes Tested in Steam with Internal Heaters, ORNL/NUREG/TM-245 and NUREG/CR-0345, October 1978.

3. R. H. Chapman, Multirod Burst Test Program Quarterly Progress Report for April--June 1976, ORNL/NUREG/TM-74, January 1977.

4. R. H. Chapman, Multirod Burst Test Program Progress Report for July--December 1977, ORNL/NUREG/TM-200, June 1978.

5. R. H. Chapman, Multirod Burst Test Program Progress Report for January--March 1978, ORNL/NUREG/TM-217 and NUREG/CR-0225, August 1978.

6. R. H. Chapman, Multirod Burst Test Program Quarterly Progress Report for January--March 1976, ORNL/NUREG/TM-36, September 1976.

7. R. H. Chapman, Multirod Burst Test Program Quarterly Progress Report for October--December 1976, ORNL/NUREG/TM-95, April 1977.

8. R. H. Chapman, Multirod Burst Test Program Quarterly Progress Report for January--March 1977, ORNL/NUREG/TM-108, May 1977.

9. D. O. Hobson and P. L. Rittenhouse, Deformation and Rupture Behavior of Light-Water Reactor Fuel Cladding, ORNL-4727, October 1971.

10. H. M. Chung and T. F. Kassner, Deformation Characteristics of Zicaloy Cladding in Vacuum and Steam Under Transient-heating Conditions: Summary Report, ANL-77-31 and NUREG/CR-0344, July 1978.

11. A. A. Bauer, L. M. Lowry and J. S. Perrin, Evaluating Strength and Ductility of Irradiated Zircaloy: Quarterly Progress Report for January through March 1976, BMI-NUREG-1948, March 1976.

12. A. A. Bauer, W. J. Gallagher, L. M. Lowry and A. J. Markworth, Evaluating Strength and Ductility of Irradiated Zircaloy. Quarterly Progress Report July through September 1977, BMI-NUREG-1985, October 1977.

13. A. A. Bauer, W. J. Gallagher, L. M. Lowry and A. J. Markworth, Evaluating Strength and Ductility of Irradiated Zircaloy. Quarterly Progress Report October through December 1977, BMI-1992 and NUREG/CR-0026, January 1978.

14. D. W. Croucher, Behavior of Defective PWR Fuel Rods During Power Ramp and Film Boiling Operation, TREE-1267 and NUREG/CR-0283, February 1979.

15. T. F. Cook, S. A. Ploger and R. R. Hobbins, Postirradiation Examination Results for the Irradiatin Effects Test IE-5, TREE-NUREG-1201, March 1978.

16. E. H. Karb, "Results of the FR-2 Nuclear Tests on the Behavior of Zircaloy Clad fuel Rods," Paper Presented at the 6th NRC Water Reactor Safety Research Information Meeting, Gaithersburg, MD, November 7, 1978.

17. K. Wiehr, H. Schmidt, Out-of-Pile Versuche zum Aufblahvorgang von Zirkaloy-Hullen Ergenbnisse aus Vorversuchen mit verkurzten Brennstabsimulatoren, KfK 2345, October 1977.

18. L. J. Siefken, M. P. Bohn, S. O. Peck, J. A. Dearien, FRAP-T5: A Computer Code for the Transient Analysis of Oxide Fuel Rods, TREE-1280 NUREG-CR-0840, June 1979.

19. D. W. Croucher, T. R. Yackle, C. M. Allison and S. A. Ploger, Irradiation Effects Test Series IE 5 Test Results Report, TREE-NUREG-1130, January 1978.

20. R. H. Chapman, Multirod Burst Test Program Quarterly Progress Report for October--December 1975, ORNL/NUREG/TM-10, May 1976.

21. D. L. Hagrman, G. A. Reymann and R. E. Mason, MATPRO-VERSION 11 Revision 1. A Handbook of Materials Properties for Use in the Analysis of Light Water Reactor Fuel Rod Behavior, NUREG/CR-0497 TREE-1280, Rev. 1, February 1980.

22. S. P. Timoshenko and J. N. Goodier, Theory of Elasticity, 3rd edition, New York: McGraw-Hill Book Company, 1970, p. 70.

23. J. M. Kramer and L. W. Deitrich, Cladding Failure by Local Plastic Instability, ANL-77-95, December 1977.

24. C. C. Busby and K. B. Marsh, High Temperature Deformation and Burst Characteristics of Recrystallized Zircaloy-4 Tubing, WAPD-TM-900, January 1970.

25. K. Wiehr et al., Jahreskolloquim 1977 des Projekts Nukleare Sicherheit.

26. D. A. Powers and R. O. Meyer, Cladding Swelling and Rupture Models for LOCA Analysis, NUREG-0630, April 1980.

APPENDIX A

EQUATION OF STATE FOR ZIRCALOY CLADDING PLASTIC DEFORMATION

The equation of state for Zircaloy cladding plastic deformation is taken from the MATPRO handbook of materials properties (Reference 21 of the main text). All strain or stress components are assumed to be true strain[a] or true stress.[b] The basic equation used to relate stress and plastic strain is

$$\sigma = K\varepsilon^{n}\left[\frac{\dot{\varepsilon}}{10^{-3}}\right]^{m} \qquad \text{(A-1)}$$

where

σ	=	true effective stress (Pa)
ε	=	true effective plastic strain (unitless)
$\dot{\varepsilon}$	=	rate of change of true effective plastic strain (s^{-1})
K,n,m	=	parameters which describe the metallurgical state of the cladding. These parameters will be discussed in detail below.

a. True strain equals the change in length divided by the length at the instant of change integrated from the original to the final length.

b. True stress equals the force per unit cross sectional area determined at the instant of measurement of the force.

Equation (16) of the main text, the integrated form of the equation of state, is obtained by integrating Equation (A-1) over a time interval Δt, assuming that σ, K, n, and m are constant over the interval. The equation is repeated here as Equation (A-2) and is used in the CSTRNI model of MATPRO:

$$\varepsilon_f = \left[\left(\frac{n}{m} + 1\right) 10^{-3} \left(\frac{\sigma}{K}\right)^{\frac{1}{m}} \Delta t + \varepsilon_i^{\frac{n}{m+1}} \right]^{\frac{m}{n+m}} \quad \text{(A-2)}$$

where

ε_f = true effective strain at the end of a time interval (unitless)

ε_i = true effective strain at the start of a time interval (unitless)

Δt = duration of the time interval (s).

Effective stress for use with the equation of state is obtained from stress components and Equation (25) of the main text

$$\sigma = \left[A1S\,(\sigma_1 - \sigma_2)^2 + A2S\,(\sigma_2 - \sigma_3)^2 + A3S\,(\sigma_3 - \sigma_1)^2 \right]^{1/2} \quad \text{(A-3)}$$

where

$\sigma_1, \sigma_2, \sigma_3$ = principal axis stress components (Pa)

A1S,A2S,A3S = coefficients of anisotropy provided by the CANISO subcode of the MATPRO package.

Once effective stress is known and Equation (A-2) has been used to find the end-of-step effective strain the Prandtl-Reuss flow rule, Equations (26) tnrough (28) of the main text, are used to find the strain components. The Prandtl-Reuss equations are

$$d\varepsilon_1 = \frac{d\varepsilon}{\sigma} [\sigma_1 (A1E + A3E) - \sigma_2 A1E - \sigma_3 \ A3E] \quad \text{(A-4)}$$

$$d\varepsilon_2 = \frac{d\varepsilon}{\sigma} [-\sigma_1 \ A1E + \sigma_2 (A2E + A1E) - \sigma_3 \ A2E] \quad \text{(A-5)}$$

$$d\varepsilon_3 = \frac{d\varepsilon}{\sigma} [-\sigma_1 \ A3E - \sigma_2 \ A2E + \sigma_3 (A3E + A2E)] \quad \text{(A-6)}$$

where

$d\varepsilon$ = $\varepsilon_f - \varepsilon_i$

A1E,A2E,A3E = coefficients of anisotropy provided by the CANISO subcode of the MATPRO package.

As mentioned in conjunction with Equations (A-3) through (A-6), coefficients of anisotropy are provided by the CANISO model. The information required by this model is the temperature, the three prinicpal components of plastic strain during a time interval, three constants related to the cladding basal pole distribution at the start of the time interval, and three constants related to the deformation history of the cladding prior to the time interval. For each time step, the CANISO model updates the six constants required and provides the six coefficients of anisotropy required by Equations (A-3) through (A-6). Initial (no plastic deformation) values of the constants related to the basal pole distribution and deformation history constants will be discussed in conjunction with the following summary.

For undeformed cladding with σ_1, σ_2, and σ_3 of Equations (A-3) through (A-6) taken to be the axial, circumferential, and radial components of stress, the expressions used to find the stress anisotropy constants from the basal pole distribution are

$$A1S = (1.5\ f_r - 0.5)\ g\ (T) + 0.5 \tag{A-7}$$

$$A2S = (1.5\ f_z - 0.5)\ g\ (T) + 0.5 \tag{A-8}$$

$$A3S = (1.5\ f_\theta - 0.5)\ g\ (T) + 0.5 \tag{A-9}$$

where

$g(T)$ = a function which is 1.0 for temperatures below 1090 K, 0 for temperatures above 1255 K and found by linear interpolation for temperatures between 1090 and 1255 K

f_r, f_z, f_θ = average of the squared cosine between the c axis of grains in the cladding and the radial, axial and tangential reference directions, respectively, weighted by the volume fraction of grains at each orientation. These averages can be obtained from a pole figure and the CTXTUR model of the MATRPRO package or the typical values of $f_r = 0.66$, $f_z = 0.06$ and $f_\theta = 0.28$ can be used.

The change of the factors f_r, f_θ, and f_z of Equations (A-7) through (A-9) due to deformation is modeled with the following correlations:

$$df_r = d\varepsilon_3\ (-1.505 + T\ 0.00895) \tag{A-10}$$

$$df_z = d\varepsilon_1 \, (-1.505 + T \, 0.00895) \tag{A-11}$$

$$df_\theta = d\varepsilon_2 \, (-1.505 + T \, 0.00895) \tag{A-12}$$

where

df_r, df_z, df_θ = change in f_r, f_z, and f_θ due to deformation

T = 644 K for temperature less than 644 K, the temperature when it is between 644 K and 1090 K and 1090 K when the temperature is above 1090 K

and the numbering convention of $z = 1$, $\theta = 2$ and $r = 3$ has been assumed for strain components.

The strain anisotropy coefficients A1E, A2E, and A3E are given by Equations (A-7) through (A-12) with A1S, A2S, and A3S replaced by A1E, A2E, and A3E when the cladding temperature is below 650 K. However, limited data at temperatures above 800 K have suggested initial strain anisotropy coefficients of 0.5 (the isotropic values). The description of high temperature strain isotropy thus requires a separate set of values for f, set initially at the isotropic values and changed during each time step by an amount given by Equations (A-10) through (A-12). The expressions for A1E, A2E, and A3E which are used to model this rather complex switching from texture dependent to deformation dependent strain anisotropy are

$$A1E = \frac{A1S + [(1.5\, f_r' - 0.5)g(T) + 0.5] \exp\left(\frac{T-725}{18}\right)}{\exp\left(\frac{T-725}{18}\right) + 1} \tag{A-13}$$

$$A2E = \frac{A2S + [(1.5\ f_z' - 0.5)g(T) + 0.5]\ \exp\left(\frac{T-725}{18}\right)}{\exp\left(\frac{T-725}{18}\right) + 1} \qquad \text{(A-14)}$$

$$A3E = \frac{A3S + [(1.5\ f_\theta' - 0.5)g(T) + 0.5]\ \exp\left(\frac{T-725}{18}\right)}{\exp\left(\frac{T-725}{18}\right) + 1} \qquad \text{(A-15)}$$

where

f_r', f_z', f_θ' = deformation dependent parameters set equal to 1/3 at zero deformation and changed like the parameters for f_r, f_z, and f_θ in Equations (A-10) through (A-12).

Effects of cladding temperature, cold work, irradiation, in-reactor annealing and oxidation on mechanical properties are expressed as changes in the strength coefficient, K; the strain hardening exponent, n; and tne strain rate sensitivity exponent, m, of Equations (A-1) and (A-2). For fully annealed Zircaloy cladding the temperature and sometimes strain rate or strain dependent values of m, n, and K are as shown below.

1. Values of the Strain Rate Sensitivity Exponent, m[a]

For temperature, T, less than 730 K,

$$m = 0.02. \qquad \text{(A-16a)}$$

---

a. Eignt to ten significant figures are used in these expressions to minimize discontinuities, not to imply accuracy.

For temperature between 730 and 900 K,

$$m = 2.063172161 \times 10^{1} + T\,[-7.704552983 \times 10^{-2} + T\,(9.504843067 \times 10^{-5} + T\,(-3.860960716 \times 10^{-8}))]. \quad \text{(A-16b)}$$

For temperature between 900 and 1090 K,

$$m = -6.47 \times 10^{-2} + T\,2.203 \times 10^{-4}. \quad \text{(A-16c)}$$

For temperature between 1090 K and 1172.5 K,

$$m = -6.47 \times 10^{-2} + T\,2.203 \times 10^{-4}$$

$$+ \left[\begin{array}{l} 0 \text{ for } \dot{\varepsilon} \geq 6.34 \times 10^{-3}/\text{s} \\ \text{or} \\ 6.78 \times 10^{-2} \left[\dfrac{T-1090}{82.5}\right] \ln\left[\dfrac{6.34 \times 10^{-3}}{\dot{\varepsilon}}\right] \\ \text{for } \dot{\varepsilon} < 6.34 \times 10^{-3}/\text{s} \end{array}\right] \quad \text{(A-16d)}$$

For temperature between 1172.5 K and 1255 K

$$m = -6.47 \times 10^{-2} + T\ 2.203 \times 10^{-4}$$

$$+ \begin{bmatrix} 0 \text{ for } \dot{\varepsilon} \geq 6.34 \times 10^{-3}/\text{s} \\ \text{or} \\ 6.78 \times 10^{-2} \left[\frac{1255-T}{82.5}\right] \ln \left[\frac{6.34 \times 10^{-3}}{\dot{\varepsilon}}\right] \\ \text{for } \dot{\varepsilon} < 6.34 \times 10^{-3}/\text{s} \end{bmatrix} \quad \text{(A-16e)}$$

For temperature greater than or equal to 1255 K,

$$m = -6.47 \times 10^{-2} + T\ 2.203 \times 10^{-4}. \quad \text{(A-16f)}$$

2. Values of the Strain Hardening Exponent, n The strain hardening exponent for strains larger than n/(1 + m), the ultimate strain, is given by the following equations,

For temperature, T, less than 1099.0722,

$$n = -9.490 \times 10^{-2} + T\ (1.165 \times 10^{-3}$$

$$+ T\ (-1.992 \times 10^{-6} + T\ 9.588 \times 10^{-10})). \quad \text{(A-17a)}$$

For temperature between 1099.0722 and 1600 K,

$$n = -0.22655119 + 2.5 \times 10^{-4}\ T. \quad \text{(A-17b)}$$

For temperatures above 1600 K,

$$n = 0.17344880 \tag{A-17c}$$

When the strain is less than $n/(1 + m)$ the strain hardening exponent is modified[a] to a larger value than the one given by Equations (A-17a) through (A-17c). The expression used to modify n for strains less than $n/(1 + m)$ is

$$n' = \text{the smaller of} \begin{bmatrix} \text{ANL} \quad \text{or} \\ n^2/[(1 + m) \quad \epsilon] \end{bmatrix} \tag{A-18}$$

where

$$\text{ANL} = \begin{bmatrix} 0.17 \text{ for temperatures } \leq 730 \text{ K} \\ 0.056 \cdot \text{temperature} - 11.218 \text{ for temperatures in the range } 730\text{-}780 \text{ K} \\ 0.95 \text{ for temperatures } \geq 780 \text{ K} \end{bmatrix}$$

n = the number given by Equations (A-17a) to (A-17c)

n' = the revised number to be used with Equation (A-1) or (A-2) in place of n.

a. This modification is not found in the MATPRO-11 Rev. 1 package of February 1980. The modification is proposed for future MATPRO revisions as a result of studies with the ballooning code.

3. Values of the Strength Coefficient, K

For temperature, T, less than 750 K,

$$K = 1.17628 \times 10^9 + T\,[4.54859 \times 10^5$$

$$+ T\,(-3.28185 \times 10^3 + T\,1.72752)]. \qquad \text{(A-19a)}$$

For temperature between 750 and 1090 K,

$$K = 2.522488 \times 10^6 \exp\left(\frac{2.8500027 \times 10^6}{T^2}\right) \qquad \text{(A-19b)}$$

For temperature between 1090 K and 1255 K,

$$K = 1.841376039 \times 10^8 - T\,1.4345448 \times 10^5. \qquad \text{(A-19c)}$$

For temperature between 1255 K and 2100 K,

$$K = 4.330 \times 10^7 + T\,[-6.685 \times 10^4$$

$$+ T\,(3.7579 \times 10^1 - T\,7.33 \times 10^{-3})]. \qquad \text{(A-19d)}$$

The changes in form of Equations (A-16a) through (A-19d) in various temperature ranges are caused by changes in the physical mechanism of the plastic deformation. At 700 to 900 K, the deformation becomes significantly strain rate dependent, the strength of the material begins to decrease rapidly with temperature and strain hardening becomes relatively unimportant. This change is generally attributed to thermal creep at high temperature, but the specific deformation system change has not been identified. The 1090 to 1255 K region is the alpha plus beta phase region for Zircaloy and the region above 1255 K is the beta phase region for this material.

The change in the strain hardening exponent due to irradiation and cold working of cladding is described by multiplying the value of the n given in Equations (A-17a) through (17c) by

$$R = [0.847 \exp(-39.2\ C) + 0.153 + C\ (-9.16 \times 10^{-2} + 0.229\ C)]$$

$$\exp\left[\frac{-(\phi^{1/3})}{3.73 \times 10^{7} + 2 \times 10^{8}\ C}\right] \qquad \text{(A-20)}$$

where

R = strain hardening exponent for irradiated and cold worked material divided by the expression in Equations (A-17a) through (A-17c)

C = effective cold-work for strain hardening exponent (unitless ratio of areas). Changes in the effective cold work as a function of time and temperature are modeled with the CANEAL model of MATPRO

ϕ = effective fast neutron fluence (neutrons >1.0 Mev/m^2). Changes in the effective fast neutron fluence are modeled with the CANEAL model of MATPRO.

The change in the strength coefficient due to irradiation and cold working of the cladding is modeled with the expression

$$DK = 0.546\ C\ K + 5.54 \times 10^{-18}\ \phi$$

where

DK = strength coefficient for irradiated and cold worked Zircaloy minus the expression in Equations (A-19a) through (A-19d).

The strain rate sensitivity exponent does not change as a function of irradiation or cold work.

Additional expressions for the change in m, n, and K due to oxidation of the Zircaloy are available in MATPRO, but they are not recommended for the current ballooning model because the extension of the model to treat multi-layered cladding (the oxide layers, the oxygen stabilized alpha layers and the beta layer) has not been completed.

APPENDIX B

BALON2 CODE LISTING AND EXAMPLE OUTPUT

Table B-1 is a listing of the BALON2 code which has been discussed throughout this report. Table B-2 is an example of a driver program designed to provide input data to the subroutine. Table B-3 presents example output data.

The data shown are the result of an analysis with a heater heating rate of 50 K/s starting at 600 K. Thirty-one calls to BALLOON with a given time step of 0.3 s were calculated to burst the cladding. The burst occurred during the seventy-fourth substep of the thirty-first call when the total time elapsed was 9.046 s. The last substep was 5×10^{-4} s long.

Several matrices of information are provided. In these matrices, the sixteen axial nodes are listed across the page in two groups of eight columns and the sixteen azimuthal nodes are listed in rows. The first matrix shows temperatures at the nodes at failure. Inspection of the matrix shows the hot node at the eighth axial and fourth azimuthal position of the cladding burst at 1073.5 K. An azimuthal temperature variation of 87.7 K is indicated at the eighth axial node. Even at the first axial node, where the heater's circumferential temperature variation was input as zero, there is a 61.3 K azimuthal temperature variation because of the varying gap thickness.

The second matrix shows local tangential stress components during the last time step. The next four matrices show the effective cold work and fast neutron fluences calculated with the MATPRO CANEAL model for cladding annealing. Approximately two thirds of the initial 0.5 cold work for strength remains while the cold work for strain hardening has essentially been annealed to zero. Fast neutron fluences remain at their initial values of zero.

The next group of output data shows details of calculated cladding shape for each of sixteen nodes 5 x 10^{-3} meters apart. The average radius in meters, the average wall thickness in meters, the value of a contact indicator and the total circumferential elongation (engineering or average strain) at the axial node is given. The fact that the contact switch is equal to one means the cladding has contacted the heating element. Details of the shape at each axial node are provided by printing midwall radii, wall thickness and axial lengths for each of the sixteen azimuthal nodes (J = 1 through 16) at each axial node. As expected, the minimum midwall radius occurs at the hot azimuthal node, J = 4.

TABLE B-1. LISTING OF THE BALON2 CODE

```
      SUBROUTINE BALON2(HTNC,TBULK,TCLI,TFLI,Q,RF,RO,HO,FTEMP,QL,STEMP,
     #  PC,PS,RMP,CFLUX,FA,KBALN,ZBALN,KFLG,MODE,NPRINT,GMIX,GTMPF,
     #  TIMET,TSTP,V,DELZ,TWALL,RAD,STRNC,STRNA,STRNR,STRNL,CTEMP,
     #  KNTCT,CHSTRS,KFAIL)
C
C     THE BALON2 SUBROUTINE COMPUTES NON SYMMETRIC CLADDING DEFORMATION
C
C     KFAIL        = OUTPUT FAILURE INDEX
C                          0  NO FAILURE
C                          1  FAILURE
C     CHSTRS       = OUTPUT MAXIMUM HOOP STRESS IN THE NODE
C                     CONSIDERED DURING THE CURRENT CALL (PSI)
C     KNTCT        = OUTPUT FUEL - CLADDING CONTACT INDEX
C                          0  NO CONTACT
C                          1  CONTACT DUE TO BOWING
C     CTEMP(K,J)   = OUTPUT CLADDING TEMPERATURE AT AXIAL NODE K,
C                     CIRCUMFERENTIAL NODE J AT MIDPOINT OF TIME
C                     STEP TSTP (DEGREES F).  NODES K AND J ARE
C                     DETERMINED BY BALOON INITIALIZING ROUTINE
C     STRNL(K,J)   = OUTPUT EFFECTIVE TRUE PLASTIC STRAIN AT NODE
C                     K,J AT END OF TIME STEP (UNITLESS)
C     STRNR(K,J)   = OUTPUT RADIAL COMPONENT OF TRUE PLASTIC STRAIN
C                     AT NODE K,J AT END OF TIME STEP (UNITLESS)
C     STRNA(K,J)   = OUTPUT AXIAL COMPONENT OF TRUE PLASTIC STRAIN
C                     AT NODE K,J AT END OF TIME STEP (UNITLESS)
C     STRNC(K,J)   = OUTPUT TANGENTIAL COMPOKENT OF TRUE PLASTIC STRAIN
C                     AT NODE K,J AT END OF TIME STEP (UNITLESS)
C     RAD(K,J)     = OUTPUT MIDWALL RADIUS OF CLADDING
C                     AT NODE K,J AT END OF TIME STEP (INCHES)
C     TWALL(K,J)   = OUTPUT WALL THICKNESS AT NODE K,J AT
C                     END OF TIME STEP (INCHES)
C     DELZ(K,J)    = OUTPUT AXIAL LENGTH OF NODE AT K,J AT
C                     END OF TIME STEP (INCHES)
C     V            = OUTPUT GAS VOLUME OF SWELLING NODE AT END
C                     OF TIME STEP (INCHES**3)
C     TIMET        = OUTPUT TIME AT END OF TIME STEP (S)
C     TSTP         = OUTPUT TIME STEP SIZE OF LAST INTERNAL TIME STEP (S)
C     TIMET        = OUTPUT TIME AT END OF TIME STEP
C
C
C     HTNC         = INPUT CLADDING SURFACT HEAT TRANSFER COEFFICIENT
C                     (BTU/S*(FT**2)*F)
C     TBULK        = INPUT BULK COOLANT TEMPERATURE (DEGREES F)
C     TCLI         = INPUT CLADDING AVERAGE TEMPERATURE WHEN BALOON
C                     IS FIRST CALLED (DEGREES F).  USED ONLY
C                     WHEN KFLG = 0
C     TFLI         = INPUT FUEL SURFACE TEMPERATURE WHEN BALOON IS
C                     FIRST CALLED (DEGREES F).  USED ONLY
C                     WHEN KFLG = 0.
C     Q            = INPUT ROD HEAT FLUX (BTU/(S*(FT**2))).  USED
C                     ONLY WHEN MODE = 0 AND KFLG = 0
C     RF           = INPUT HOT RADIUS OF FUEL PELLET (IN).
C     RO           = INPUT INITIAL (UNDEFORMED) CLADDING OUTSIDE
```

```
C                          RADIUS (IN)
C      HO                = INPUT INITIAL (UNDEFORMED) CLADDING WALL THICKNESS (IN)
C      FTEMP(K,J)        = INPUT FUEL SURFACE TEMPERATURE AT NODE K,J AT
C                          MIDPOINT OF TIME STEP TSTP (DEGREES F). USED
C                          ONLY WHEN MODE = 1 AND KFLG = 1
C      QL(K,J)           = INPUT ROD HEAT FLUX AT NODE K,J (BTU/(S*(FT**2))).
C      STEMP(K,J)        = INPUT SHROUD SURFACE TEMPERATURE AT NODE K,J AT
C                          MIDPOINT OF TIME STEP TSTP (DEGREES F). USED
C                          USED ONLY WHEN MODE = 0 AND KFLG = 1
C      PC                = INPUT COOLANT PRESSURE (PSI)
C      PS                = INPUT FUEL ROD PRESSURE (PSI)
C      RMP               = INPUT UNIFORMLY EXPANDED CLADDING MIDPLANE
C                          RADIUS WHEN BALOON IS FIRST CALLED (IN).
C                          USED ONLY WHEN KFLG EQUALS 0
C      CFLUX             = INPUT FAST NEUTRON FLUX (NEUTRONS/((M**2)*S))
C      FA                = INPUT ADDITIONAL AXIAL FORCE APPLIED TO CLADDING
C                          BY CONSTRAINTS (POUNDS)
C      KBALN             = INPUT FRAT-T INDEX OF BALLOONING NODE
C                         ONLY WHEN MODE = 1
C      ZBALN             = INPUT LENGTH OF FRAP-T NODE (INCHES).  USED
C                          ONLY WHEN KFLG EQUALS 0
C      KFLG              = INPUT INITIALIZATION FLAG
C                                0  CAUSES BALOON TO INITILIZE ITSELF
C                                1  NO INITIALIZATION
C      MODE              = INPUT SWITCH WHICH DETERMINES METHOD OF
C                          FINDING CLADDING TEMPERATURES AND ANNEALING
C                                0  CAUSES CLADDING TEMPERATURES TO BE
C                                   CALCULATED USING CONSTANT FUEL SURFACE
C                                   HEAT FLUX ASSUMPTION
C                                1  CAUSES CLADDING TEMPERATURES TO BE
C                                   CALCULATED USING CONSTANT FUEL SURFACE
C                                   TEMPERATURE ASSUMPTION
C                                2  CAUSES CLADDING TEMPERATURES AND PRESSURES
C                                   TO BE TAKEN FROM A TABLE READ IN DURING
C                                   INITIALIZATION
C                                3  CAUSES CLADDING TEMPERATURES TO BE
C                                   CONSTANT DURING THE ENTIRE FRAP - T TIME
C                                   STEP.  UNLIKE MODES 0 TO 2 CLADDING
C                                   ANNEALING IS NOT CONSIDERED INTERNALLY
C                                   IN THIS MODE
C      NPRINT            = INPUT SWITCH WHICH DETERMINES THE AMOUNT OF
C                          INFORMATION PRINTED FROM WITHIN THE SUBROUTINE
C                                0  NO PRINT OUT UNLESS THE TIME STEP FROM
C                                    FRAT-T WAS DIVIDED INTO MORE THAN
C                                    300 SUB-STEPS
C                                1  PRINTS SUB-STEP NUMBER
C                                          SUBSTEP DURATION (S)
C                                          AVERAGE MIDWALL RADIUS AT EACH
C                                             AXIAL SUB-NODE (M)
C                                          AVERAGE WALL THICKNESS AT EACH
C                                             AXIAL SUB-NODE (M)
C                                          VALUE OF KNTCT
C                                          CLADDING FAILURE LOCATION
```

```
C                                       CLADDING TANGENTIAL STRESS
C                                          AT FAILURE (PA)
C                              2  IN ADDITION TO THE INFORMATION PRINTED
C                                 WHEN NPRINT = 1 VALUES OF THE FOLLOWING
C                                 ARGUMENTS ARE PRINTED FOR EACH TIME
C                                       CTEMP(K,J) IN KELVINS
C                                       STRESF(K,J) IN N/(M**2)
C                                       RAD(K,J) IN METERS
C                                       TWALL(K,J) IN METERS
C                                       DELZ(K,J) IN METERS
C                              3  IN ADDITION TO THE INFORMATION PRINTED
C                                 WHEN NPRINT = 2 VALUES OF THE FOLLOWING
C                                 ARGUMENTS ARE PRINTED FOR EACH TIME
C                                 STEP
C                                       CWNF(K,J)
C                                       CWKF(K,J)
C                              4  IN ADDITION TO THE INFORMATION PRINTED
C                                 WHEN NPRINT = 3 VALUES OF THE FOLLOWING
C                                 ARGUMENTS ARE PRINTED FOR EACH TIME
C                                 STEP
C                                       FNCN(K,J) IN NEUTRONS/(M**2)
C                                       FNCK(K,J) IN NEUTRONS/(M**2)
C     GMIX(L)      = INPUT MOLE FRACTIONS OF THE GAS COMPONENTS
C                    FOUND IN THE GAP (UNITLESS).  USED ONLY FOR MODE
C                    EQUAL TO 1
C                       L =  1 IS HELIUM
C                       L =  2 IS ARGON
C                       L =  3 IS KRYPTON
C                       L =  4 IS XENON
C                       L =  5 IS HYDROGEN
C                       L =  6 IS NITROGEN
C                       L =  7 IS OXYGEN
C                       L =  8 IS CARBON MONOXIDE
C                       L =  9 IS CARBON DIOXIDE
C                       L = 10 IS WATER VAPOR
C     GTMPF        = INPUT GAP GAS TEMPERATURE (DEGREES F)
C     TIMET        = INPUT TIME AT START OF TIME STEP.  USED
C                    ONLY WITH CLADDING TEMPERATURE AND
C                    TIME TABLE OF MODE = 2 (S).
C     TSTP         = INPUT FRAP TIME STEP SIZE (S)
C     V            = INPUT GAS VOLUME OF SWELLING NODE AT START OF
C                    TIME STEP (INCHES**3)
C     DELZ(K,J)    = INPUT AXIAL LENGTH OF NODE AT K,J AT
C                    START OF TIME STEP (INCHES)
C     TWALL(K,J)   = INPUT WALL THICKNESS AT NODE K,J AT
C                    START OF TIME STEP (INCHES). USED
C                    ONLY WHEN KFLG = 1
C     RAD(K,J)     = INPUT MIDWALL RADIUS OF CLADDING
C                    AT NODE K,J AT START OF TIME STEP (INCHES).
C                    USED ONLY WHEN KFLG = 1.
C     STRNC(K,J)   = INPUT TANGENTIAL COMPONENT OF TRUE PLASTIC STRAIN
C                    AT NODE K,J AT START OF TIME STEP (UNITLESS)
C                    USED ONLY WHEN KFLG = 1.
```

```
C       STRNA(K,J) = INPUT AXIAL COMPONENT OF TRUE PLASTIC STRAIN
C                      AT NODE K,J AT START OF TIME STEP (UNITLESS)
C                      USED ONLY WHEN KFLG = 1.
C       STRNR(K,J) = INPUT RADIAL COMPONENT OF TRUE PLASTIC STRAIN
C                      AT NODE K,J AT START OF TIME STEP (UNITLESS)
C                      USED ONLY WHEN KFLG = 1.
C       STRNL(K,J) = INPUT EFFECTIVE TRUE PLASTIC STRAIN AT NODE K,J
C                      AT START OF TIME STEP (UNITLESS). USED
C                      ONLY WHEN KFLG = 1
C       CTEMP(K,J) = INPUT CLADDING TEMPERATURE AT NODE K,J AT MIDPOINT
C                      OF PREVIOUS TIME STEP. USED ONLY IF KFLG = 1.
C       KNTCT      = INPUT FUEL - CLADDING CONTACT INDEX AT END OF
C                      PREVIOUS TIME STEP.  USED ONLY IF KFLG = 1.
C                         0  NO CONTACT
C                         1  CONTACT DUE TO BOWING
C       KFAIL      = INPUT FAILURE INDEX.  BALOON DOES NOTHING BUT
C                      RETURN IF KFAIL IS NOT EQUAL TO 0
C
C       COMMON BLOCK/MATPRC/STORES MATPRO PARAMETERS USED TO DETERMINE
C       CLADDING MATERIAL PROPERTIES
C
        COMMON /MATPRC/ AMATPC(1) ,
     # FNCK1(1    ) , FNCN1(1    ), CWKF1(1    ) , CWNF1(1    ),
     # COBAA1(1    ), COBAB1(1    ), COBAC1(1    ),
     # COBAD1(1    ), COBAE1(1    ), COBAF1(1    ), COBAG1(1    ),
     # COBAH1(1    ), COBAI1(1    ), DOXCFR(1    ), WOXC(1    ),
     # EMETWA(1    ), DAOXFR(1), DTMPCL , CANRIN, KAXMTP
C
C       ARRAYS IN COMMON BLOCK  /MATPRC/ ARE INDEXED WITH AXIAL NODE
C
C       FNCK1    = EFFECTIVE FAST FLUENCE FOR STRENGTH COEFFICIENT (N/M**2)
C       FNCN1    = EFFECTIVE FAST FLUENCE FOR STRAIN HARDENING EXPONENT
C                  (N/M**2)
C       CWKF1    = EFFECTIVE COLD WORK FOR STRENGTH COEFFICIENT (AO-A)/AO
C       CWNF1    = EFFECTIVE COLD WORK FOR STRAIN HARDENING EXPONENT
C                  (AO-A)/A
C
C       COBAA1 THRU COBAI1 OXYGEN CONCENTRATIONS AT BETA-ALPHA+BETA
C       INTERFACES IN SUBROUTINE COBILD CALCULATIONS
C
C       DOXCFR   = AVERAGE OXYGEN CONCENTRATION IN BETA (WT. FRACTION)
C       DAOXFR   = AVERAGE OXYGEN CONCENTRATION IN ALPHA (WT. FRACTION)
C       WOXC     = TOTAL OXYGEN UPTAKE (KG/M**2)
C       EMETWA   = HEAT GENERATED BY ZR-H2O REACTION   (W/M)
C       DTMPCL   = MAXIMUM CIRCUMFERENTIAL VARIATION IN CLADDING TEMPERA-
C                  TURE (K)
C       CANRIN   = CONTRACTILE STRAIN RATIO DURING UNIAXIAL TENSILE TEST.
C                  CIRCUMFERENTIAL STRAIN/RADIAL STRAIN
C       KAXMTP   = AXIAL NODE NUMBER
C       COMMON BLOCK/BLN/ STORES INFORMATION NEEDED TO RESTART BALOON
C
        COMMON /BLN/ KSUB(1),DZO(1,16),TSTPO(1),CWKF2(1,1,1),
     # CWNF2(1,1,1),FNCK2(1,1,1),FNCN2(1,1,1),FCP2(1,1,1),
```

```
     # FRP2(1,1,1),FAP2(1,1,1),ACD2(1,1,1),AAD2(1,1,1),
     # ARD2(1,1,1)
C
C      KSUB(I)       = NUMBER OF SUBCODES USED WITHIN THE I TH AXIAL
C                        NODE OF FRAP (UNITLESS)
C      DZO(I,K)      = INITIAL LENGTH OF K TH SUB-NODE OF THE I TH
C                        AXIAL NODE OF FRAP (M)
C      TSTPO(I)      = PREVIOUS TIME STEP SIZE (S)
C      CWKF2(I,K,J)  = EFFECTIVE COLD WORK FOR STRENGTH COEFFICIENT
C                         AT FRAP AXIAL NODE I, BALOON AXIAL SUB-NODE K
C                         AND AZIMUTHAL SUB-NODE J
C                         (UNITLESS)
C      CWNF2(I,K,J)  = EFFECTIVE COLD WORK FOR STRAIN HARDENING EXPONENT
C                         AT FRAP AXIAL NODE I, BALOON AXIAL SUB-NODE K
C                         AND AZIMUTHAL SUB-NODE J
C                         (UNITLESS)
C      FNCK2NI,K,J)  = EFFECTIVE FAST NEUTRON FLUENCE FOR STRENGTH COEFF
C                         AT FRAP AXIAL NODE I, BALOON AXIAL SUB-NODE K
C                         AND AZIMUTHAL SUB-NODE J
C                         (NEUTRONS/M**2)
C      FNCN2(I,K,J)  = EFFECTIVE FAST NEUTRON FLUENCE FOR STRAIN
C                         HARDENING EXPONENT AT FRAP AXIAL NODE I,
C                         BALOON AXIAL SUBNODE K AND AZIMUTHAL SUB-NODE J
C                         (NEUTRONS/M**2)
C      FCP2(I,K,J)   = VOLUME WEIGHTED AVERAGE COSINE OF THE ANGLE
C                         BETWEEN CLADDING BASAL POLES AND THE TANGENTIAL
C                         DIRECTION AT FRAP AXIAL NODE I, BALOON AXIAL
C                         SUB-NODE K AND AZIMUTHAL SUB-NODE J
C      FRP2(I,K,J)   = VOLUME WEIGHTED AVERAGE COSINE OF THE ANGLE
C                         BETWEEN CLADDING BASAL POLES AND THE RADIAL
C                         DIRECTION AT FRAP AXIAL NODE I, BALOON AXIAL
C                         SUB-NODE K AND AZIMUTHAL SUB-NODE J
C      FAP2(I,K,J)   = VOLUME WEIGHTED AVERAGE COSINE OF THE ANGLE
C                         BETWEEN CLADDING BASAL POLES AND THE AXIAL
C                         DIRECTION AT FRAP AXIAL NODE I, BALOON AXIAL
C                         SUB-NODE K AND AZIMUTHAL SUB-NODE J
C      ACD2(I,K,J)   = HIGH TEMPERATURE STRAIN AXISOTROPY COEFFECIENT
C                         AT FRAP AXIAL NODE I, BALOON AXIAL SUB-NODE K
C                         AND AZIMUTHAL SUB-NODE J
C      AAD2(I,K,J)   = HIGH TEMPERATURE STRAIN AXISOTROPY COEFFECIENT
C                         AT FRAP AXIAL NODE I, BALOON AXIAL SUB-NODE K
C                         AND AZIMUTHAL SUB-NODE J
C      ARD2(I,K,J)   = HIGH TEMPERATURE STRAIN AXISOTROPY COEFFECIENT
C                         AT FRAP AXIAL NODE I, BALOON AXIAL SUB-NODE K
C                         AND AZIMUTHAL SUB-NODE J
C                         SEE SUBROUTINE LISTING FOR RELATION BETWEEN
C                         ACD2, AAD2,ARD2, STRAIN COMPONENTS AND EFFECTIVE
C                         STRAIN
C
       DIMENSION HTCS(16,16),TSTM(16,16),QL(16,16)
       DIMENSION DELZ(16,16),TWALL(16,16),RAD(16,16),CTEMP(16,16)
       DIMENSION DELOXY(16,16)
       DIMENSION FTEMP(16,16),STEMP(16,16)
```

```
      DIMENSION ACS(16,16),AAS(16,16),ARS(16,16)
      DIMENSION ACE(16,16),AAE(16,16),ARE(16,16)
      DIMENSION ACD(16,16),AAD(16,16),ARD(16,16)
      DIMENSION FCP(16,16),FRP(16,16),FAP(16,16)
      DIMENSION STRNC(16,16),STRNR(16,16),STRNA(16,16),STRNL(16,16)
      DIMENSION RTEMP(16,16),RSTRAN(16,16)
      DIMENSION DBYTH(16,16),DBYZ(16,16)
      DIMENSION RAVE(16)
      DIMENSION STRESR(16),STRESA(16),STRESF(16,16),TSTRES(16,16)
      DIMENSION FNCK(16,16),FNCN(16,16),CWKF(16,16),CWNF(16,16)
      DIMENSION GMIX(10)
      DIMENSION TM(20),TMTT(16,16,20),TMP(20),TPIT(20),TPOT(20)
      DIMENSION DEH(16),DEA(16)
      DIMENSION DISP(16,16),RADC(16),RADR(16)
C
C     THE EQUATIONS USED IN THIS SUBROUTINE ARE BASED ON
C     RESULTS DISCUSSED IN
C     (1) J. M. KRAMER AND L. W. DEITRICH, CLADDING FAILURE BY
C         LOCAL PLASTIC INSTABILITY, ANL-77-95 (DECEMBER 1977)
C     (2) L. J. SIEFKEN, ET. AL., FRAP-T5 A COMPUTER CODE FOR THE
C         TRANSIENT ANALYSIS OF OXIDE FUEL RODS, TREE-1281 AND
C         NUREG/CR-0840  (JUNE 1979)
C
C     THE FOLLOWING SUBCODES ARE CALLED IN THIS SUBROUTINE
C     CANISO OF JULY 1979
C     CSTRNI OF OCTOBER 1978
C     CANEAL OF JUNE 1978
C     CMLIMT OF FEBRUARY 1980
C     CELMOD OF DECEMBER 1977
C     CKMN OF OCTOBER 1978
C     CCP OF FEBUARY 1980
C     POLATE OF TO BE PUBLISHED
C     GTHCON OF OCTOBER 1979
C
C
C     CODED BY J. A. DEARIEN
C     MODIFIED BY D. L. HAGRMAN DECEMBER 1980
C
C
C     AN MODIFIED FOR SMALL STRAINS OPTION IN CSTRNI
C
C
C     THE FOLLOWING ARE DUMMY ARGUMENTS FOR CMLIMT
      CINWID = 1.2E-04
      CINRAD = 1.0E-02
      CAXRAD = 1.0E+03
      CAXSTR = 1.0E+06
      DELTMP = 50.
C
C     NJ = NUMBER OF CIRCUMFERENTIAL NODES USED
      NJ = 16
      ND = NJ/2
      M1 = ND + 1
```

TABLE B-1. (CONTINUED)

```
      DELTH = 6.28/NJ
      NJ1 = NJ - 1
      NJ2 = NJ - 2
C
C     CONVERT INPUT TO SI UNITS
      HTCM   = HTNC * 2.044E+04
      TBLKM  = (TBULK + 459.67)/1.8
      QM     = Q * 1.136E+04
      RHTR   = RF * 2.54E-02
      ROUT   = RO * 2.54E-02
      WO     = HO * 2.54E-02
      PO     = PC /1.45E-04
      PI     = PS /1.45E-04
      FAX    = FA * 4.448
      VM     = V * 1.6387E-05
      RBAR = ROUT - 0.5 * WO
      GTEMP = (GTMPF + 459.67)/1.8
C     CONVERT INPUT REQUIRED ONLY FOR INITIALIZATION
C      AND FIND AXIAL SUB-NODE LENGTHS
      IF(KFLG .GT. 0) GO TO 20
      FR = 0.0
      TCLO   = (TCLI + 459.67)/1.8
      TFLO   = (TFLI + 459.67)/1.8
      RAI    = RMP * 2.54E-02
      ZBLNN = ZBALN * 2.54E-02
      NK = 18
    5 NK = NK - 2
      IF((ZBLNN - (5.0E-03 * (NK - 4) )) .LE. 0.) GO TO 5
      IF(NK .LT. 4) NK = 4
      KSUB(KBALN) = NK
      NK1 = NK - 1
      NK2 = NK - 2
      DZO(KBALN,1) = (ZBLNN - (5.0E-03 * (NK - 4)))/4.
      DZO(KBALN,2) = DZO(KBALN,1)
      DZO(KBALN,NK1) = DZO(KBALN,1)
      DZO(KBALN,NK)  = DZO(KBALN,1)
      IF(NK .EQ. 4) GO TO 15
      DO 10 K=3,NK2
   10 DZO(KBALN,K) = 5.0E-03
   15 CONTINUE
      DELTO = TSTP
C     CONVERT INPUT REQUIRED ONLY FOR UPDATES
C     SET NK EQUAL TO NUMBER OF AXIAL SUB-NODES
   20 IF(KFLG .LT. 1) GO TO 40
      NK = KSUB(KBALN)
      DELTO = TSTPO(KBALN)
      DO 30 K=1,NK
      DO 30 J=1,NJ
      DELZ(K,J) = DELZ(K,J) * 2.54E-02
      RAD(K,J) = RAD(K,J) * 2.54E-02
      TWALL(K,J) = TWALL(K,J) * 2.54E-02
C     FNCK(K,J) = FNCK2(KBALN,K,J)
C     FNCN(K,J) = FNCN2(KBALN,K,J)
```

```
C       CWKF(K,J)  =  CWKF2(KBALN,K,J)
C       CWNF(K,J)  =  CWNF2(KBALN,K,J)
C       FCP(K,J)   =  FCP2(KBALN,K,J)
C       FRP(K,J)   =  FRP2(KBALN,K,J)
C       FAP(K,J)   =  FAP2(KBALN,K,J)
C       ACD(K,J)   =  ACD2(KBALN,K,J)
C       AAD(K,J)   =  AAD2(KBALN,K,J)
C       ARD(K,J)   =  ARD2(KBALN,K,J)
        FTEMP(K,J) =  (FTEMP(K,J)  + 459.67)/1.8
C        QL(K,J) = QL(K,J)  * 1.136E+04
        STEMP(K,J) =  (STEMP(K,J)  + 459.67)/1.8
     30 CTEMP(K,J) =  (CTEMP(K,J)  + 459.67)/1.8
     40 CONTINUE
C
        DO 50 K=1,NK
        DO 50 J=1,NJ
C       ALLOW FOR FUTURE INPUT OF SPACE VARYING PARAMETERS
        HTCS(K,J) = HTCM
        TSTM(K,J) = TBLKM
        RSTRAN(K,J) = 1.0E-02
     50 DELOXY(K,J) = DOXCFR(KBALN)
C
C       SET UP QUANTITIES REQUIRED FOR EACH CALL
        CDPRES = PI - PO
        DTIME = 0.0
        NSTEP = 0
C       CLADDING DENSITY FROM WCAP-3269-41 (CONVERTED TO KG/(M**3))
        CDENS = 6.55E+03
C       ZBEND IS THE BENDING RADIUS ASSUMED TO ESTIMATE CLADDING BENDING
        ZBEND = 1.0E-01
C
        MAX = 600
C       INITIALIZE ASSUMENG A THETA INVARIENT INITIAL GEOMETRY
C       AND TEMPERATURE
C       NOTE NO SYMMETRY BREAK IN HERE YET
        IF(KFLG .EQ. 1) GO TO 100
C        KAN IS A SWITCH TO AVOID LONG TIMES AT PREINSTABILITY STRAINS
        KAN = 0
C
        KFAIL = 0
        KNTCT = 0
        DO 60 K=1,NK
        DO 60 J=1,NJ
        CTEMP(K,J) = TCLO
C        QL(K,J) = QM
        FTEMP(K,J) = TFLO
        DELZ(K,J)  = DZO(KBALN,K)
C       THE FOLLOWING TEXTURE INITIALIZATIONS ARE TEMPORARY
C       AND FOR TYPICAL CLADDING ONLY
C       THE PARAMETERS SHOULD BE PASSED INTO BALOON WHEN FRAP
C       MODELS THE EFFECT OF DEFORMATION ON ANISOTROPY USING
C       THE MATRPO SUBROUTINE CANISO
        FCP(K,J) = 0.28
```

```
      FRP(K,J) = 0.66
      FAP(K,J) = 0.06
      ACD(K,J) = 0.5
      AAD(K,J) = 0.5
      ARD(K,J) = 0.5
C     SET UP INITIAL COLD WORKS AND FLUENCES
      FNCK(K,J) = FNCK1(KBALN)
      FNCN(K,J) = FNCN1(KBALN)
      CWKF(K,J) = CWKF1(KBALN)
      CWNF(K,J) = CWNF1(KBALN)
C     SET UP INITIAL STRAINS, DIMENSIONS
      STRNC(K,J) = ALOG(RAI/(ROUT - 0.5 * WO))
      IF(STRNC(K,J) .LT. 1.0E-06) STRNC(K,J) = 1.0E-06
      STRNA(K,J) = 0.0
      STRNR(K,J) = -STRNC(K,J)
      RAD(K,J) = RAI
      TWALL(K,J) = WO *  EXP(STRNR(K,J))
      CALL CANISO(STRNC(K,J),STRNA(K,J),STRNR(K,J),CTEMP(K,J),FCP(K,J)
     #,FAP(K,J),FRP(K,J),ACD(K,J),AAD(K,J),ARD(K,J),ACS(K,J),AAS(K,J),A
     #RS(K,J),ACE(K,J),AAE(K,J),ARE(K,J))
      SQ = ACE(K,J)*((AAE(K,J)*STRNC(K,J)-ARE(K,J)*STRNA(K,J))**2)  +
     # AAE(K,J)*((ARE(K,J)*STRNA(K,J) -  ACE(K,J)*STRNR(K,J)   )**2)  +
     # ARE(K,J)*((ACE(K,J)*STRNR(K,J) - AAE(K,J)*STRNC(K,J) )**2)
      IF(SQ .LT. 1.0E-20) STRNL(K,J) = 0.0
      IF(SQ .GE. 1.0E-20) STRNL(K,J) = (SQ**0.5)/(ACE(K,J)*AAE(K,J) +
     # AAE(K,J)*ARE(K,J) + ARE(K,J)*ACE(K,J))
   60 CONTINUE
C     CONSTRUCT TIME - TEMPERATURE TABLES FOR MODE 2 ONLY
      IF(MODE .NE. 2) GO TO 100
      READ 901,NTTTP
  901 FORMAT(I10)
C     NTTTP IS NUMBER OF TIME - TEMPERATURE PAIRS TO BE READ IN
C     FOR THE MODE 2 TABLE.  NOTE 16 AXIAL NODES ARE READ IN NO MATTER
C     WHAT NK IS AND NOTE DIMENSIONING LIMITS NTTTP TO 20
      PRINT 919
  919 FORMAT(/23H TIME-TEMPERATURE PAIRS)
      DO 98 M=1,NTTTP
      READ 902,TM(M)
      DO 62 J=4,NJ,4
      READ 903,(TMTT(K,J,M),K=1,8)
      READ 903,(TMTT(K,J,M),K=9,16)
  902 FORMAT(E10.2)
  903 FORMAT(8E10.2)
   62 CONTINUE
C     PRINT TIME-TEMPERATURE PAIRS
      PRINT 920,TM(M)
  920 FORMAT(//7H TIME =,E12.5//)
      DO 63 J=4,NJ,4
   63 PRINT 906,(TMTT(K,J,M),K=1,8)
      PRINT 907
      DO 64 J=4,NJ,4
   64 PRINT 906,(TMTT(K,J,M),K=9,16)
C     INTERPOLATE AROUND CIRCUMFERENCE
```

```
      DO 98 K=1,NK
      DO 92 J=1,3
   92 TMTT(K,J,M) = (TMTT(K,16,M)*(4-J) + TMTT(K,4,M)*J)/4.
      DO 94 J=5,7
   94 TMTT(K,J,M) = (TMTT(K,4,M)*(8-J) + TMTT(K,8,M)*(J-4))/4.
      DO 96 J=9,11
   96 TMTT(K,J,M) = (TMTT(K,8,M)*(12-J) + TMTT(K,12,M)*(J-8))/4.
      DO 98 J=13,15
   98 TMTT(K,J,M) = (TMTT(K,12,M)*(16-J) + TMTT(K,16,M)*(J-12))/4.
      READ 901,NTPTP
C     NTPTP IS NUMBER OF TIME - PRESSURE PAIRS TO BE READ IN
C     FOR THE MODE 2 TABLE
      DO 99 M=1,NTPTP
      READ 904,TMP(M),TPIT(M),TPOT(M)
  904 FORMAT(3E10.2)
   99 CONTINUE
C     PRINT TIME - PRESSURE TRIPLETS
      PRINT 921
  921 FORMAT(/43H TIME-PRESSURE TRIPLETS-TIME INSIDE OUTSIDE)
      DO 65 M=1,NTPTP
   65 PRINT 922,TMP(M),TPIT(M),TPOT(M)
  922 FORMAT(10X,3E15.5)
C
  100 NSTEP = NSTEP + 1
      IF(NSTEP .GE. MAX) GO TO 890
      IF(KFAIL .GT. 0) GO TO 1000
      IF(MODE .LT. 5) GO TO 105
C     ESTIMATE PRESSURE DECREASE DUE TO EXPANSION
      PI = PS*100./((1.45E-04)*(97.+3.*((RAVE(8)-4.699E-03)
     # / (5.1308E-03 - 4.699E-03))))
      COPRES = PI - PO
  105 CONTINUE
C     FIND LOCAL STRESS AND MAXIMUM TIME STEP SIZE
C     FIRST FIND AZMUTHAL RADII OF CURVATURE
C     IF(FR .LT. 1.0E-02) GO TO 225
C     DO 220 K=1,NK
C     DBYTH(K,1) = ( RAD(K,3)    + RAD(K,NJ1) + 2.0 *( RAD(K,2) +
C    # RAD(K,NJ)   ) - 6.0 * RAD(K,1) ) / (6.0 * (DELTH**2) )
C     DBYTH(K,2) = ( RAD(K,4)    + RAD(K,NJ)   + 2.0 *( RAD(K,3) +
C    # RAD(K,1)    ) - 6.0 * RAD(K,2) ) / (6.0 * (DELTH**2) )
C     DBYTH(K,NJ1)=( RAD(K,1)    + RAD(K,NJ1-2)+2.0 *(RAD(K,NJ) +
C    # RAD(K,NJ2) ) - 6.0 * RAD(K,NJ1))/ (6.0 * (DELTH**2) )
C     DBYTH(K,NJ) =( RAD(K,2)    + RAD(K,NJ2) + 2.0 *( RAD(K,1) +
C    # RAD(K,NJ1) ) - 6.0 * RAD(K,NJ) )/ (6.0 * (DELTH**2) )
C     DO 220 J = 3,NJ2
C 220 DBYTH(K,J) = ( RAD(K,J+2) + RAD(K,J-2) + 2.0 *( RAD(K,J+1) +
C    # RAD(K,J-1) ) - 6.0 * RAD(K,J) ) / (6.0 * (DELTH**2) )
C 225 CONTINUE
C     FIND AXIAL RADII OF CURVATURE
      NK1 = NK - 1
      DO 260 J =1,NJ
C     ASSUME TOP AND BOTTOM AXIAL NODES HAVE A VIRTUAL NEIGHBOR
C     WITH A RADIUS THAT PRESERVES THE SLOPE
```

```
      DBYZ(1,J) = 0.0
      DBYZ(NK,J) = 0.0
      DO 260 K=2,NK1
  260 DBYZ(K,J) = 8.0 * ((RAD(K+1,J) - RAD(K,J))/(DZO(KBALN,K+1) +
     # DZO(KBALN,K)) - (RAD(K,J) - RAD(K-1,J))/(DZO(KBALN,K) +
     # DZO(KBALN,K-1)) )/(DZO(KBALN,K+1) + 2.0 * DZO(KBALN,K) +
     # DZO(KBALN,K-1))
C     FIND STRESS COMPONENTS
C     FIND AVERAGE THICKNESS, INSIDE AND OUTSIDE RADII
      DO 308 K=1,NK
      T = 0.0
      R = 0.0
      DO 305 J=1,NJ
      R = R + EXP(STRNC(K,J))
  305 T = T + TWALL(K,J)
      RAVE(K) = R*RBAR/NJ
      TWALA = T/NJ
      RI = RAVE(K) - (TWALA/2.)
      RO = RAVE(K) + (TWALA/2.)
      STRESR(K) = -(PI*RI + PO*RO)/(RI + RO)
      STRESA(K) = (PI*RI*RI - PO*RO*RO + FAX/3.14)/(RO*RO - RI*RI)
C     IF(FR .LT. 1.0E-02) GO TO 306
C     DO 300 J=1,NJ
C 300 STRESF(K,J)    = CDPRES * RAD(K,J) / TWALA
C    #  - RAVE(K) * CDPRES * (TWALL(K,J) - TWALA)/(TWALA * TWALA)
C    # + RAVE(K) * STRESA(K)    * DBYZ(K,J) / (( EXP(STRNA(K,J)))**2)
C    #  + CDPRES * DBYTH(K,J) / TWALA - (PI + PO)/2.
C     GO TO 308
  306 DO 307 J=1,NJ
  307 STRESF(K,J) = CDPRES * RAVE(K)/TWALA
     # - RAVE(K) * CDPRES * (TWALL(K,J) - TWALA)/(TWALA * TWALA)
     # + RAVE(K) * STRESA(K) * DBYZ(K,J) / (( EXP(STRNA(K,J)))**2)
     # - (PI + PO)/2.
  308 CONTINUE
C     DETERMINE SIZE OF POSSIBLE TIME STEP SUBDIVISION
C
C     CALCULATE CLADDING TEMPERATURES USING CONSTANT HEAT FLUX
C     ASSUMPTION
C
C     START BY DETERMINING THE MAXIMUM SIZE OF THE TIME STEP
C     USING NEW DIMENSIONS AND NEW STRESS BUT OLD TEMPERATURES
C
C     IF OUTSIDE PRESSURE IS NOT LESS THAN INSIDE PRESSURE SKIP
C     TO DEFORMATION CALCULATIOIN
      IF(CDPRES .LE. 0) GO TO 415
C
C
      TIMAX = TSTP - DTIME
      IF(KNTCT .EQ. 1 .AND. TIMAX .GT. 1.00) TIMAX = 1.00
      DO 320 K=1,NK
      DO 320 J=1,NJ
      CALL CKMN(CTEMP(K,J),DELOXY(K,J),FNCK(K,J),FNCN(K,J),
     #  CWKF(K,J),CWNF(K,J),RSTRAN(K,J),AK,AN,AM)
```

```
C      MODIFICATION TO AVOID LONG TIME STEPS AT PRE INSTABILITY STRAINS
C      NOT NEEDED IN FRAT T BECAUSE FRAP T DOESNT CALL UNTIL AFTER
C      AFTER INSTABILITY STRAIN
       IF(STRNC(K,J) .GE. (AN/(1. +AM))) KAN = 1
       IF(KAN .LT. 1) GO TO 315
       IF(STRNC(K,J) .LT. (AN/(1. + AM))) AN = AN * AN / ((1. + AM)
     #* STRNC(K,J))
       ANL = 0.17
C      IF(CTEMP(K,J) .GT. 730.) ANL = 1.56E-02 * CTEMP(K,J) - 11.218
C      IF(CTEMP(K,J) .GE. 780.) ANL = 0.95
       IF(AN .GT. ANL) AN = ANL
   315 IF(STRESF(K,J) .LT. ((STRNC(K,J)**AN)*AK)) GO TO 320
       TITEST = (((STRNC(K,J)**AN)*AK/STRESF(K,J))**(1.0/AM ))
     # * 10.0
       IF(CTEMP(K,J) .GT. 1090. .AND. CTEMP(K,J) .LT. 1255.)
     #TITEST = TITEST * 5.0
       IF(TITEST .LT. TIMAX) TIMAX = TITEST
   320 CONTINUE
       DELT = TIMAX
       IF(DELT .LT. 5.0E-04) DELT = 5.0E-04
       DTCR = (DELT + DELTO)/2.0
       DELTO = DELT
C
C      SELECT UPDATE MODE FOR TEMPERATURES
C
       IF(MODE .GT. 0) GO TO 340
C      GET NEW TEMPERATURES USING TIME STEP JUST SELECTED
C      AND CONSTANT-FUEL-SURFACE-HEAT-FLUX ASSUMPTION
       DO 330 K=1,NK
       DO 330 J=1,NJ
       CTEMPO = CTEMP(K,J)
       CP = CCP(CTEMP(K,J))
       RTMC = HTCS(K,J)/(CDENS * CP * TWALL(K,J))
       TSS = (QL(K,J) * RHTR + HTCS(K,J) * RAD(K,J) * TSTM(K,J))
     # /HTCS(K,J) * RAD(K,J)
       CTEMP(K,J) = CTEMP(K,J) *  EXP(-(RTMC * DTCR))
     #   + TSS * (1. - EXP(-(RTMC * DTCR)))
   330 RTEMP(K,J) = (CTEMP(K,J) - CTEMPO) / DTCR
       TIMET = TIMET + DELT
       GO TO 397
C
C       GET NEW TEMPERATURES USING TIME STEP JUST SELECTED
C       AND CONSTANT-FUEL-SURFACE-TEMPERATURE ASSUMPTION
   340 IF(MODE .GT. 1) GO TO 360
       DO 350 K=1,NK
       DO 350 J=1,NJ
       CTEMPO = CTEMP(K,J)
       GPTHK = RAD(K,J) - TWALL(K,J) / 2. - RHTR
       CP = CCP(CTEMP(K,J))
       CVT = CP * CDENS / DTCR
       HTCG = GTHCON(GMIX,GTEMP,PI,GPTHK)
       HTCG = HTCG + 0.8 * 5.67E-08 * (FTEMP(K,J) + CTEMP(K,J))
     # * (FTEMP(K,J)*FTEMP(K,J) + CTEMP(K,J)*CTEMP(K,J))
```

```
C       HTCG MODIFICATION IS RADIATION HEAT TRANSFER HEATER TO CLADDING
C
C       HTCR IS EFFECTIVE HEAT TRANSFER COEFF TO SHROUD BY RADIATION
        HTCR = 0.4 * 5.67E-08 * (CTEMP(K,J) + STEMP(K,J))
       # * (CTEMP(K,J)*CTEMP(K,J) + STEMP(K,J)*STEMP(K,J))
        CTEMP(K,J) = (HTCG * FTEMP(K,J) + HTCS(K,J) * TSTM(K,J)
       #  + CVT * TWALL(K,J) * CTEMP(K,J) + HTCR*STEMP(K,J))
       #  /(HTCG + HTCS(K,J) + CVT*TWALL(K,J) + HTCR)
   350  RTEMP(K,J) = (CTEMP(K,J) - CTEMPO) / DTCR
        TIMET = TIMET + DELT
        GO TO 397
C       GET NEW TEMPERATURES USING TIME - TEMPERATURE TABLE READ
C       IN DURING INITIALIZATION
C
   360  IF(MODE .GT. 2) GO TO 400
        TIMEM = TIMET + DELT/2.
        TIMET = TIMET + DELT
        NTM = 1
        DO 365 M=1,NTTTP
   365  IF(TM(M) .LT. TIMEM) NTM = NTM + 1
        NTM = NTM - 1
        IF(NTM .GE. NTTTP) GO TO 375
        XFR = (TIMEM - TM(NTM)) / (TM(NTM+1) - TM(NTM))
        DO 370 K=1,NK
        DO 370 J=1,NJ
        CTEMPO = CTEMP(K,J)
        CTEMP(K,J) = TMTT(K,J,NTM) + (TMTT(K,J,NTM+1) - TMTT(K,J,NTM))
       # * XFR
   370  RTEMP(K,J) = (CTEMP(K,J) - CTEMPO) / DTCR
        GO TO 385
   375  DO 380 K=1,NK
        DO 380 J=1,NJ
   380  CTEMP(K,J) = TMTT(K,J,NTTTP)
C
   385  NTM = 1
        DO 390 M=1,NTPTP
   390  IF(TMP(M) .LT. TIMEM) NTM = NTM + 1
        NTM = NTM - 1
        IF(NTM .GE. NTPTP) GO TO 395
        XFR = (TIMEM - TMP(NTM)) / (TMP(NTM+1) - TMP(NTM))
        PO = TPOT(NTM) + (TPOT(NTM+1) - TPOT(NTM)) * XFR
        PI = TPIT(NTM) + (TPIT(NTM+1) - TPIT(NTM)) * XFR
        CDPRES = PI - PO
        GO TO 397
   395  PI = TPIT(NTPTP)
        PO = TPOT(NTPTP)
        CDPRES = PI - PO
C
C       FIND ANNEALING AND OXIDATION EFFECTS FOR MODES 0 TO 2
C
   397  IF(MODE .GT. 2) GO TO 399
        DO 398 K=1,NK
        DO 398 J=1,NJ
```

```
C         OXIDATION IGNORED FOR NOW
          TSTART = CTEMP(K,J) - (RTEMP(K,J) * DTCR)
  398     CALL CANEAL(CFLUX,DTCR,TSTART,RTEMP(K,J),FNCK(K,J),FNCN(K,J),
         # CWKF(K,J),CWNF(K,J))
  399     IF(MODE .GT. 2) TIMET = TIMET + DELT
C
C          PRINT START-OF-STEP INFORMATION IF DESIRED
C
  400     IF(NPRINT .EQ. 0) GO TO 405
          PRINT 905,NSTEP,DELT,TIMET,CDPRES
  905     FORMAT(//30H                    TIME STEP    ,I3,14H       DURATION,
         #E16.5,4H SEC,10H       NET =,E15.4,16H PRESSURE DIFF =,E15.5)
          IF(NPRINT .LT. 2) GO TO 405
          PRINT 917
  917     FORMAT(/99H             TEMPERATURES DURING TIME STEP -- AXIAL NODES
         #ACROSS  CIRCUMFERENTIAL NODES DOWN THE TABLE//)
          PRINT 906,((CTEMP(K,J),K=1,8),J=1,NJ)
  906     FORMAT(8E16.5)
          PRINT 907
  907     FORMAT (3H    )
          PRINT 906,((CTEMP(K,J),K=9,16),J=1,NJ)
          PRINT 908
  908     FORMAT(/55H             TANGENTIAL STRESS COMPONENTS DURING TIME STEP
         #//)
          PRINT 906,((STRESF(K,J),K=1,8),J=1,NJ)
          PRINT 907
          PRINT 906,((STRESF(K,J),K=9,16),J=1,NJ)
          IF(NPRINT .LT. 3) GO TO 405
          PRINT 913
  913     FORMAT(/51H             COLD WORK FOR STRENGTH DURING TIME STEP   //)
          PRINT 906,((CWKF(K,J),K=1,8),J=1,NJ)
          PRINT 907
          PRINT 906,((CWKF(K,J),K=9,16),J=1,NJ)
          PRINT 909
  909     FORMAT(/67H             COLD WORK FOR STRAIN HARDENING EXPONENT DURIN
         #G TIME STEP //)
          PRINT 906,((CWNF(K,J),K=1,8),J=1,NJ)
          PRINT 907
          PRINT 906,((CWNF(K,J),K=9,16),J=1,NJ)
          IF(NPRINT .LT. 4) GO TO 405
          PRINT 915
  915     FORMAT(/60H             FAST NEUTRON FLUENCE FOR STRENGTH DURING TIME
         # STEP//)
          PRINT 906,((FNCK(K,J),K=1,8),J=1,NJ)
          PRINT 907
          PRINT 906,((FNCK(K,J),K=9,16),J=1,NJ)
          PRINT 916
  916     FORMAT(/77H             FAST NEUTRON FLUENCE FOR STRAIN HARDENING EXP
         #ONENT DURING TIME STEP//)
          PRINT 906,((FNCN(K,J),K=1,8),J=1,NJ)
          PRINT 907
          PRINT 906,((FNCN(K,J),K=9,16),J=1,NJ)
          IF(KFAIL .NE. 1) GO TO 405
```

```
      DO 402 K=1,NK
      T = 0.0
      R = 0.0
      DO 401 J=1,NJ
      R = R + EXP(STRNC(K,J))
  401 T = T + TWALL(K,J)
      RAVE(K) = R*RBAR/NJ
      TAVE = T/NJ
      TCE = (RAVE(K) - RBAR)/RBAR
      PRINT 911,K,RAVE(K),TAVE,KNTCT,TCE
  402 PRINT 912,(J,RAD(K,J),TWALL(K,J),DELZ(K,J),J=1,NJ)
  405 CONTINUE
C
C       TEST FOR FAILURE
C
      IF(KFAIL .GT. 0) GO TO 800
      DO 410 K=1,NK
      DO 410 J=1,NJ
      CALL CMLIMT(CTEMP(K,J),DELOXY(K,J),FNCK(K,J),FNCN(K,J),
     # CWKF(K,J),CWNF(K,J),CINWID,CINRAD,CDPRES,CAXRAD,CAXSTR,
     # RSTRAN(K,J),DELTMP,DUM1,DUM2,DUM3,DUM4,DUM5,DUM6,DUM7,
     # DUM8,DUM9,DUM10,DUM11,CTSTRT)
      IF(STRESF(K,J).GE.CTSTRT) KFAIL = 1
      IF(NPRINT .EQ. 0) GO TO 410
      IF(K .EQ. 8 .AND. J .EQ. 4) PRINT 918,STRESF(8,4),CTSTRT
      IF(STRESF(K,J).LT.CTSTRT) GO TO 410
      PRINT 910,J,K,STRESF(K,J),CTSTRT
  910 FORMAT(53H  FAILED DUE TO LOCAL STRESS AT CIRCUMFERENTIAL NODE ,I2
     #,12H AXIAL NODE ,I2,9H STRESS =,E12.5,25H FAILURE STRESS AT NODE =
     #,E12.5)
  410 CONTINUE
  918 FORMAT(/38H            HOOP STRESS AT K=8 J=4 IS = ,E16.6,21H
     #   FAILURE AT ,E16.6,7H N/M**2/)
      IF(KFAIL .GT. 0) NPRINT = 4
      IF(KFAIL .GT. 0) GO TO 400
  415 CONTINUE
      DO 490 K=1,NK
      DO 420 J=1,NJ
C       CALL CANISO FOR TEMPERATURE EFFECT ONLY
      CALL CANISO(0.0,0.0,0.0,CTEMP(K,J),FCP(K,J),FAP(K,J),
     # FRP(K,J),ACD(K,J),AAD(K,J),ARD(K,J),ACS(K,J),AAS(K,J),ARS(K,J),
     # ACE(K,J),AAE(K,J),ARE(K,J))
C       FIND TRUE EFFECTIVE STRESS
      TSTRES(K,J) = (ACS(K,J)*((STRESF(K,J)-STRESA(K))**2)
     #  +AAS(K,J)*((STRESA(K) - STRESR(K))**2)
     #  +ARS(K,J)*((STRESR(K) - STRESF(K,J))**2)
     #  )**0.5
C
C       FIND DEFORMATIONS DURING TIME STEP
C
C      INSERT CREEP-DOWN CALCULATION HERE IF IT IS DESIRED
C
      STRNLL = STRNL(K,J)
```

```
      CALL CSTRNI(DELT,CTEMP(K,J),DELOXY(K,J),FNCK(K,J),FNCN(K,J),
     # CWKF(K,J),CWNF(K,J),TSTRES(K,J),STRNLL)
      IF(STRNLL.LT.STRNL(K,J)) STRNLL = STRNL(K,J)
      DEP = STRNLL - STRNL(K,J)
      RSTRAN(K,J) = DEP/DELT
      DEH(J) = DEP * (ACE(K,J) * (STRESF(K,J) - STRESA(K))
     # + ARE(K,J) * (STRESF(K,J) - STRESR(K)))
     # /TSTRES(K,J)
      DEA(J) = DEP * (AAE(K,J) * (STRESA(K) - STRESR(K))
     # +     ACE(K,J) * (STRESA(K) - STRESF(K,J)))
     # /TSTRES(K,J)
      DER = DEP * (ARE(K,J) * (STRESR(K) - STRESF(K,J))
     # + AAE(K,J) * (STRESR(K) - STRESA(K)))
     # /TSTRES(K,J)
      STRNC(K,J) = STRNC(K,J) + DEH(J)
      STRNA(K,J) = STRNA(K,J) + DEA(J)
      STRNR(K,J) = STRNR(K,J) + DER
      STRNL(K,J) = STRNLL
C       CALL CANISO FOR EFFECT OF DEFORMATION ON TEXTURE
      CALL CANISO(DEH(J),DEA(J),DER,CTEMP(K,J),FCP(K,J),FAP(K,J),
     # FRP(K,J),ACD(K,J),AAD(K,J),ARD(K,J),ACS(K,J),AAS(K,J),ARS(K,J),
     # ACE(K,J),AAE(K,J),ARE(K,J))
C
C       FIND END OF TIME STEP DIMENSIONS
C
      TWALL(K,J) = TWALL(K,J) * EXP(DER)
      RAD(K,J) = RAD(K,J) * EXP(DEH(J))
  420 DELZ(K,J) = DELZ(K,J) * EXP(DEA(J))
      T = 0.0
      R = 0.0
      DO 421 J=1,NJ
      R = R + EXP(STRNC(K,J))
  421 T = T + TWALL(K,J)
      RAVE(K) = R*RBAR/NJ
      TAVE = T/NJ
C       FIND RADIAL DISPLACEMENT DUE TO BENDING
      IF(KNTCT .EQ. 1) GO TO 458
      DO 430 J=1,ND
      M = J + ND
      DISP(K,J) = (DEA(J) - DEA(M) - (STRNA(K,J) - STRNA(K,M)) *
     # (DEH(J) + DEH(M))/2.0) * (ZBEND**2) /
     # ((RAD(K,J) + RAD(K,M)) * 4.0)
  430 DISP(K,M) = -DISP(K,J)
C       ADD BENDING INCREMENT TO RADIUS
      DO 440 J=1,ND
      M = J + ND
      RAD(K,J) = RAD(K,J) + DISP(K,J)
      RMIN = RHTR + (TWALL(K,J) / 2.)
      IF(RAD(K,J).GE.RMIN) GO TO 440
      RAD(K,M) = RAD(K,M) - (RMIN - RAD(K,J))
      KNTCT = 1
      RAD(K,J) = RMIN
  440 CONTINUE
```

```
          DO 450 J=M1,NJ
          M = J - ND
          RAD(K,J) = RAD(K,J) + DISP(K,J)
          RMIN = RHTR + (TWALL(K,J) / 2.)
          IF(RAD(K,J).GE.RMIN) GO TO 450
          RAD(K,M) = RAD(K,M) - (RMIN - RAD(K,J))
          KNTCT = 1
          RAD(K,J) = RMIN
  450     CONTINUE
C         SMOOTH PRE-CONTACT RADII TO COMPENSATE FOR
C         FAILURE OF BENDING MODEL TO CONSIDER AZMUTHAL NEIGHBOR INTERACTIONS
          RADH1 = RAD(K,1)
          RADHL = RAD(K,1)
          RAD(K,1) = (RAD(K,NJ) + RAD(K,1) + RAD(K,2) )/3.
          DO 451 J=2,NJ1
          RADH = RAD(K,J)
          RAD(K,J) = (RADHL + RAD(K,J) + RAD(K,J+1) )/3.
          RADHL = RADH
  451     CONTINUE
          RAD(K,NJ) = (RADHL + RAD(K,NJ) + RADH1 )/3.
C
C         CIRCULAR CROSS SECTION DISPLACEMENT MODEL
          RSML = 10.0
          JMIN = 0
          DO 453 J=1,NJ
          IF(RAD(K,J) .LT. RSML) JMIN = J
  453     IF(RAD(K,J) .LT. RSML) RSML = RAD(K,J)
          JLOK = JMIN
  458     CONTINUE
          DO 454 J=1,NJ
          IF(CTEMP(K,J) .GT. 1172.5) FR = 1.0
  454     RADR(J) = RAD(K,J)
  456     IF(KNTCT .NE. 1) GO TO 457
          JMIN = JLOK
          RSML = RHTR + (TWALL(K,JMIN) * 0.5)
  457     DSPMX = RAVE(K) - RSML
C         FIND ANGLE BETWEEN J AND JMAX THEN CALCULATE
C         DISPLACED CIRCLE RADII
          DO 455 J=1,NJ
          DISPA = 6.28 * (JMIN - J)/NJ
  455     RADC(J) = (RAVE(K)*RAVE(K) - SIN(DISPA)*SIN(DISPA)
         # * DSPMX*DSPMX)**0.5  - COS(DISPA) * DSPMX
C
C          PRINT END OF TIME STEP INFORMATION IF DESIRED
C
C
C         MIX RADIAL DISPLACEMENT AND CIRCULAR SECTION MODELS
C         AS INSTRUCTED BY FR = FRACTION RADIAL DISPLACEMENT MODEL
          DO 460 J=1,NJ
  460     RAD(K,J) = RADC(J)
          IF(NPRINT .EQ. 0) GO TO 490
          TCE = (RAVE(K) - RBAR)/RBAR
          PRINT 911,K,RAVE(K),TAVE,KNTCT,TCE
  911     FORMAT(12H AXIAL NODE ,I2,16H     AVE RADIUS =,E13.6,24H     AVE WAL
```

```
     #L THICKNESS =,E13.6,20H     CONTACT SWITCH =,I2,9H     TCE =,E10.3)
      IF(NPRINT .LT. 2) GO TO 490
      PRINT 912,(J,RAD(K,J),TWALL(K,J),DELZ(K,J),J=1,NJ)
  912 FORMAT(5H  J =,I2,17H MIDWALL RADIUS =,E11.5,17H WALL THICKNESS =,
     #E12.6,7H DELZ =,E12.6)
C
  490 CONTINUE
  500 IF(NSTEP.GE.MAX) GO TO 890
C
C     COMPARE TOTAL TIME SINCE CALL TO INPUT TIME STEP SIZE AND BRANCH
      DTIME = DTIME + DELT
      IF((TSTP - DTIME).GT.0) GO TO 100
C
C     FIND MAX HOOP STRESS FOR FRAIL
      CHSTRS = 0.0
      DO 510 K=1,NK
      DO 510 J=1,NJ
  510 IF(CHSTRS .LT. STRESF(K,J)) CHSTRS = STRESF(K,J)
C
C     STORE COMMON BLOCK INFORMATION FOR NEXT CALL
  800 TSTPO(KBALN) = DELTO
C      DO 810 K=1,NK
C      DO 810 J=1,NJ
C     CWKF2(KBALN,K,J) = CWKF(K,J)
C     CWNF2(KBALN,K,J) = CWNF(K,J)
C     FNCK2(KBALN,K,J) = FNCK(K,J)
C     FNCN2(KBALN,K,J) = FNCN(K,J)
C     FCP2(KBALN,K,J) = FCP(K,J)
C     FRP2(KBALN,K,J) = FRP(K,J)
C     FAP2(KBALN,K,J) = FAP(K,J)
C     ACD2(KBALN,K,J) = ACD(K,J)
C     AAD2(KBALN,K,J) = AAD(K,J)
C 810 ARD2(KBALN,K,J) = ARD(K,J)
C
C     CONVERT OUTPUT FROM SI UNITS TO ENGLISH UNITS
      CHSTRS = CHSTRS * 1.45E-04
      V = VM / 1.6387E-05
      DO 820 K=1,NK
      DO 820 J=1,NJ
      FTEMP(K,J) = FTEMP(K,J) * 1.8 - 459.67
      STEMP(K,J) = STEMP(K,J) * 1.8 - 459.67
C      QL(K,J) = QL(K,J) / 1.136E+04
      CTEMP(K,J) = CTEMP(K,J) * 1.8 - 459.67
      RAD(K,J) = RAD(K,J) / 2.54E-02
      TWALL(K,J) = TWALL(K,J) / 2.54E-02
      DELZ(K,J) = DELZ(K,J) / 2.54E-02
  820 CONTINUE
C
      GO TO 1000
C
C     NOTE MAX-OUT IF IT OCCURED
  890 PRINT 914,MAX
  914 FORMAT(15H     MAX STEPS-,I3,30H- EXCEEDED IN BALOON-2 SUBCODE)
      STOP
 1000 RETURN
      END
```

TABLE B-2. BALON2 CODE DRIVER PROGRAM

```
      PROGRAM PERTB(INPUT,OUTPUT, TAPE 5 = INPUT)
C
C     CODED BY D. L. HAGRMAN AUGUST 1980
C     MODIFIED BY D. L. HAGRMAN DECEMBER 1980
C
      DIMENSION DELZ(16,16),TWALL(16,16),RAD(16,16),CTEMP(16,16)
      DIMENSION FTEMP(16,16),STEMP(16,16),QL(16,16)
      DIMENSION STRNC(16,16),STRNR(16,16),STRNA(16,16),STRNL(16,16)
      DIMENSION GMIX(10)
C
C     FOR INTER-CALL UPDATE ONLY
      DIMENSION DTSURF(16,16)
C
      COMMON /MATPRC/ AMATPC(1) ,
     # FNCK1(1   ) , FNCN1(1   ), CWKF1(1    ) , CWNF1(1    ),
     # COBAA1(1    ), COBAB1(1    ), COBAC1(1    ),
     # COBAD1(1    ), COBAE1(1    ), COBAF1(1    ), COBAG1(1    ),
     # COBAH1(1    ), COBAI1(1    ), DOXCFR(1    ), WOXC(1      ),
     # EMETWA(1    ), DAOXFR(1), DTMPCL , CANRIN, KAXMTP
C
      COMMON /BLN/ KSUB(1),DZO(1,16),TSTPO(1),CWKF2(1,1,1),
     # CWNF2(1,1,1),FNCK2(1,1,1),FNCN2(1,1,1),FCP2(1,1,1),
     # FRP2(1,1,1),FAP2(1,1,1),ACD2(1,1,1),AAD2(1,1,1),
     # ARD2(1,1,1)
      KBALN = 1
      DOXCFR(KBALN) = 0.0
      KSUB(KBALN) = 16
      NK = KSUB(KBALN)
      TSTPO(KBALN) = 1.0
      HTNC = 3.0 / 3600.
      TBULK = 1025.
      TCLI = 620.33
      TFLI = 620.33
      Q = 0.5
      RF  = 0.185
      RO     = 0.215
      HO     = 0.026
      PC     = 14.5
      PS     = 2114.1
      RMP = RO - 0.5 * HO
      CFLUX = 0.0
      FA     = 0.0
      ZBALN = 8./2.54
      KFLG = 0
      MODE = 1
      NPRINT = 0
      GMIX(1) = 1.
      GMIX(2) = 0.
      GMIX(3) = 0.
      GMIX(4) = 0.
      GMIX(5) = 0.
      GMIX(6) = 0.
      GMIX(7) = 0.
```

```
      GMIX(8) = 0.
      GMIX(9) = 0.
      GMIX(10) = 0.
      GTMPF = 620.33
      TIMET = 0.0
      TSTP = 0.3
      FNCK1(KBALN) = 0.0
      FNCN1(KBALN) = 0.0
      CWKF1(KBALN) = 0.50
      CWNF1(KBALN) = 0.04
      V = 1.0
C
C     STEPS FOR INTER-CALL UPDATE ONLY
C     FTRAT = HEATING RATE OF FUEL SURFACE TEMPERATURE (DEGREES F)
      FTRAT = 50. * 1.8
C     THE FOLLOWING 16 STEPS SET UP SYMMETRY BREAKING FRACTIONS
      NJ = 16
      CIRMP = 0.010
      AXAMP = 0.01
      DO 5 K=5,12
      DO 5 J=1,NJ
    5 DTSURF(K,J) = 1.0 + (CIRMP * (1.0 + SIN(6.2832*J/NJ))/2.0)
     # + AXAMP * SIN(3.14159 * (K-4)/8)
      DO 10 J=1,NJ
      DTSURF(1,J) = 1.0
      DTSURF(2,J) = 1.0
      DTSURF(3,J) = 1.0
      DTSURF(4,J) = 1.0
      DTSURF(13,J) = 1.0
      DTSURF(14,J) = 1.0
      DTSURF(15,J) = 1.0
   10 DTSURF(16,J) = 1.0
C
C
      DO 15 K=1,NK
      DZO(KBALN,K) = 8./2.54
      DO 15 J=1,NJ
      FTEMP(K,J) = 621.33
      QL(K,J) = 0
      STEMP(K,J) = 1025.
   15 CONTINUE
      KNTCT = 0
      KFAIL = 0
      N = 1
      PRINT 901,N
      CALL BALON2(HTNC,TBULK,TCLI,TFLI,Q,RF,RO,HO,FTEMP,QL,STEMP,
     #  PC,PS,RMP,CFLUX,FA,KBALN,ZBALN,KFLG,MODE,NPRINT,GMIX,GTMPF,
     #  TIMET,TSTP,V,DELZ,TWALL,RAD,STRNC,STRNA,STRNR,STRNL,CTEMP,
     #  KNTCT,CHSTRS,KFAIL)
      NPRINT = 0
C     BREAK SYMMETRY OF FTEMP(K,J).   FOR MODE = 1
C     BREAK SYMMETRY OF QL(K,J).   FOR MODE = 0
C     SYMMETRY OF CTEMP(K,J) SHOULD BE BROKEN IN A SIMILAR FASHON
```

```
C       FOR MODE = 3.  FAILURE TO DO THIS WILL CAUSE UNREALISTICALLY
C       LARGE STRAINS AT FAILURE
        DO 18 K=1,NK
        DO 18 J=1,NJ
   18   QL(K,J) = Q * DTSURF(K,J)
        KFLG = 1
   20   TSURF = FTRAT * (TIMET + TSTP/2.) + 620.33
        DO 25 K=1,NK
        DO 25 J=1,NJ
   25   FTEMP(K,J) = TSURF * DTSURF(K,J)
        GTMPF = FTEMP(8,1)
        N = N + 1
        PRINT 901,N
  901   FORMAT(//10X,I3,18H TH CALL OF BALOON)
        CALL BALON2(HTNC,TBULK,TCLI,TFLI,Q,RF,RO,HO,FTEMP,QL,STEMP,
      #  PC,PS,RMP,CFLUX,FA,KBALN,ZBALN,KFLG,MODE,NPRINT,GMIX,GTMPF,
      #  TIMET,TSTP,V,DELZ,TWALL,RAD,STRNC,STRNA,STRNR,STRNL,CTEMP,
      #  KNTCT,CHSTRS,KFAIL)
        IF(N .LT. 60 .AND. KFAIL .EQ. 0) GO TO 20
        PRINT 902,DELZ(8,4),TWALL(8,4),RAD(8,4),STRNC(8,4),STRNA(8,4),STRN
      #R(8,4),STRNL(8,4),CTEMP(8,4)
  902   FORMAT(/8E16.5)
        PRINT 903,TIMET
  903   FORMAT(16H            TIME =,E16.6,4H SEC)
        PRINT 904
  904   FORMAT(//50H          HOT AXIAL NODE TEMPERATURES IN DEGREES F)
        PRINT 905,(CTEMP(8,J),J=1,10)
  905   FORMAT(/10E12.4)
        PRINT 905,(CTEMP(8,J),J=11,NJ)
        STOP
        END
```

TABLE B-3. EXAMPLE OUTPUT

27 TH CALL OF BALOON

28 TH CALL OF BALOON

29 TH CALL OF BALOON

30 TH CALL OF BALOON

31 TH CALL OF BALOON

TIME STEP 74 DURATION .50000E-03 SEC NET = .9046E+01 PRESSURE DIFF = .14480E+08

TEMPERATURES DURING TIME STEP -- AXIAL NODES ACROSS CIRCUMFERENTIAL NODES DOWN THE TABLE

.10216E+04	.10216E+04	.10216E+04	.10214E+04	.10260E+04	.10267E+04	.10269E+04	.10268E+04
.10346E+04	.10346E+04	.10346E+04	.10344E+04	.10412E+04	.10425E+04	.10434E+04	.10434E+04
.10466E+04	.10466E+04	.10466E+04	.10464E+04	.10559E+04	.10577E+04	.10600E+04	.10608E+04
.10575E+04	.10575E+04	.10575E+04	.10575E+04	.10686E+04	.10712E+04	.10729E+04	.10735E+04
.10466E+04	.10466E+04	.10466E+04	.10464E+04	.10559E+04	.10577E+04	.10600E+04	.10608E+04
.10346E+04	.10346E+04	.10346E+04	.10344E+04	.10412E+04	.10425E+04	.10434E+04	.10434E+04
.10216E+04	.10216E+04	.10216E+04	.10214E+04	.10260E+04	.10267E+04	.10269E+04	.10268E+04
.10109E+04	.10109E+04	.10109E+04	.10108E+04	.10127E+04	.10129E+04	.10127E+04	.10123E+04
.10037E+04	.10037E+04	.10037E+04	.10037E+04	.10022E+04	.10021E+04	.10013E+04	.10008E+04
.99932E+03	.99932E+03	.99930E+03	.99952E+03	.99475E+03	.99429E+03	.99319E+03	.99250E+03
.99697E+03	.99697E+03	.99694E+03	.99722E+03	.99025E+03	.98958E+03	.96825E+03	.98746E+03
.99623E+03	.99623E+03	.99620E+03	.99664E+03	.98873E+03	.98799E+03	.98658E+03	.98577E+03
.99696E+03	.99696E+03	.99693E+03	.99731E+03	.99023E+03	.98956E+03	.98822E+03	.98744E+03
.99930E+03	.99930E+03	.99928E+03	.99949E+03	.99471E+03	.99425E+03	.99314E+03	.99245E+03
.10037E+04	.10037E+04	.10037E+04	.10037E+04	.10022E+04	.10020E+04	.10013E+04	.10007E+04
.10109E+04	.10109E+04	.10109E+04	.10107E+04	.10126E+04	.10128E+04	.10126E+04	.10122E+04

.10269E+04	.10267E+04	.10260E+04	.10246E+04	.10216E+04	.10217E+04	.10217E+04	.10217E+04
.10434E+04	.10425E+04	.10413E+04	.10394E+04	.10344E+04	.10346E+04	.10346E+04	.10346E+04
.10600E+04	.10577E+04	.10560E+04	.10534E+04	.10464E+04	.10465E+04	.10465E+04	.10465E+04
.10729E+04	.10712E+04	.10686E+04	.10655E+04	.10575E+04	.10575E+04	.10575E+04	.10575E+04
.10600E+04	.10577E+04	.10560E+04	.10534E+04	.10464E+04	.10465E+04	.10465E+04	.10465E+04
.10434E+04	.10425E+04	.10413E+04	.10394E+04	.10344E+04	.10346E+04	.10346E+04	.10346E+04
.10269E+04	.10267E+04	.10260E+04	.10246E+04	.10216E+04	.10217E+04	.10217E+04	.10217E+04
.10127E+04	.10129E+04	.10127E+04	.10117E+04	.10107E+04	.10108E+04	.10108E+04	.10108E+04
.10013E+04	.10021E+04	.10023E+04	.10017E+04	.10033E+04	.10033E+04	.10033E+04	.10033E+04
.99319E+03	.99428E+03	.99491E+03	.99456E+03	.99871E+03	.99860E+03	.99861E+03	.99861E+03
.98825E+03	.98957E+03	.99043E+03	.99027E+03	.99626E+03	.99607E+03	.99608E+03	.99608E+03
.98658E+03	.98798E+03	.98893E+03	.98884E+03	.99549E+03	.99527E+03	.99528E+03	.99528E+03
.98822E+03	.98955E+03	.99041E+03	.99025E+03	.99625E+03	.99606E+03	.99607E+03	.99607E+03
.99314E+03	.99424E+03	.99487E+03	.99452E+03	.99868E+03	.99857E+03	.99858E+03	.99858E+03
.10013E+04	.10020E+04	.10023E+04	.10016E+04	.10032E+04	.10032E+04	.10033E+04	.10033E+04
.10126E+04	.10128E+04	.10126E+04	.10116E+04	.10107E+04	.10107E+04	.10108E+04	.10108E+04

TABLE B-3. (CONTINUED)

TANGENTIAL STRESS COMPONENTS DURING TIME STEP

.11867E+09	.11867E+09	.11880E+09	.12068E+09	.12697E+09	.13367E+09	.14213E+09	.14444E+09
.12111E+09	.12111E+09	.12119E+09	.12195E+09	.13327E+09	.14081E+09	.15124E+09	.16202E+09
.12417E+09	.12417E+09	.12422E+09	.12429E+09	.14272E+09	.15421E+09	.16968E+09	.19261E+09
.12607E+09	.12607E+09	.12613E+09	.12572E+09	.14878E+09	.16239E+09	.19044E+09	.23377E+09
.12417E+09	.12417E+09	.12422E+09	.12429E+09	.14272E+09	.15421E+09	.16968E+09	.19261E+09
.12111E+09	.12111E+09	.12119E+09	.12195E+09	.13326E+09	.14081E+09	.15123E+09	.16201E+09
.11867E+09	.11867E+09	.11880E+09	.12068E+09	.12697E+09	.13367E+09	.14213E+09	.14444E+09
.11737E+09	.11730E+09	.11757E+09	.12079E+09	.12334E+09	.13047E+09	.13828E+09	.13143E+09
.11673E+09	.11674E+09	.11699E+09	.12166E+09	.12119E+09	.12924E+09	.13712E+09	.12007E+09
.11641E+09	.11642E+09	.11674E+09	.12272E+09	.11996E+09	.12903E+09	.13720E+09	.11037E+09
.11627E+09	.11628E+09	.11664E+09	.12355E+09	.11929E+09	.12916E+09	.13776E+09	.10362E+09
.11622E+09	.11624E+09	.11661E+09	.12386E+09	.11907E+09	.12923E+09	.13797E+09	.10116E+09
.11627E+09	.11628E+09	.11664E+09	.12355E+09	.11929E+09	.12916E+09	.13776E+09	.10358E+09
.11641E+09	.11642E+09	.11674E+09	.12273E+09	.11996E+09	.12903E+09	.13729E+09	.11030E+09
.11672E+09	.11673E+09	.11699E+09	.12167E+09	.12118E+09	.12924E+09	.13712E+09	.11999E+09
.11737E+09	.11737E+09	.11756E+09	.12079E+09	.12332E+09	.13045E+09	.13826E+09	.13134E+09
.14214E+09	.13367E+09	.12816E+09	.12371E+09	.11995E+09	.11890E+09	.11883E+09	.11883E+09
.15124E+09	.14084E+09	.13351E+09	.12841E+09	.12178E+09	.12137E+09	.12132E+09	.12132E+09
.16967E+09	.15433E+09	.14188E+09	.13482E+09	.12457E+09	.12449E+09	.12446E+09	.12446E+09
.19041E+09	.16252E+09	.14843E+09	.13907E+09	.12609E+09	.12637E+09	.12634E+09	.12634E+09
.16967E+09	.15433E+09	.14188E+09	.13482E+09	.12457E+09	.12449E+09	.12446E+09	.12446E+09
.15123E+09	.14084E+09	.13351E+09	.12841E+09	.12178E+09	.12137E+09	.12132E+09	.12132E+09
.14214E+09	.13367E+09	.12816E+09	.12371E+09	.11995E+09	.11890E+09	.11883E+09	.11883E+09
.13830E+09	.13043E+09	.12544E+09	.12101E+09	.11936E+09	.11755E+09	.11745E+09	.11745E+09
.13716E+09	.12917E+09	.12422E+09	.11948E+09	.11949E+09	.11680E+09	.11675E+09	.11674E+09
.13734E+09	.12893E+09	.12380E+09	.11866E+09	.11990E+09	.11657E+09	.11641E+09	.11640E+09
.13782E+09	.12904E+09	.12372E+09	.11823E+09	.12027E+09	.11643E+09	.11625E+09	.11624E+09
.13804E+09	.12911E+09	.12372E+09	.11810E+09	.12041E+09	.11639E+09	.11621E+09	.11620E+09
.13783E+09	.12904E+09	.12372E+09	.11823E+09	.12027E+09	.11643E+09	.11625E+09	.11624E+09
.13735E+09	.12894E+09	.12380E+09	.11865E+09	.11990E+09	.11657E+09	.11641E+09	.11640E+09
.13716E+09	.12917E+09	.12421E+09	.11947E+09	.11949E+09	.11688E+09	.11675E+09	.11674E+09
.13829E+09	.13041E+09	.12543E+09	.12100E+09	.11936E+09	.11754E+09	.11744E+09	.11744E+09

COLD WORK FOR STRENGTH DURING TIME STEP

.38894E+00	.38894E+00	.38893E+00	.38925E+00	.37600E+00	.37423E+00	.37311E+00	.37275E+00
.37866E+00	.37866E+00	.37865E+00	.37903E+00	.35925E+00	.35634E+00	.35401E+00	.35307E+00
.36874E+00	.36874E+00	.36873E+00	.36906E+00	.34519E+00	.34137E+00	.33802E+00	.33663E+00
.36435E+00	.36435E+00	.36434E+00	.36462E+00	.33929E+00	.33505E+00	.33147E+00	.32992E+00
.36874E+00	.36874E+00	.36873E+00	.36906E+00	.34519E+00	.34137E+00	.33802E+00	.33663E+00
.37866E+00	.37866E+00	.37865E+00	.37902E+00	.35925E+00	.35634E+00	.35401E+00	.35307E+00
.38894E+00	.38894E+00	.38893E+00	.38924E+00	.37600E+00	.37423E+00	.37311E+00	.37275E+00
.39620E+00	.39620E+00	.39620E+00	.39627E+00	.39139E+00	.39072E+00	.39081E+00	.39099E+00
.40063E+00	.40063E+00	.40065E+00	.40035E+00	.40387E+00	.40409E+00	.40513E+00	.40573E+00
.40319E+00	.40319E+00	.40321E+00	.40256E+00	.41291E+00	.41375E+00	.41542E+00	.41628E+00
.40451E+00	.40451E+00	.40454E+00	.40363E+00	.41835E+00	.41954E+00	.42154E+00	.42253E+00
.40492E+00	.40491E+00	.40496E+00	.40395E+00	.42017E+00	.42147E+00	.42357E+00	.42460E+00
.40451E+00	.40451E+00	.40455E+00	.40364E+00	.41837E+00	.41956E+00	.42156E+00	.42256E+00
.40320E+00	.40320E+00	.40323E+00	.40258E+00	.41296E+00	.41380E+00	.41547E+00	.41633E+00
.40066E+00	.40066E+00	.40067E+00	.40038E+00	.40394E+00	.40417E+00	.40522E+00	.40582E+00
.39624E+00	.39624E+00	.39624E+00	.39631E+00	.39149E+00	.39082E+00	.39092E+00	.39111E+00
.37311E+00	.37423E+00	.37607E+00	.37886E+00	.38844E+00	.38827E+00	.38827E+00	.38827E+00
.35401E+00	.35634E+00	.35940E+00	.36319E+00	.37769E+00	.37748E+00	.37748E+00	.37748E+00
.33802E+00	.34137E+00	.34533E+00	.34994E+00	.35760E+00	.36740E+00	.36740E+00	.36740E+00
.33147E+00	.33504E+00	.33947E+00	.34439E+00	.36317E+00	.36300E+00	.36301E+00	.36301E+00
.33802E+00	.34137E+00	.34533E+00	.34994E+00	.36760E+00	.36740E+00	.36741E+00	.36741E+00
.35401E+00	.35634E+00	.35940E+00	.36318E+00	.37769E+00	.37748E+00	.37749E+00	.37749E+00
.37311E+00	.37423E+00	.37607E+00	.37886E+00	.38844E+00	.38827E+00	.38827E+00	.38827E+00
.39081E+00	.39072E+00	.39135E+00	.39313E+00	.39628E+00	.39624E+00	.39624E+00	.39624E+00
.40513E+00	.40410E+00	.40372E+00	.40465E+00	.40109E+00	.40127E+00	.40126E+00	.40126E+00
.41542E+00	.41376E+00	.41269E+00	.41300E+00	.40383E+00	.40421E+00	.40420E+00	.40420E+00
.42153E+00	.41954E+00	.41809E+00	.41803E+00	.40522E+00	.40575E+00	.40573E+00	.40573E+00
.42357E+00	.42147E+00	.41990E+00	.41972E+00	.40565E+00	.40623E+00	.40621E+00	.40621E+00
.42156E+00	.41957E+00	.41812E+00	.41805E+00	.40523E+00	.40576E+00	.40574E+00	.40574E+00
.41547E+00	.41381E+00	.41274E+00	.41304E+00	.40385E+00	.40423E+00	.40421E+00	.40421E+00
.40522E+00	.40417E+00	.40379E+00	.40471E+00	.40112E+00	.40129E+00	.40129E+00	.40129E+00
.39092E+00	.39083E+00	.39144E+00	.39322E+00	.39633E+00	.39629E+00	.39629E+00	.39629E+00

TABLE B-3. (CONTINUED)

COLD WORK FOR STRAIN HARDENING EXPONENT DURING TIME STEP

.53619E-02	.53620E-02	.53610E-02	.53962E-02	.40907E-02	.39388E-02	.38461E-02	.38160E-02
.43280E-02	.43280E-02	.43270E-02	.43616E-02	.28413E-02	.26621E-02	.25258E-02	.24730E-02
.35000E-02	.35000E-02	.34993E-02	.35243E-02	.20643E-02	.18884E-02	.17453E-02	.16885E-02
.31801E-02	.31801E-02	.31795E-02	.31989E-02	.17983E-02	.16260E-02	.14925E-02	.14372E-02
.35001E-02	.35001E-02	.34993E-02	.35243E-02	.20643E-02	.18884E-02	.17453E-02	.16885E-02
.43282E-02	.43282E-02	.43271E-02	.43616E-02	.28413E-02	.26620E-02	.25258E-02	.24730E-02
.53623E-02	.53623E-02	.53613E-02	.53961E-02	.40907E-02	.39388E-02	.38461E-02	.38160E-02
.62178E-02	.62178E-02	.62177E-02	.62260E-02	.56308E-02	.55618E-02	.55721E-02	.55929E-02
.67965E-02	.67964E-02	.67983E-02	.67584E-02	.72479E-02	.72801E-02	.74315E-02	.75197E-02
.71508E-02	.71507E-02	.71547E-02	.70627E-02	.86526E-02	.87947E-02	.90817E-02	.92330E-02
.73401E-02	.73400E-02	.73455E-02	.72145E-02	.96076E-02	.98282E-02	.10209E-01	.10403E-01
.73997E-02	.73995E-02	.74057E-02	.72603E-02	.99467E-02	.10195E-01	.10609E-01	.10818E-01
.73408E-02	.73407E-02	.73463E-02	.72154E-02	.96119E-02	.98329E-02	.10214E-01	.10408E-01
.71525E-02	.71524E-02	.71565E-02	.70647E-02	.86606E-02	.89035E-02	.90914E-02	.92431E-02
.67996E-02	.67996E-02	.68016E-02	.67619E-02	.72583E-02	.72915E-02	.74440E-02	.75327E-02
.62230E-02	.62230E-02	.62231E-02	.62316E-02	.56499E-02	.55737E-02	.55851E-02	.56064E-02
.38461E-02	.39389E-02	.40968E-02	.43461E-02	.53079E-02	.52886E-02	.52890E-02	.52890E-02
.25258E-02	.26619E-02	.28503E-02	.30996E-02	.42403E-02	.42213E-02	.42217E-02	.42216E-02
.17453E-02	.18883E-02	.20711E-02	.23027E-02	.34140E-02	.33995E-02	.33998E-02	.33998E-02
.14925E-02	.16259E-02	.18060E-02	.20265E-02	.30988E-02	.30874E-02	.30877E-02	.30877E-02
.17453E-02	.18883E-02	.20711E-02	.23027E-02	.34140E-02	.33996E-02	.33999E-02	.33999E-02
.25258E-02	.26619E-02	.28503E-02	.30996E-02	.42403E-02	.42214E-02	.42218E-02	.42218E-02
.38461E-02	.39388E-02	.40968E-02	.43461E-02	.53079E-02	.52889E-02	.52893E-02	.52893E-02
.55720E-02	.55621E-02	.56339E-02	.58427E-02	.62272E-02	.62230E-02	.62230E-02	.62230E-02
.74315E-02	.72808E-02	.72269E-02	.73605E-02	.68587E-02	.68827E-02	.68818E-02	.68818E-02
.90817E-02	.87957E-02	.86162E-02	.86669E-02	.72426E-02	.72975E-02	.72957E-02	.72957E-02
.10209E-01	.98293E-02	.95606E-02	.95496E-02	.74443E-02	.75225E-02	.75199E-02	.75199E-02
.10609E-01	.10197E-01	.98960E-02	.98622E-02	.75071E-02	.75938E-02	.75910E-02	.75910E-02
.10214E-01	.98341E-02	.95649E-02	.95535E-02	.74454E-02	.75234E-02	.75208E-02	.75209E-02
.90914E-02	.88045E-02	.86240E-02	.96742E-02	.72450E-02	.72997E-02	.72978E-02	.72978E-02
.74440E-02	.72921E-02	.72372E-02	.73700E-02	.68629E-02	.68866E-02	.68856E-02	.68856E-02
.55850E-02	.55740E-02	.56449E-02	.58532E-02	.62335E-02	.62291E-02	.62290E-02	.62290E-02

FAST NEUTRON FLUENCE FOR STRENGTH DURING TIME STEP

0.	0.	0.	0.	0.	0.	0.	0.
0.	0.	0.	0.	0.	0.	0.	0.
0.	0.	0.	0.	0.	0.	0.	0.
0.	0.	0.	0.	0.	0.	0.	0.
0.	0.	0.	0.	0.	0.	0.	0.
0.	0.	0.	0.	0.	0.	0.	0.
0.	0.	0.	0.	0.	0.	0.	0.
0.	0.	0.	0.	0.	0.	0.	0.
0.	0.	0.	0.	0.	0.	0.	0.
0.	0.	0.	0.	0.	0.	0.	0.
0.	0.	0.	0.	0.	0.	0.	0.
0.	0.	0.	0.	0.	0.	0.	0.
0.	0.	0.	0.	0.	0.	0.	0.
0.	0.	0.	0.	0.	0.	0.	0.
0.	0.	0.	0.	0.	0.	0.	0.
0.	0.	0.	0.	0.	0.	0.	0.
0.	0.	0.	0.	0.	0.	0.	0.
0.	0.	0.	0.	0.	0.	0.	0.
0.	0.	0.	0.	0.	0.	0.	0.
0.	0.	0.	0.	0.	0.	0.	0.
0.	0.	0.	0.	0.	0.	0.	0.
0.	0.	0.	0.	0.	0.	0.	0.
0.	0.	0.	0.	0.	0.	0.	0.
0.	0.	0.	0.	0.	0.	0.	0.
0.	0.	0.	0.	0.	0.	0.	0.
0.	0.	0.	0.	0.	0.	0.	0.
0.	0.	0.	0.	0.	0.	0.	0.
0.	0.	0.	0.	0.	0.	0.	0.
0.	0.	0.	0.	0.	0.	0.	0.
0.	0.	0.	0.	0.	0.	0.	0.
0.	0.	0.	0.	0.	0.	0.	0.
0.	0.	0.	0.	0.	0.	0.	0.

```
FAST NEUTRON FLUENCE FOR STRAIN HARDENING EXPONENT DURING TIME STEP

   0.          0.          0.          0.          0.          0.          0.          0.
   0.          0.          0.          0.          0.          0.          0.          0.
   0.          0.          0.          0.          0.          0.          0.          0.
   0.          0.          0.          0.          0.          0.          0.          0.
   0.          0.          0.          0.          0.          0.          0.          0.
   0.          0.          0.          0.          0.          0.          0.          0.
   0.          0.          0.          0.          0.          0.          0.          0.
   0.          0.          0.          0.          0.          0.          0.          0.
   0.          0.          0.          0.          0.          0.          0.          0.
   0.          0.          0.          0.          0.          0.          0.          0.
   0.          0.          0.          0.          0.          0.          0.          0.
   0.          0.          0.          0.          0.          0.          0.          0.
   0.          0.          0.          0.          0.          0.          0.          0.
   0.          0.          0.          0.          0.          0.          0.          0.
   0.          0.          0.          0.          0.          0.          0.          0.
   0.          0.          0.          0.          0.          0.          0.          0.

   0.          0.          0.          0.          0.          0.          0.          0.
   0.          0.          0.          0.          0.          0.          0.          0.
   0.          0.          0.          0.          0.          0.          0.          0.
   0.          0.          0.          0.          0.          0.          0.          0.
   0.          0.          0.          0.          0.          0.          0.          0.
   0.          0.          0.          0.          0.          0.          0.          0.
   0.          0.          0.          0.          0.          0.          0.          0.
   0.          0.          0.          0.          0.          0.          0.          0.
   0.          0.          0.          0.          0.          0.          0.          0.
   0.          0.          0.          0.          0.          0.          0.          0.
   0.          0.          0.          0.          0.          0.          0.          0.
   0.          0.          0.          0.          0.          0.          0.          0.
   0.          0.          0.          0.          0.          0.          0.          0.
   0.          0.          0.          0.          0.          0.          0.          0.
   0.          0.          0.          0.          0.          0.          0.          0.
   0.          0.          0.          0.          0.          0.          0.          0.
AXIAL NODE  1    AVE RADIUS =  .549451E-02    AVE WALL THICKNESS =  .629816E-03   CONTACT SWITCH = 1    TCE =  .709E-01
  J = 1 MIDWALL RADIUS = .52842E-02 WALL THICKNESS = .631392E-03 DELZ = .491490E-02
  J = 2 MIDWALL RADIUS = .51307E-02 WALL THICKNESS = .619213E-03 DELZ = .484800E-02
  J = 3 MIDWALL RADIUS = .50308E-02 WALL THICKNESS = .603960E-03 DELZ = .476336E-02
  J = 4 MIDWALL RADIUS = .49962E-02 WALL THICKNESS = .594465E-03 DELZ = .470288E-02
  J = 5 MIDWALL RADIUS = .50308E-02 WALL THICKNESS = .603960E-03 DELZ = .476337E-02
  J = 6 MIDWALL RADIUS = .51307E-02 WALL THICKNESS = .619214E-03 DELZ = .484802E-02
  J = 7 MIDWALL RADIUS = .52842E-02 WALL THICKNESS = .631393E-03 DELZ = .491492E-02
  J = 8 MIDWALL RADIUS = .54715E-02 WALL THICKNESS = .637838E-03 DELZ = .494954E-02
  J = 9 MIDWALL RADIUS = .56654E-02 WALL THICKNESS = .641067E-03 DELZ = .496457E-02
  J =10 MIDWALL RADIUS = .58351E-02 WALL THICKNESS = .642636E-03 DELZ = .497072E-02
  J =11 MIDWALL RADIUS = .59513E-02 WALL THICKNESS = .643366E-03 DELZ = .497333E-02
  J =12 MIDWALL RADIUS = .59928E-02 WALL THICKNESS = .643582E-03 DELZ = .497408E-02
  J =13 MIDWALL RADIUS = .59519E-02 WALL THICKNESS = .643369E-03 DELZ = .497334E-02
  J =14 MIDWALL RADIUS = .58363E-02 WALL THICKNESS = .642644E-03 DELZ = .497075E-02
  J =15 MIDWALL RADIUS = .56669E-02 WALL THICKNESS = .641084E-03 DELZ = .496464E-02
  J =16 MIDWALL RADIUS = .54731E-02 WALL THICKNESS = .637870E-03 DELZ = .494971E-02
AXIAL NODE  2    AVE RADIUS =  .549451E-02    AVE WALL THICKNESS =  .629815E-03   CONTACT SWITCH = 1    TCE =  .709E-01
  J = 1 MIDWALL RADIUS = .52842E-02 WALL THICKNESS = .631391E-03 DELZ = .491490E-02
  J = 2 MIDWALL RADIUS = .51307E-02 WALL THICKNESS = .619213E-03 DELZ = .484801E-02
  J = 3 MIDWALL RADIUS = .50308E-02 WALL THICKNESS = .603962E-03 DELZ = .476338E-02
  J = 4 MIDWALL RADIUS = .49962E-02 WALL THICKNESS = .594469E-03 DELZ = .470291E-02
  J = 5 MIDWALL RADIUS = .50308E-02 WALL THICKNESS = .603963E-03 DELZ = .476339E-02
  J = 6 MIDWALL RADIUS = .51307E-02 WALL THICKNESS = .619215E-03 DELZ = .484802E-02
  J = 7 MIDWALL RADIUS = .52842E-02 WALL THICKNESS = .631393E-03 DELZ = .491491E-02
  J = 8 MIDWALL RADIUS = .54715E-02 WALL THICKNESS = .637836E-03 DELZ = .494954E-02
  J = 9 MIDWALL RADIUS = .56654E-02 WALL THICKNESS = .641065E-03 DELZ = .496456E-02
  J =10 MIDWALL RADIUS = .58351E-02 WALL THICKNESS = .642634E-03 DELZ = .497071E-02
  J =11 MIDWALL RADIUS = .59513E-02 WALL THICKNESS = .643364E-03 DELZ = .497333E-02
  J =12 MIDWALL RADIUS = .59928E-02 WALL THICKNESS = .643580E-03 DELZ = .497407E-02
  J =13 MIDWALL RADIUS = .59519E-02 WALL THICKNESS = .643367E-03 DELZ = .497334E-02
  J =14 MIDWALL RADIUS = .58363E-02 WALL THICKNESS = .642642E-03 DELZ = .497074E-02
  J =15 MIDWALL RADIUS = .56669E-02 WALL THICKNESS = .641082E-03 DELZ = .496463E-02
  J =16 MIDWALL RADIUS = .54731E-02 WALL THICKNESS = .637869E-03 DELZ = .494971E-02
```

TABLE B-3. (CONTINUED)

```
AXIAL NODE  3     AVE RADIUS =  .549500E-02      AVE WALL THICKNESS =  .629750E-03    CONTACT SWITCH = 1     TCE =  .710E-01
  J = 1 MIDWALL RADIUS = .52845E-02 WALL THICKNESS = .631320E-03 DELZ = .491464E-02
  J = 2 MIDWALL RADIUS = .51308E-02 WALL THICKNESS = .619141E-03 DELZ = .484749E-02
  J = 3 MIDWALL RADIUS = .50308E-02 WALL THICKNESS = .603893E-03 DELZ = .476284E-02
  J = 4 MIDWALL RADIUS = .49962E-02 WALL THICKNESS = .594301E-03 DELZ = .470837E-02
  J = 5 MIDWALL RADIUS = .50308E-02 WALL THICKNESS = .603893E-03 DELZ = .476284E-02
  J = 6 MIDWALL RADIUS = .51308E-02 WALL THICKNESS = .619142E-03 DELZ = .484750E-02
  J = 7 MIDWALL RADIUS = .52845E-02 WALL THICKNESS = .631321E-03 DELZ = .491465E-02
  J = 8 MIDWALL RADIUS = .54719E-02 WALL THICKNESS = .637774E-03 DELZ = .494919E-02
  J = 9 MIDWALL RADIUS = .56661E-02 WALL THICKNESS = .641012E-03 DELZ = .496431E-02
  J =10 MIDWALL RADIUS = .58359E-02 WALL THICKNESS = .642586E-03 DELZ = .497051E-02
  J =11 MIDWALL RADIUS = .59523E-02 WALL THICKNESS = .643319E-03 DELZ = .497314E-02
  J =12 MIDWALL RADIUS = .59938E-02 WALL THICKNESS = .643536E-03 DELZ = .497389E-02
  J =13 MIDWALL RADIUS = .59529E-02 WALL THICKNESS = .643322E-03 DELZ = .497315E-02
  J =14 MIDWALL RADIUS = .58371E-02 WALL THICKNESS = .642594E-03 DELZ = .497054E-02
  J =15 MIDWALL RADIUS = .56676E-02 WALL THICKNESS = .641029E-03 DELZ = .496439E-02
  J =16 MIDWALL RADIUS = .54735E-02 WALL THICKNESS = .637812E-03 DELZ = .494938E-02
AXIAL NODE  4     AVE RADIUS =  .551059E-02      AVE WALL THICKNESS =  .628615E-03    CONTACT SWITCH = 1     TCE =  .740E-01
  J = 1 MIDWALL RADIUS = .52933E-02 WALL THICKNESS = .630474E-03 DELZ = .490950E-02
  J = 2 MIDWALL RADIUS = .51352E-02 WALL THICKNESS = .619008E-03 DELZ = .484729E-02
  J = 3 MIDWALL RADIUS = .50325E-02 WALL THICKNESS = .604092E-03 DELZ = .476146E-02
  J = 4 MIDWALL RADIUS = .49969E-02 WALL THICKNESS = .595798E-03 DELZ = .471424E-02
  J = 5 MIDWALL RADIUS = .50325E-02 WALL THICKNESS = .604091E-03 DELZ = .476145E-02
  J = 6 MIDWALL RADIUS = .51352E-02 WALL THICKNESS = .619008E-03 DELZ = .484729E-02
  J = 7 MIDWALL RADIUS = .52933E-02 WALL THICKNESS = .630473E-03 DELZ = .490949E-02
  J = 8 MIDWALL RADIUS = .54862E-02 WALL THICKNESS = .636424E-03 DELZ = .494131E-02
  J = 9 MIDWALL RADIUS = .56862E-02 WALL THICKNESS = .639179E-03 DELZ = .495514E-02
  J =10 MIDWALL RADIUS = .58614E-02 WALL THICKNESS = .640407E-03 DELZ = .496046E-02
  J =11 MIDWALL RADIUS = .59814E-02 WALL THICKNESS = .640894E-03 DELZ = .496236E-02
  J =12 MIDWALL RADIUS = .60243E-02 WALL THICKNESS = .641020E-03 DELZ = .496281E-02
  J =13 MIDWALL RADIUS = .59821E-02 WALL THICKNESS = .640897E-03 DELZ = .496237E-02
  J =14 MIDWALL RADIUS = .58626E-02 WALL THICKNESS = .640414E-03 DELZ = .496049E-02
  J =15 MIDWALL RADIUS = .56878E-02 WALL THICKNESS = .639195E-03 DELZ = .495521E-02
  J =16 MIDWALL RADIUS = .54878E-02 WALL THICKNESS = .636601E-03 DELZ = .494151E-02
AXIAL NODE  5     AVE RADIUS =  .577664E-02      AVE WALL THICKNESS =  .615162E-03    CONTACT SWITCH = 1     TCE =  .126E+00
  J = 1 MIDWALL RADIUS = .54151E-02 WALL THICKNESS = .620156E-03 DELZ = .485797E-02
  J = 2 MIDWALL RADIUS = .51714E-02 WALL THICKNESS = .593575E-03 DELZ = .470667E-02
  J = 3 MIDWALL RADIUS = .50153E-02 WALL THICKNESS = .552258E-03 DELZ = .445317E-02
  J = 4 MIDWALL RADIUS = .49617E-02 WALL THICKNESS = .525463E-03 DELZ = .427892E-02
  J = 5 MIDWALL RADIUS = .50153E-02 WALL THICKNESS = .552260E-03 DELZ = .445319E-02
  J = 6 MIDWALL RADIUS = .51714E-02 WALL THICKNESS = .593577E-03 DELZ = .470668E-02
  J = 7 MIDWALL RADIUS = .54151E-02 WALL THICKNESS = .620157E-03 DELZ = .485797E-02
  J = 8 MIDWALL RADIUS = .57182E-02 WALL THICKNESS = .634367E-03 DELZ = .493408E-02
  J = 9 MIDWALL RADIUS = .60384E-02 WALL THICKNESS = .641818E-03 DELZ = .496913E-02
  J =10 MIDWALL RADIUS = .63233E-02 WALL THICKNESS = .645408E-03 DELZ = .498081E-02
  J =11 MIDWALL RADIUS = .65206E-02 WALL THICKNESS = .647102E-03 DELZ = .498526E-02
  J =12 MIDWALL RADIUS = .65915E-02 WALL THICKNESS = .647622E-03 DELZ = .498649E-02
  J =13 MIDWALL RADIUS = .65217E-02 WALL THICKNESS = .647109E-03 DELZ = .498527E-02
  J =14 MIDWALL RADIUS = .63253E-02 WALL THICKNESS = .645424E-03 DELZ = .498086E-02
  J =15 MIDWALL RADIUS = .60410E-02 WALL THICKNESS = .641852E-03 DELZ = .496925E-02
  J =16 MIDWALL RADIUS = .57208E-02 WALL THICKNESS = .634447E-03 DELZ = .493447E-02
AXIAL NODE  6     AVE RADIUS =  .596663E-02      AVE WALL THICKNESS =  .606491E-03    CONTACT SWITCH = 1     TCE =  .163E+00
  J = 1 MIDWALL RADIUS = .54991E-02 WALL THICKNESS = .615038E-03 DELZ = .483258E-02
  J = 2 MIDWALL RADIUS = .51987E-02 WALL THICKNESS = .582572E-03 DELZ = .464817E-02
  J = 3 MIDWALL RADIUS = .50083E-02 WALL THICKNESS = .524081E-03 DELZ = .428555E-02
  J = 4 MIDWALL RADIUS = .49433E-02 WALL THICKNESS = .488620E-03 DELZ = .404923E-02
  J = 5 MIDWALL RADIUS = .50083E-02 WALL THICKNESS = .524092E-03 DELZ = .428562E-02
  J = 6 MIDWALL RADIUS = .51987E-02 WALL THICKNESS = .592576E-03 DELZ = .464820E-02
  J = 7 MIDWALL RADIUS = .54991E-02 WALL THICKNESS = .615040E-03 DELZ = .483260E-02
  J = 8 MIDWALL RADIUS = .58774E-02 WALL THICKNESS = .631546E-03 DELZ = .492079E-02
  J = 9 MIDWALL RADIUS = .62819E-02 WALL THICKNESS = .640160E-03 DELZ = .496324E-02
  J =10 MIDWALL RADIUS = .66452E-02 WALL THICKNESS = .644380E-03 DELZ = .497789E-02
  J =11 MIDWALL RADIUS = .68986E-02 WALL THICKNESS = .646309E-03 DELZ = .498312E-02
  J =12 MIDWALL RADIUS = .69900E-02 WALL THICKNESS = .646884E-03 DELZ = .498452E-02
  J =13 MIDWALL RADIUS = .69000E-02 WALL THICKNESS = .646316E-03 DELZ = .498314E-02
  J =14 MIDWALL RADIUS = .66478E-02 WALL THICKNESS = .644398E-03 DELZ = .497794E-02
  J =15 MIDWALL RADIUS = .62851E-02 WALL THICKNESS = .640199E-03 DELZ = .496340E-02
  J =16 MIDWALL RADIUS = .58807E-02 WALL THICKNESS = .631639E-03 DELZ = .492125E-02
```

TABLE B-3. (CONTINUED)

```
AXIAL NODE  7    AVE RADIUS =  .626506E-02    AVE WALL THICKNESS =  .596999E-03   CONTACT SWITCH = 1    TCE =  .221E+00
 J = 1 MIDWALL RADIUS = .56179E-02 WALL THICKNESS = .611141E-03 DELZ = .481450E-02
 J = 2 MIDWALL RADIUS = .52306E-02 WALL THICKNESS = .572753E-03 DELZ = .458904E-02
 J = 3 MIDWALL RADIUS = .49889E-02 WALL THICKNESS = .498763E-03 DELZ = .412366E-02
 J = 4 MIDWALL RADIUS = .49073E-02 WALL THICKNESS = .416520E-03 DELZ = .355612E-02
 J = 5 MIDWALL RADIUS = .49889E-02 WALL THICKNESS = .498774E-03 DELZ = .412378E-02
 J = 6 MIDWALL RADIUS = .52306E-02 WALL THICKNESS = .572760E-03 DELZ = .458911E-02
 J = 7 MIDWALL RADIUS = .56179E-02 WALL THICKNESS = .611144E-03 DELZ = .481453E-02
 J = 8 MIDWALL RADIUS = .61151E-02 WALL THICKNESS = .630286E-03 DELZ = .491623E-02
 J = 9 MIDWALL RADIUS = .66564E-02 WALL THICKNESS = .639946E-03 DELZ = .496370E-02
 J =10 MIDWALL RADIUS = .71498E-02 WALL THICKNESS = .644538E-03 DELZ = .497913E-02
 J =11 MIDWALL RADIUS = .74971E-02 WALL THICKNESS = .646603E-03 DELZ = .498440E-02
 J =12 MIDWALL RADIUS = .76229E-02 WALL THICKNESS = .647217E-03 DELZ = .498579E-02
 J =13 MIDWALL RADIUS = .74990E-02 WALL THICKNESS = .646610E-03 DELZ = .498442E-02
 J =14 MIDWALL RADIUS = .71534E-02 WALL THICKNESS = .644557E-03 DELZ = .497918E-02
 J =15 MIDWALL RADIUS = .66608E-02 WALL THICKNESS = .639989E-03 DELZ = .496388E-02
 J =16 MIDWALL RADIUS = .61194E-02 WALL THICKNESS = .630392E-03 DELZ = .491674E-02
AXIAL NODE  8    AVE RADIUS =  .673875E-02    AVE WALL THICKNESS =  .508260E-03   CONTACT SWITCH = 1    TCE =  .313E+00
 J = 1 MIDWALL RADIUS = .57965E-02 WALL THICKNESS = .610299E-03 DELZ = .481115E-02
 J = 2 MIDWALL RADIUS = .52844E-02 WALL THICKNESS = .566547E-03 DELZ = .455875E-02
 J = 3 MIDWALL RADIUS = .49721E-02 WALL THICKNESS = .471356E-03 DELZ = .393101E-02
 J = 4 MIDWALL RADIUS = .48680E-02 WALL THICKNESS = .337915E-03 DELZ = .294029E-02
 J = 5 MIDWALL RADIUS = .49721E-02 WALL THICKNESS = .471372E-03 DELZ = .393117E-02
 J = 6 MIDWALL RADIUS = .52844E-02 WALL THICKNESS = .566556E-03 DELZ = .455884E-02
 J = 7 MIDWALL RADIUS = .57965E-02 WALL THICKNESS = .610304E-03 DELZ = .481119E-02
 J = 8 MIDWALL RADIUS = .64724E-02 WALL THICKNESS = .630935E-03 DELZ = .492104E-02
 J = 9 MIDWALL RADIUS = .72273E-02 WALL THICKNESS = .640910E-03 DELZ = .496839E-02
 J =10 MIDWALL RADIUS = .79286E-02 WALL THICKNESS = .645440E-03 DELZ = .498215E-02
 J =11 MIDWALL RADIUS = .84277E-02 WALL THICKNESS = .647480E-03 DELZ = .498681E-02
 J =12 MIDWALL RADIUS = .86095E-02 WALL THICKNESS = .648097E-03 DELZ = .498805E-02
 J =13 MIDWALL RADIUS = .84306E-02 WALL THICKNESS = .647488E-03 DELZ = .498683E-02
 J =14 MIDWALL RADIUS = .79336E-02 WALL THICKNESS = .645459E-03 DELZ = .498220E-02
 J =15 MIDWALL RADIUS = .72334E-02 WALL THICKNESS = .640952E-03 DELZ = .496055E-02
 J =16 MIDWALL RADIUS = .64783E-02 WALL THICKNESS = .631042E-03 DELZ = .492171E-02
AXIAL NODE  9    AVE RADIUS =  .626482E-02    AVE WALL THICKNESS =  .597001E-03   CONTACT SWITCH = 1    TCE =  .221E+00
 J = 1 MIDWALL RADIUS = .56178E-02 WALL THICKNESS = .611133E-03 DELZ = .481445E-02
 J = 2 MIDWALL RADIUS = .52306E-02 WALL THICKNESS = .572751E-03 DELZ = .458903E-02
 J = 3 MIDWALL RADIUS = .49890E-02 WALL THICKNESS = .498783E-03 DELZ = .412382E-02
 J = 4 MIDWALL RADIUS = .49073E-02 WALL THICKNESS = .416590E-03 DELZ = .355667E-02
 J = 5 MIDWALL RADIUS = .49890E-02 WALL THICKNESS = .498794E-03 DELZ = .412393E-02
 J = 6 MIDWALL RADIUS = .52306E-02 WALL THICKNESS = .572758E-03 DELZ = .458910E-02
 J = 7 MIDWALL RADIUS = .56178E-02 WALL THICKNESS = .611137E-03 DELZ = .481448E-02
 J = 8 MIDWALL RADIUS = .61149E-02 WALL THICKNESS = .630277E-03 DELZ = .491618E-02
 J = 9 MIDWALL RADIUS = .66561E-02 WALL THICKNESS = .639938E-03 DELZ = .496367E-02
 J =10 MIDWALL RADIUS = .71494E-02 WALL THICKNESS = .644532E-03 DELZ = .497911E-02
 J =11 MIDWALL RADIUS = .74966E-02 WALL THICKNESS = .646597E-03 DELZ = .498438E-02
 J =12 MIDWALL RADIUS = .76223E-02 WALL THICKNESS = .647211E-03 DELZ = .498578E-02
 J =13 MIDWALL RADIUS = .74985E-02 WALL THICKNESS = .646605E-03 DELZ = .498440E-02
 J =14 MIDWALL RADIUS = .71530E-02 WALL THICKNESS = .644551E-03 DELZ = .497916E-02
 J =15 MIDWALL RADIUS = .66605E-02 WALL THICKNESS = .639981E-03 DELZ = .496384E-02
 J =16 MIDWALL RADIUS = .61192E-02 WALL THICKNESS = .630384E-03 DELZ = .491669E-02
```

TABLE B-3. (CONTINUED)

```
AXIAL NODE 10     AVE RADIUS = .596822E-02     AVE WALL THICKNESS = .606440E-03     CONTACT SWITCH = 1     TCE = .163E+00
 J = 1 MIDWALL RADIUS = .54998E-02 WALL THICKNESS = .615065E-03 DELZ = .483278E-02
 J = 2 MIDWALL RADIUS = .51989E-02 WALL THICKNESS = .582550E-03 DELZ = .464794E-02
 J = 3 MIDWALL RADIUS = .50082E-02 WALL THICKNESS = .523764E-03 DELZ = .428352E-02
 J = 4 MIDWALL RADIUS = .49431E-02 WALL THICKNESS = .488271E-03 DELZ = .404619E-02
 J = 5 MIDWALL RADIUS = .50082E-02 WALL THICKNESS = .523774E-03 DELZ = .428359E-02
 J = 6 MIDWALL RADIUS = .51989E-02 WALL THICKNESS = .582554E-03 DELZ = .464798E-02
 J = 7 MIDWALL RADIUS = .54998E-02 WALL THICKNESS = .615067E-03 DELZ = .483279E-02
 J = 8 MIDWALL RADIUS = .58787E-02 WALL THICKNESS = .631583E-03 DELZ = .492104E-02
 J = 9 MIDWALL RADIUS = .62839E-02 WALL THICKNESS = .640191E-03 DELZ = .496339E-02
 J =10 MIDWALL RADIUS = .66479E-02 WALL THICKNESS = .644406E-03 DELZ = .497798E-02
 J =11 MIDWALL RADIUS = .69017E-02 WALL THICKNESS = .646333E-03 DELZ = .498320E-02
 J =12 MIDWALL RADIUS = .69933E-02 WALL THICKNESS = .646908E-03 DELZ = .498460E-02
 J =13 MIDWALL RADIUS = .69032E-02 WALL THICKNESS = .646340E-03 DELZ = .498322E-02
 J =14 MIDWALL RADIUS = .66505E-02 WALL THICKNESS = .644424E-03 DELZ = .497804E-02
 J =15 MIDWALL RADIUS = .62871E-02 WALL THICKNESS = .640230E-03 DELZ = .496355E-02
 J =16 MIDWALL RADIUS = .58820E-02 WALL THICKNESS = .631676E-03 DELZ = .492150E-02
AXIAL NODE 11     AVE RADIUS = .577506E-02     AVE WALL THICKNESS = .614814E-03     CONTACT SWITCH = 1     TCE = .126E+00
 J = 1 MIDWALL RADIUS = .54142E-02 WALL THICKNESS = .619179E-03 DELZ = .485270E-02
 J = 2 MIDWALL RADIUS = .51709E-02 WALL THICKNESS = .593707E-03 DELZ = .470974E-02
 J = 3 MIDWALL RADIUS = .50150E-02 WALL THICKNESS = .555037E-03 DELZ = .447959E-02
 J = 4 MIDWALL RADIUS = .49615E-02 WALL THICKNESS = .525100E-03 DELZ = .428815E-02
 J = 5 MIDWALL RADIUS = .50150E-02 WALL THICKNESS = .555039E-03 DELZ = .447960E-02
 J = 6 MIDWALL RADIUS = .51709E-02 WALL THICKNESS = .593709E-03 DELZ = .470975E-02
 J = 7 MIDWALL RADIUS = .54142E-02 WALL THICKNESS = .619180E-03 DELZ = .485270E-02
 J = 8 MIDWALL RADIUS = .57168E-02 WALL THICKNESS = .633208E-03 DELZ = .492739E-02
 J = 9 MIDWALL RADIUS = .60365E-02 WALL THICKNESS = .640714E-03 DELZ = .496422E-02
 J =10 MIDWALL RADIUS = .63208E-02 WALL THICKNESS = .644465E-03 DELZ = .497746E-02
 J =11 MIDWALL RADIUS = .65178E-02 WALL THICKNESS = .646212E-03 DELZ = .498243E-02
 J =12 MIDWALL RADIUS = .65886E-02 WALL THICKNESS = .646739E-03 DELZ = .498379E-02
 J =13 MIDWALL RADIUS = .65189E-02 WALL THICKNESS = .646219E-03 DELZ = .498245E-02
 J =14 MIDWALL RADIUS = .63228E-02 WALL THICKNESS = .644482E-03 DELZ = .497751E-02
 J =15 MIDWALL RADIUS = .60390E-02 WALL THICKNESS = .640750E-03 DELZ = .496436E-02
 J =16 MIDWALL RADIUS = .57194E-02 WALL THICKNESS = .633288E-03 DELZ = .492781E-02
AXIAL NODE 12     AVE RADIUS = .565408E-02     AVE WALL THICKNESS = .621142E-03     CONTACT SWITCH = 1     TCE = .102E+00
 J = 1 MIDWALL RADIUS = .53591E-02 WALL THICKNESS = .623817E-03 DELZ = .487557E-02
 J = 2 MIDWALL RADIUS = .51536E-02 WALL THICKNESS = .602372E-03 DELZ = .475722E-02
 J = 3 MIDWALL RADIUS = .50211E-02 WALL THICKNESS = .572666E-03 DELZ = .457804E-02
 J = 4 MIDWALL RADIUS = .49754E-02 WALL THICKNESS = .552867E-03 DELZ = .446129E-02
 J = 5 MIDWALL RADIUS = .50211E-02 WALL THICKNESS = .572666E-03 DELZ = .457804E-02
 J = 6 MIDWALL RADIUS = .51536E-02 WALL THICKNESS = .602372E-03 DELZ = .475722E-02
 J = 7 MIDWALL RADIUS = .53591E-02 WALL THICKNESS = .623818E-03 DELZ = .487557E-02
 J = 8 MIDWALL RADIUS = .56127E-02 WALL THICKNESS = .635743E-03 DELZ = .493966E-02
 J = 9 MIDWALL RADIUS = .58783E-02 WALL THICKNESS = .642150E-03 DELZ = .496955E-02
 J =10 MIDWALL RADIUS = .61129E-02 WALL THICKNESS = .645342E-03 DELZ = .498018E-02
 J =11 MIDWALL RADIUS = .62747E-02 WALL THICKNESS = .646874E-03 DELZ = .498442E-02
 J =12 MIDWALL RADIUS = .63327E-02 WALL THICKNESS = .647349E-03 DELZ = .498563E-02
 J =13 MIDWALL RADIUS = .62756E-02 WALL THICKNESS = .646880E-03 DELZ = .498444E-02
 J =14 MIDWALL RADIUS = .61146E-02 WALL THICKNESS = .645356E-03 DELZ = .498023E-02
 J =15 MIDWALL RADIUS = .58804E-02 WALL THICKNESS = .642190E-03 DELZ = .496966E-02
 J =16 MIDWALL RADIUS = .56148E-02 WALL THICKNESS = .635798E-03 DELZ = .493995E-02
AXIAL NODE 13     AVE RADIUS = .550626E-02     AVE WALL THICKNESS = .628998E-03     CONTACT SWITCH = 1     TCE = .732E-01
 J = 1 MIDWALL RADIUS = .52906E-02 WALL THICKNESS = .630435E-03 DELZ = .490955E-02
 J = 2 MIDWALL RADIUS = .51336E-02 WALL THICKNESS = .618437E-03 DELZ = .484364E-02
 J = 3 MIDWALL RADIUS = .50315E-02 WALL THICKNESS = .602665E-03 DELZ = .475629E-02
 J = 4 MIDWALL RADIUS = .49962E-02 WALL THICKNESS = .594414E-03 DELZ = .470533E-02
 J = 5 MIDWALL RADIUS = .50315E-02 WALL THICKNESS = .602665E-03 DELZ = .475628E-02
 J = 6 MIDWALL RADIUS = .51336E-02 WALL THICKNESS = .618437E-03 DELZ = .484364E-02
 J = 7 MIDWALL RADIUS = .52906E-02 WALL THICKNESS = .630435E-03 DELZ = .490955E-02
 J = 8 MIDWALL RADIUS = .54822E-02 WALL THICKNESS = .637034E-03 DELZ = .494490E-02
 J = 9 MIDWALL RADIUS = .56808E-02 WALL THICKNESS = .640320E-03 DELZ = .496084E-02
 J =10 MIDWALL RADIUS = .58546E-02 WALL THICKNESS = .641887E-03 DELZ = .496721E-02
 J =11 MIDWALL RADIUS = .59737E-02 WALL THICKNESS = .642578E-03 DELZ = .496976E-02
 J =12 MIDWALL RADIUS = .60163E-02 WALL THICKNESS = .642776E-03 DELZ = .497045E-02
 J =13 MIDWALL RADIUS = .59744E-02 WALL THICKNESS = .642582E-03 DELZ = .496977E-02
 J =14 MIDWALL RADIUS = .58559E-02 WALL THICKNESS = .641895E-03 DELZ = .496724E-02
 J =15 MIDWALL RADIUS = .56823E-02 WALL THICKNESS = .640338E-03 DELZ = .496092E-02
 J =16 MIDWALL RADIUS = .54838E-02 WALL THICKNESS = .637075E-03 DELZ = .494512E-02
```

TABLE B-3. (CONTINUED)

```
AXIAL NODE 14    AVE RADIUS =  .549825E-02    AVE WALL THICKNESS =  .629637E-03    CONTACT SWITCH = 1    TCE =  .716E-01
 J = 1 MIDWALL RADIUS = .52860E-02 WALL THICKNESS = .630921E-03 DELZ = .491254E-02
 J = 2 MIDWALL RADIUS = .51313E-02 WALL THICKNESS = .618512E-03 DELZ = .484373E-02
 J = 3 MIDWALL RADIUS = .50306E-02 WALL THICKNESS = .602875E-03 DELZ = .475630E-02
 J = 4 MIDWALL RADIUS = .49958E-02 WALL THICKNESS = .593507E-03 DELZ = .469770E-02
 J = 5 MIDWALL RADIUS = .50306E-02 WALL THICKNESS = .602875E-03 DELZ = .475630E-02
 J = 6 MIDWALL RADIUS = .51313E-02 WALL THICKNESS = .618513E-03 DELZ = .484374E-02
 J = 7 MIDWALL RADIUS = .52860E-02 WALL THICKNESS = .630[illegible]22E-0[illegible] DELZ = .491255E-02
 J = 8 MIDWALL RADIUS = .54748E-02 WALL THICKNESS = .637817E-03 DELZ = .494944E-02
 J = 9 MIDWALL RADIUS = .56704E-02 WALL THICKNESS = .641322E-03 DELZ = .496563E-02
 J =10 MIDWALL RADIUS = .58416E-02 WALL THICKNESS = .643022E-03 DELZ = .497214E-02
 J =11 MIDWALL RADIUS = .59588E-02 WALL THICKNESS = .643813E-03 DELZ = .497488E-02
 J =12 MIDWALL RADIUS = .60007E-02 WALL THICKNESS = .644048E-03 DELZ = .497566E-02
 J =13 MIDWALL RADIUS = .59595E-02 WALL THICKNESS = .643817E-03 DELZ = .497489E-02
 J =14 MIDWALL RADIUS = .58428E-02 WALL THICKNESS = .643031E-03 DELZ = .497217E-02
 J =15 MIDWALL RADIUS = .56720E-02 WALL THICKNESS = .641340E-03 DELZ = .496570E-02
 J =16 MIDWALL RADIUS = .54764E-02 WALL THICKNESS = .637853E-03 DELZ = .494963E-02
AXIAL NODE 15    AVE RADIUS =  .549778E-02    AVE WALL THICKNESS =  .629668E-03    CONTACT SWITCH = 1    TCE =  .715E-01
 J = 1 MIDWALL RADIUS = .52858E-02 WALL THICKNESS = .630960E-03 DELZ = .491256E-02
 J = 2 MIDWALL RADIUS = .51312E-02 WALL THICKNESS = .618547E-03 DELZ = .484400E-02
 J = 3 MIDWALL RADIUS = .50306E-02 WALL THICKNESS = .602913E-03 DELZ = .475660E-02
 J = 4 MIDWALL RADIUS = .49958E-02 WALL THICKNESS = .593548E-03 DELZ = .469803E-02
 J = 5 MIDWALL RADIUS = .50306E-02 WALL THICKNESS = .602914E-03 DELZ = .475660E-02
 J = 6 MIDWALL RADIUS = .51312E-02 WALL THICKNESS = .618551E-03 DELZ = .484401E-02
 J = 7 MIDWALL RADIUS = .52858E-02 WALL THICKNESS = .630962E-03 DELZ = .491257E-02
 J = 8 MIDWALL RADIUS = .54744E-02 WALL THICKNESS = .637844E-03 DELZ = .494960E-02
 J = 9 MIDWALL RADIUS = .56698E-02 WALL THICKNESS = .641349E-03 DELZ = .496575E-02
 J =10 MIDWALL RADIUS = .58408E-02 WALL THICKNESS = .643046E-03 DELZ = .497223E-02
 J =11 MIDWALL RADIUS = .59579E-02 WALL THICKNESS = .643836E-03 DELZ = .497496E-02
 J =12 MIDWALL RADIUS = .59998E-02 WALL THICKNESS = .644070E-03 DELZ = .497574E-02
 J =13 MIDWALL RADIUS = .59586E-02 WALL THICKNESS = .643839E-03 DELZ = .497498E-02
 J =14 MIDWALL RADIUS = .58420E-02 WALL THICKNESS = .643055E-03 DELZ = .497226E-02
 J =15 MIDWALL RADIUS = .56713E-02 WALL THICKNESS = .641367E-03 DELZ = .496583E-02
 J =16 MIDWALL RADIUS = .54760E-02 WALL THICKNESS = .637885E-03 DELZ = .494981E-02
AXIAL NODE 16    AVE RADIUS =  .549777E-02    AVE WALL THICKNESS =  .629669E-03    CONTACT SWITCH = 1    TCE =  .715E-01
 J = 1 MIDWALL RADIUS = .52858E-02 WALL THICKNESS = .630961E-03 DELZ = .491257E-02
 J = 2 MIDWALL RADIUS = .51312E-02 WALL THICKNESS = .618550E-03 DELZ = .484401E-02
 J = 3 MIDWALL RADIUS = .50306E-02 WALL THICKNESS = .602913E-03 DELZ = .475659E-02
 J = 4 MIDWALL RADIUS = .49958E-02 WALL THICKNESS = .593547E-03 DELZ = .469802E-02
 J = 5 MIDWALL RADIUS = .50306E-02 WALL THICKNESS = .602914E-03 DELZ = .475660E-02
 J = 6 MIDWALL RADIUS = .51312E-02 WALL THICKNESS = .618551E-03 DELZ = .484402E-02
 J = 7 MIDWALL RADIUS = .52858E-02 WALL THICKNESS = .630963E-03 DELZ = .491258E-02
 J = 8 MIDWALL RADIUS = .54744E-02 WALL THICKNESS = .637846E-03 DELZ = .494961E-02
 J = 9 MIDWALL RADIUS = .56698E-02 WALL THICKNESS = .641350E-03 DELZ = .496576E-02
 J =10 MIDWALL RADIUS = .58408E-02 WALL THICKNESS = .643048E-03 DELZ = .497224E-02
 J =11 MIDWALL RADIUS = .59579E-02 WALL THICKNESS = .643838E-03 DELZ = .497497E-02
 J =12 MIDWALL RADIUS = .59998E-02 WALL THICKNESS = .644072E-03 DELZ = .497575E-02
 J =13 MIDWALL RADIUS = .59586E-02 WALL THICKNESS = .643841E-03 DELZ = .497498E-02
 J =14 MIDWALL RADIUS = .58420E-02 WALL THICKNESS = .643057E-03 DELZ = .497227E-02
 J =15 MIDWALL RADIUS = .56713E-02 WALL THICKNESS = .641369E-03 DELZ = .496583E-02
 J =16 MIDWALL RADIUS = .54760E-02 WALL THICKNESS = .637887E-03 DELZ = .494982E-02
```

APPENDIX C

DERIVATION OF KRAMER AND DEITRICH'S EXPRESSION FOR STRESS

The theory of Kramer and Deitrich is summarized here because the theory is basic to understanding cladding deformation. In the Kramer and Deitrich approach, forces on an element of cladding are summed and set equal to zero as in any statics problem. However, Kramer and Deitrich express these forces as a function of a general transformation and they divide the transformation into two parts--a large symmetric deformation which preserves the cylindrical shape of the cladding and small perturbation terms which are a function of position. The cladding deformation is viewed as a transformation of an element of material from its initial coordinates to a new location

$$r = f_1\,(\theta_o, Z_o, t) = a(t) + \delta\,(\theta_o, Z_o, t) \qquad \text{(C-1a)}$$

$$\theta = f_2\,(\theta_o, Z_o\ t) = \theta_o \qquad \text{(C-1b)}$$

$$Z = f_3\,(\theta_o, Z_o, t) = \exp\,(\bar{\varepsilon}_Z)\ Z_o = \lambda(t) \qquad \text{(C-1c)}$$

where

(r,θ,Z)	=	new coordinates of the element of material initially located at (r_o, θ_o, Z_o)
f_1,f_2,f_3	=	functions describing a general transformation
$a(t)$	=	zero-th order, the radius one would find if the cylinder remained cylindrical

$\delta(\theta_0, Z_0, t)$ = local perturbations of the radius

$\bar{\varepsilon}_Z$ = average axial strain component.

Equation (C-1b) assumes radial displacement but that assumption is not used in this model. The quantity that is used is the position vector of the deformed element in cylindrical coordinates

$$\vec{r} = [a(t) + \delta(\theta_0, Z_0, t)]\, \hat{r} + \lambda\ (t)\ Z_0\ \hat{Z}. \tag{C-2}$$

This position vector is used to define two (non-unit) basis vectors tangent to the deformed surface

$$\vec{\beta}_1 = \frac{\partial \vec{r}}{\partial \theta_0} = \frac{\partial \delta}{\partial \theta_0}\, \hat{r} + [a(t) + \delta(\theta_0, Z_0, t)]\, \frac{\partial \hat{r}}{\partial \theta_0} + 0 + 0$$

$$= \frac{\partial \delta}{\partial \theta_0}\, \hat{r} + [a(t) + \delta\ (\theta_0, Z_0, t)]\ \hat{\theta} \tag{C-3}$$

$$\vec{\beta}_2 = \frac{\partial \vec{r}}{\partial Z_0} = \frac{\partial \delta}{\partial Z_0}\, \hat{r} + [a(t) + \delta\ (\theta_0, Z_0, t)]\, \frac{\partial \hat{r}}{\partial Z_0} + \lambda(t)\ \hat{Z}$$

$$= \frac{\partial \delta}{\partial Z_0}\, \hat{r} + \lambda(t)\ \hat{Z}. \tag{C-4}$$

Figure C-1 illustrates typical orientations of $\vec{r}$, $\vec{\beta}_1$, and $\vec{\beta}_2$.

Bending stresses from thermal expansion and swelling are neglected so the forces on a surface element come from membrane stresses in the plane and pressures normal to the plane. The force per unit area on the edges of the surface element are the inner product of the stress tensor and a unit vector normal to the edge. The force per unit area on the Z_0 = constant and θ_0 = constant edges is

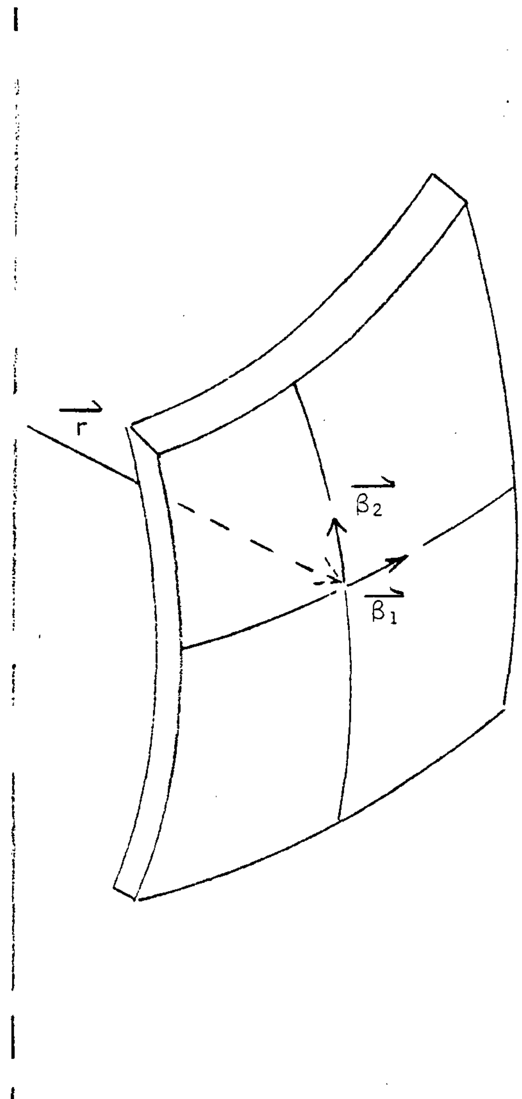

Figure C-1. Schematic illustration of the position vector, $\vec{r}$, and two bases vectors tangent to the deformed surface element.

$$\vec{F}_{Z_0} = \bar{\bar{\sigma}} \cdot \frac{\vec{\beta^2}}{\left|\vec{\beta^2}\right|} \tag{C-5}$$

$$\vec{F}_{\theta_0} = \bar{\bar{\sigma}} \cdot \frac{\vec{\beta^1}}{\left|\vec{\beta^1}\right|} \tag{C-6}$$

where

$\vec{F}_{Z_0}$ = force per unit area on the Z_0 = constant edge

$\vec{F}_{\theta_0}$ = force per unit area on the θ_0 = constant edge

$\dfrac{\vec{\beta^2}}{\left|\vec{\beta^2}\right|}$ = unit vector normal to Z_0 = constant edge. The vector $\vec{\beta^2}$ equals $\vec{\nabla} Z_0$.

$\dfrac{\vec{\beta^1}}{\left|\vec{\beta^1}\right|}$ = unit vector normal to θ_0 = constant edge. The vector $\vec{\beta^1}$ equals $\vec{\nabla}\theta_0$.

Figure C-2 shows typical orientations of $\dfrac{\vec{\beta^2}}{\left|\vec{\beta^2}\right|}$ and $\dfrac{\vec{\beta^1}}{\left|\vec{\beta^1}\right|}$.

$\vec{F}_Z$ and $\vec{F}_{\theta_0}$ must be multiplied by the edge areas to find the force due to stress on the edges of the surface element under consideration. The length of each edge can be found by realizing that the differential vector connecting two neighboring points is

$$\vec{dr} = \frac{\partial \vec{r}}{\partial \theta_0}\, d\theta_0 + \frac{\partial \vec{r}}{\partial Z_0}\, dZ_0 \ . \tag{C-7}$$

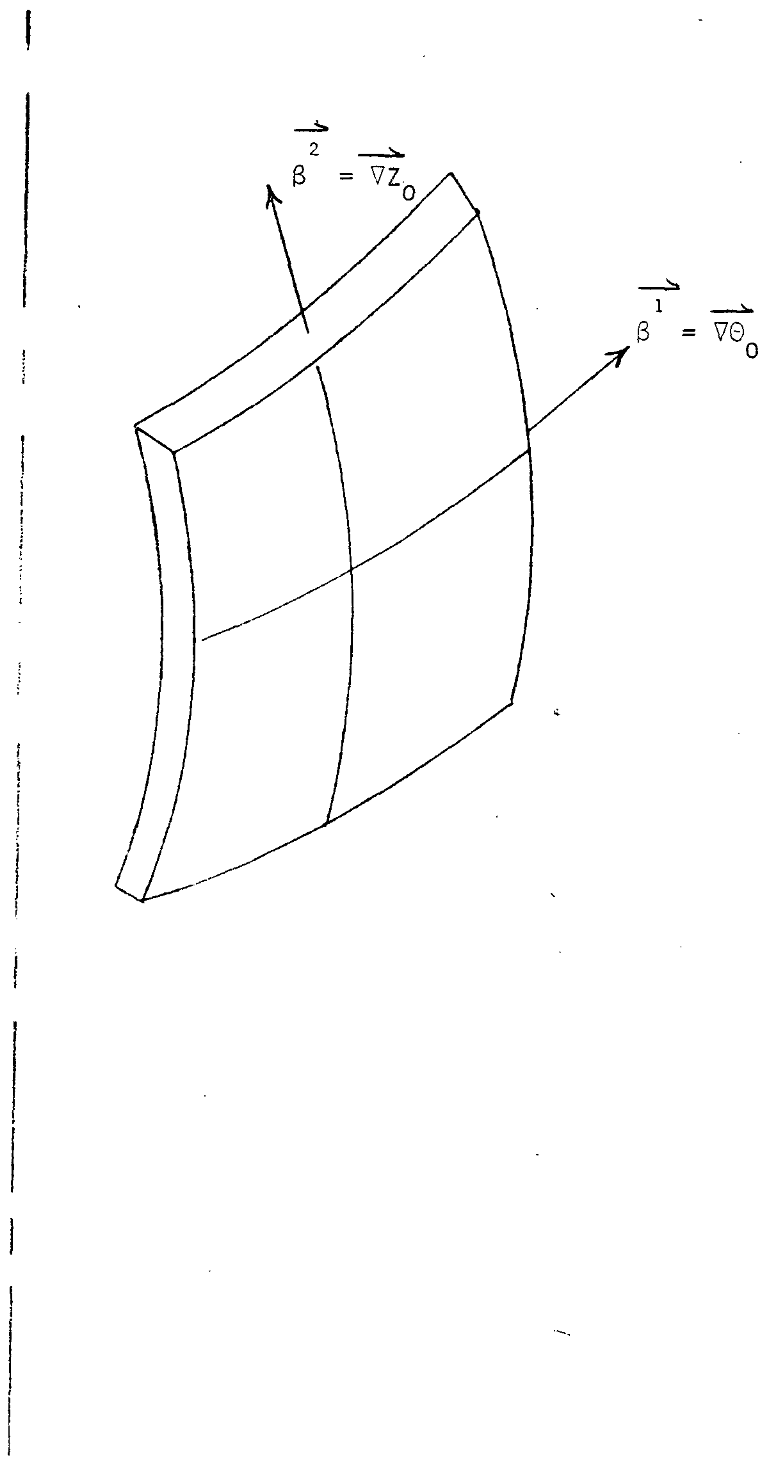

Figure C-2. Schematic illustration of typical orientations of vectors normal to the Z_0 = constant and Θ_0 = constant edges.

The differential arc length is the square root of

$$ds^2 = \vec{dr} \cdot \vec{dr} = \left[\left(\frac{\partial\delta}{\partial\theta_o}\right)^2 + [a(t) + \delta\ (\theta_o,\ Z_o,\ t)]^2\right] d\theta_o{}^2$$

$$+ 2\ \frac{\partial\delta}{\partial\theta_o}\ \frac{\partial\delta}{\partial Z_o}\ d\theta_o\ dZ_o + \left[\left(\frac{\partial\delta}{\partial Z_o}\right)^2 + \lambda(t)^2\right] dZ_o{}^2\ . \tag{C-8}$$

The Z_o = constant edge is thus $\sqrt{E}\ d\theta_o$ long and the θ_o = constant edge is $\sqrt{G}\ dZ_o$ long

where

$$E = \left(\frac{\partial\delta}{\partial\theta_o}\right)^2 + [a(t) + \delta(\theta_o,\ Z_o,\ t)]^2 = |\vec{\beta_1}|^2 \tag{C-9}$$

$$G = \left(\frac{\partial\delta}{\partial Z_o}\right)^2 + \lambda(t)^2 = |\vec{\beta_2}|^2 . \tag{C-10}$$

Thus for an element h thick, the forces on the Z_o = constant and θ_o = constant edges are

$$\vec{F}_{Z_o} = \bar{\bar{\sigma}} \cdot \frac{\vec{\beta^2}}{|\vec{\beta^2}|}\ h\sqrt{E}\ d\theta_o \tag{C-11}$$

and

$$\vec{F}_\theta = \bar{\bar{\sigma}} \cdot \frac{\vec{\beta^1}}{|\vec{\beta^1}|}\ h\sqrt{G}\ dZ_o \tag{C-12}$$

Using the orthonormal relations between $\vec{\beta}^1$, $\vec{\beta}^2$, $\vec{\beta}_1$, and $\vec{\beta}_2$,

$$\vec{\beta}^1 \cdot \vec{\beta}_1 = 1 \tag{C-13a}$$

$$\vec{\beta}^2 \cdot \vec{\beta}_2 = 1 \tag{C-13b}$$

$$\vec{\beta}^1 \cdot \vec{\beta}_2 = 0 \tag{C-13c}$$

$$\vec{\beta}^2 \cdot \vec{\beta}_1 = 0 \tag{C-13d}$$

$$\vec{\beta}^1 \cdot (\vec{\beta}_1 \times \vec{\beta}_2) = 0 \tag{C-13e}$$

$$\vec{\beta}^2 \cdot (\vec{\beta}_1 \times \vec{\beta}_2) = 0 \tag{C-13f}$$

and the definitions of $\vec{\beta}_1$ and $\vec{\beta}_2$, it is possible to solve for the six unknown components of $\vec{\beta}^1$ and $\vec{\beta}^2$. The components can in turn be used to show

$$\left|\vec{\beta}^1\right| = \frac{\sqrt{G}}{H} \tag{C-14}$$

$$\left|\vec{\beta}^2\right| = \frac{\sqrt{E}}{H} \tag{C-15}$$

where

$$H = \sqrt{EG - 2 \frac{\partial \delta}{\partial \theta_o} \frac{\partial \delta}{\partial Z_o}} \quad . \qquad \text{(C-16)}$$

Equations (C-11) and (C-12) can be rewritten using these expressions and the orthonormal relations

$$\vec{F}_{Z_o} = \bar{\bar{\sigma}} \cdot \vec{\beta}^2 \, h \, H \, d\theta_o$$

$$= [\sigma^{12} \vec{\beta}_1 + \sigma^{22} \vec{\beta}_2] \, h \, H \, d\theta_o \qquad \text{(C-17)}$$

and

$$\vec{F}_{\theta_o} = \bar{\bar{\sigma}} \cdot \vec{\beta}^1 \, h \, H \, dZ_o$$

$$= [\sigma^{11} \vec{\beta}_1 + \sigma^{21} \vec{\beta}_2] \, h \, H \, dZ_o . \qquad \text{(C-18)}$$

In addition to these stress-caused forces on the element there is a force exerted by the pressure on the element. The force due to pressure is

$$\vec{F}_n = \Delta P \, \vec{dA} \qquad \text{(C-19)}$$

where

ΔP = the pressure inside the cladding minus the pressure outside the cladding

$\vec{dA}$ = the surface area of the element times a unit vector normal to the element.

Since $\vec{\beta_1} \times \vec{\beta_2}$ is normal to the surface and the edges have been shown to be $\left|\vec{\beta_1}\right| d\theta_o = \sqrt{E}\, d\theta_o$ and $\left|\vec{\beta_2}\right| dZ_o = \sqrt{G}\, dZ_o$ in length,

$$\vec{dA} = d\theta_o\, dZ_o\, \vec{\beta_1} \times \vec{\beta_2}$$

$$= d\theta_o\, dZ_o\, H\, \hat{n} \tag{C-20}$$

where $\hat{n}$ is a unit normal to the surface,

$$\frac{\lambda(a + \delta)\,\hat{r} - \lambda \frac{\partial\delta}{\partial\theta_o}\,\hat{\theta} - (a + \delta)\frac{\partial\delta}{\partial Z_o}\,\hat{Z}}{H}.$$

The force exerted by pressure is thus

$$\vec{F_n} = \Delta P\, H\, d\theta_o dZ_o\, \hat{n}. \tag{C-21}$$

Since the element is in equilibrium (small forces required to accelerate the cladding mass are neglected), the normal components of the stress-caused forces and the pressure-caused force must sum to zero.

$$\vec{F_n} \cdot \hat{n} = \frac{d\vec{F}_{Z_o}}{dZ_o}\, dZ_o \cdot \hat{n} + \frac{d\vec{F}_{\theta_o}}{d\theta_o}\, d\theta_o \cdot \hat{n}\ . \tag{C-22}$$

The forces acting on the element are shown schematically in Figure C-3. Using expressions (C-17) and (C-18) for $\vec{F}_{Z_o}$ and $\vec{F}_{\theta_o}$, the fact that $\hat{n}$ is orthogonal to $\vec{\beta_1}$ and $\vec{\beta_2}$, Equations (C-3) and (C-4) for $\vec{\beta_1}$ and $\vec{\beta_2}$, and the expression given after Equation (C-20) for $\hat{n}$ in conjunction with Equation (C-22) leads to the expression

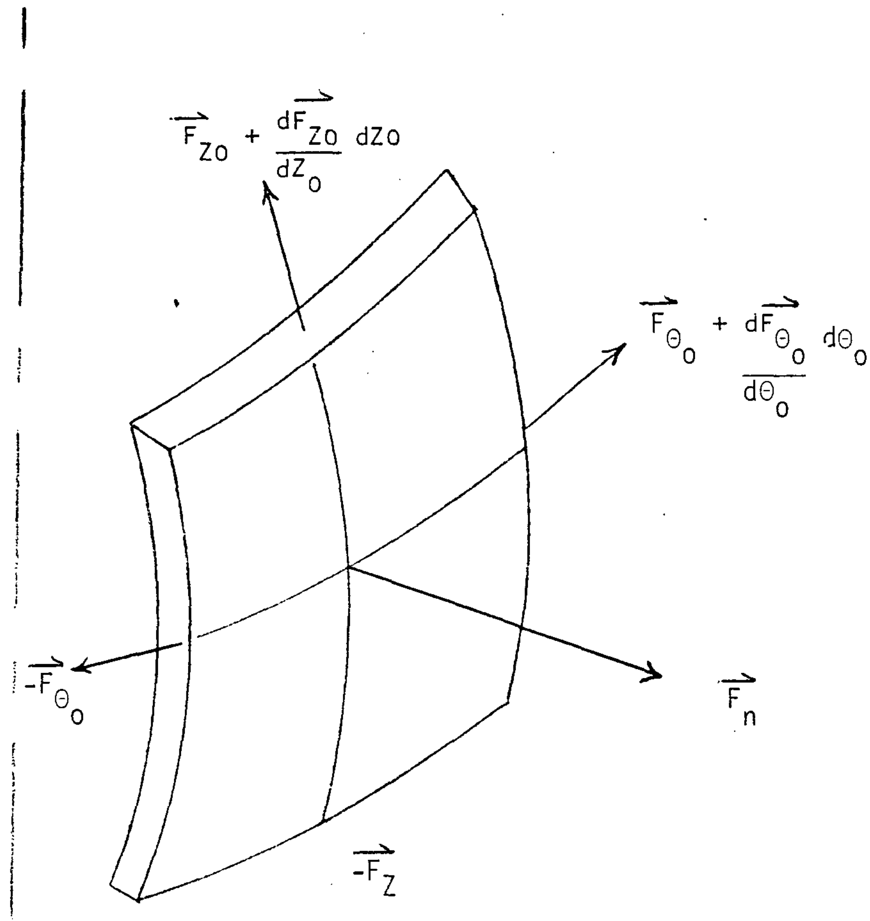

Figure C-3. Forces acting on an element of deformed cladding surface.

$$\frac{\Delta P}{h} = L\,\sigma^{11} + 2\,M\,\sigma^{12} + N\,\sigma^{22} \tag{C-23}$$

where

$$L = \left[-\,(a+\delta)\left(\frac{\partial^2\delta}{\partial\theta_o^{\,2}} - a - \delta\right) + 2\left(\frac{\partial\delta}{\partial\theta_o}\right)\right]\frac{\lambda}{H}$$

$$M = \left[-\,(a+\delta)\,\frac{\partial^2\delta}{\partial\theta_o\,\partial Z_o} + \frac{\partial\delta}{\partial\theta_o}\,\frac{\partial\delta}{\partial Z_o}\right]\frac{\lambda}{H}$$

$$N = -\,(a+\delta)\,\frac{\partial^2\delta}{\partial Z_o^{\,2}}\cdot\frac{\lambda}{H}$$

Although Equation (C-23) is only one equation in the three unknowns σ^{11}, σ^{12}, and σ^{22}, it will turn out that two of the three stress components have no first order change when the cladding shape is perturbed from cylindrical so the equation is sufficient to solve for the one non-zero component.

In order to get a convenient basis for the perturbation theory that will be used with the equilibrium relation, Equation (C-23), a new basis is defined

$$\overset{=}{\sigma} = \sigma^{ij}\,\vec{\beta}_i\,\vec{\beta}_j \equiv \sigma^i{}_j\,\frac{\vec{\beta}_i}{\left|\vec{\beta}_i\right|}\,\vec{\beta}^j\,\left|\vec{\beta}_j\right| \quad . \tag{C-24}$$

The new components, σ^i_j, can be related to the old using inner products along with the defining relation, Equation (C-24). The inner products are

$$\vec{\beta}_1 \cdot \vec{\beta}_1 = E \tag{C-25}$$

$$\vec{\beta}_2 \cdot \vec{\beta}_2 = G \tag{C-26}$$

$$\vec{\beta}_1 \cdot \vec{\beta}_2 = 2 \frac{\partial\delta}{\partial\theta_o} \frac{\partial\delta}{\partial Z_o} \equiv F \tag{C-27}$$

$$\vec{\beta}^i \cdot \vec{\beta}_j = \delta_{ij}. \tag{C-28}$$

The new components expressed in terms of the old components are

$$\sigma^1_1 = E\ \sigma^{11} + F\ \sigma^{12} \tag{C-29}$$

$$\sigma^1_2 = \sqrt{\frac{E}{G}}\ (F\ \sigma^{11} + G\ \sigma^{12}) \tag{C-30}$$

$$\sigma^2_2 = F\ \sigma^{21} + G\ \sigma^{22}$$

$$= F\ \sigma^{12} + G\ \sigma^{22}. \tag{C-31}$$

These components are convenient for the perturbation theory approach because they reduce to the familiar principal stress components in the limit of no perturbation:

As $\delta \to 0$,

$$L \to a \tag{C-32}$$

$$M \to 0 \tag{C-33}$$

$$N \to 0 \tag{C-34}$$

$$E \to a^2 \tag{C-35}$$

$$F \to 0 \tag{C-36}$$

$$E \to \lambda^2 \tag{C-37}$$

and Equation (C-23) becomes

$$\frac{\Delta P}{h_{cyl}} = a\, \sigma^{11}. \tag{C-38}$$

Thus, using Equations (C-29) to (C-38)

$$\sigma_1^1 \to a^2\, \sigma^{11} = a\, \frac{\Delta P}{h_{cyl}} \tag{C-39}$$

$$\sigma_2^1 \to a\lambda\, \sigma^{12} \tag{C-40}$$

$$\sigma_2^2 \to \lambda^2 \sigma^{22}. \tag{C-41}$$

The right side of (C-40) is zero. This can be seen by noting that as $\delta \to 0$

$$\vec{\beta_1} \to a\,\hat{\theta} \tag{C-42}$$

$$\vec{\beta_2} \to \lambda\,\hat{Z}\ . \tag{C-43}$$

This means that in the limit $\delta \to 0$

$$\sigma^{12} \to \frac{1}{a\lambda}\,\sigma_{\theta Z_{cyl}} = 0\ . \tag{C-44}$$

Similar logic can be used to identify the limit of σ^{22}. From Equation (C-43),

$$\sigma^{22} \to \frac{1}{\lambda^2}\,\sigma_{ZZ_{cyl}}\ . \tag{C-45}$$

Combining Equations (C-39), (C-40), (C-41), (C-44), and (C-45) leads to the conclusion that σ_1^1, σ_2^1 and σ_2^2 do reduce to the familiar principal stress components as $\delta \to 0$:

$$\sigma_1^1 \to \frac{\Delta P}{h_{cyl}}\,a \tag{C-46}$$

$$\sigma_2^1 \to 0 \tag{C-47}$$

$$\sigma_2^2 \to \sigma_{ZZ_{cyl}}\ . \tag{C-48}$$

The final part of deriving the Kramer and Deitrich expression for stress is to carry out the perturbation approximation. In order to do this, the stress components σ^i_j are written as the sum of the cylindrical shape stresses given by Equations (C-46) to (C-48) and a small change

$$\sigma^i{}_j = \sigma_a{}^i{}_j + \sigma_\delta{}^i{}_j \tag{C-49}$$

where

$\sigma_a{}^i{}_j$ = cylindrical shape stresses given as limits in Equations (C-46) to (C-48)

$\sigma_\delta{}^i{}_j$ = $\sigma^i{}_j - \sigma_a{}^i{}_j$.

A second preliminary step is to invert the transformation relations of Equations (C-29) to (C-31) and a third is to express the deformed wall thickness, h, as the cylinder wall thickness, h_{cyl}, less a small change of order δ

$$h = h_{cyl} - h_\delta \ . \tag{C-50}$$

The perturbation calculation itself is carried out by substituting the expressions for σ^{ij} as functions of $\sigma^i{}_j$ into Equation (C-23). With some algebra and subsequent use of Equations (C-49) and (C-50) the following expression is obtained:

$$\begin{aligned}
&\frac{\Delta P}{h_{cyl} - h_\delta}\left[GE - F^2\right] \\
&\quad = \left[LG - 2MF + NF^2\right]\left[\frac{\Delta P\ a}{h_{cyl}} + \sigma_\delta{}^1{}_1\right] \\
&\quad + \sqrt{\frac{G}{E}}\left[-LF + 2ME - NF\frac{E}{G}\right]\left[0 + \sigma_\delta{}^1{}_2\right] \\
&\quad + N\left[E - \frac{F^2}{G}\right]\left[\sigma_{ZZ_{cyl}} + \sigma_\delta{}^2{}_2\right].
\end{aligned} \tag{C-51}$$

Next the expressions following Equation (C-23) for L, M, and N and the defining equations for E, G, and F [Equations (C-9), (C-10) and (C-27)] are used to express L, M, N, G, E, and F in Equation (C-51) as functions of δ. The resultant expression is then expanded in orders of δ where

$$h_\delta, \ \frac{\partial^2 \delta}{\delta \theta_o^2}, \ \frac{\partial^2 \delta}{\partial Z_o^2}, \text{ and } \sigma_\delta{}^i{}_j$$

are considered to be or order δ. The zero-th order terms are an identity

$$\frac{\Delta P}{h_{cyl}} a = \frac{\Delta P}{h_{cyl}} a \ . \tag{C-52}$$

The first order terms lead to the following expression

$$\sigma_\delta{}^1{}_1 \approx \frac{\Delta P \delta}{h_{cyl}} - \frac{a \ \Delta P \ h_\delta}{h^2_{cyl}} + \frac{\Delta P}{h_{cyl}} \frac{\partial^2 \delta}{\partial \theta_o{}^2} + \frac{\sigma_{ZZ_{cyl}}}{\lambda^2} a \frac{\partial^2 \delta}{\partial Z_o{}^2} \tag{C-53}$$

which is the expression used for the change in hoop stress due to a change in shape. Since there are no first-order terms involving any other stress components, the cylinder expressions for these other components are correct to first order without modification.

APPENDIX D

DERIVATION OF MODEL FOR BENDING

This appendix is a derivation of Equation (29) of the main text, the expression used to model the effect of bending due to different changes in cladding length as the ballooning proceeds. A highly simplified model for this bending is employed. In this model the cladding is assumed to be bent into a circular arc of radius r_Z as illustrated in Figure D-1. Since both the right and the left side subtend an angle ϕ,

$$\phi = \frac{Z_r}{r_Z} \tag{D-1}$$

$$\phi = \frac{Z_L}{r_Z + d} \tag{D-2}$$

where

ϕ = angle subtended by the bending cladding

r_Z = radius of curvature of the inside bend of the cladding viewed from the side

Z_r = length of the right side of the cladding

Z_L = length of the left side of the cladding

d = cladding diameter.

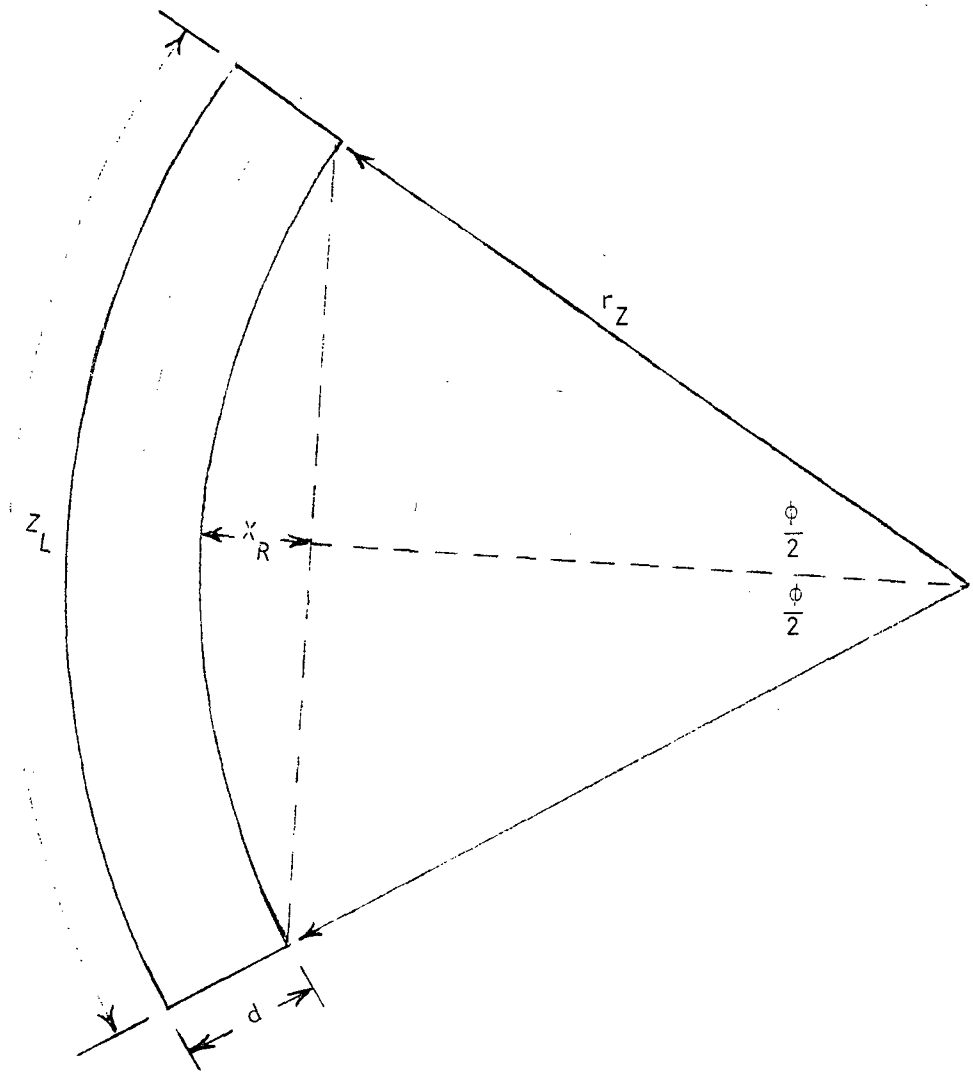

Figure D-1. Cladding configuration assumed for bending model.

At the midpoint of the arc the right hand side of the cladding is displaced a distance

$$X_R \approx r_Z - r_Z \cos\left(\frac{\phi}{2}\right) \tag{D-3a}$$

or

$$X_R \approx r_Z \frac{\phi^2}{8} \tag{D-3b}$$

by the bending. X_R can be expressed in terms of Z_R and Z_L by eliminating ϕ and r_Z from Equations (D-1), (D-2), and (D-3b). The resultant expression is

$$X_R = \frac{Z_R\ (Z_L - Z_R)}{8d}\ . \tag{D-4}$$

Similarly, the left hand side of the cladding is displaced a distance

$$X_L \approx \frac{Z_L\ (Z_L - Z_R)}{8d}\ . \tag{D-5}$$

Equations (D-4) and (D-5) show that the average bending displacement at the center of the arc is

$$X = \left(\frac{Z_L + Z_R}{2}\right)\left(\frac{Z_L - Z_R}{8d}\right) \tag{D-6a}$$

$$= \text{ZBEND}\ \frac{Z_L - Z_R}{8d} \tag{D-6b}$$

where ZBEND is the average length contributing to the bending.

A complete calculation of cladding bending would have to ensure that length changes and local stresses are consistent all around the cladding circumference and allow for variation in strains over the length of the bowed cladding. This careful calculation of the cladding bending would be both expensive and inconsistent with the approximations made to model the effect of shape on the local stress of the ballooning cladding and to account for tangential displacement. The detailed calculation was avoided by assuming

$$Z_R \approx \text{ZBEND} \exp\left[\varepsilon_{ZZ}(K,J)\right] \tag{D-7}$$

$$Z_L \approx \text{ZBEND} \exp\left[\varepsilon_{ZZ}\left(K, J + \frac{NJ}{2}\right)\right] \tag{D-8}$$

$$d \approx r_o \left\{\exp\left[e_{\theta\theta}(K,J)\right] + \exp\left[e_{\theta\theta}\left(K, J + \frac{NJ}{2}\right)\right]\right\} \tag{D-9}$$

where

$\varepsilon_{ZZ}(K,L)$ = axial component of strain of the cladding element at the K-th axial and L-th circumferential node

$\varepsilon_{\theta\theta}(K,L)$ = tangential component of strain of the cladding element at the K-th axial and L-th circumferential node

r_o = initial midwall radius of the cladding

NJ = number of circumferential nodes used to represent the cladding.

Equations (D-6b) to (D-9) can be combined to find the net displacement of the cladding midwall radius due to bending

$$X = \frac{\text{ZBEND}}{8r_o} \frac{\exp\left[\varepsilon_{ZZ}\left(K, J + \frac{NJ}{2}\right)\right] - \exp\left[\varepsilon_{ZZ}(K,J)\right]}{\exp\left[\varepsilon_{\theta\theta}(K,J)\right] + \exp\left[\varepsilon_{\theta\theta}\left(K, J + \frac{NJ}{2}\right)\right]} \; . \tag{D-10}$$

Since the code is an incremental code, the expression actually used is the change in midwall radius during a time step. This change is obtained from Equation (D-10) and the chain rule:

$$dX = \frac{\partial X}{\partial \varepsilon_{ZZ}(K,J)} d\varepsilon_{ZZ}(K,J) + \frac{\partial X}{\partial \varepsilon_{ZZ}\left(K,J + \frac{NJ}{2}\right)} d\varepsilon_{ZZ}\left(K,J + \frac{NJ}{2}\right)$$

$$+ \frac{\partial X}{\partial \varepsilon_{\theta\theta}(K,J)} d\varepsilon_{\theta\theta}(K,J) + \frac{\partial X}{\partial \varepsilon_{\theta\theta}\left(K,J + \frac{NJ}{2}\right)} d\varepsilon_{\theta\theta}\left(K,J + \frac{NJ}{2}\right). \quad \text{(D-11)}$$

The resultant expression is Equation (29) of the main text.